Politecnico di Torino

Master of science program in

ENERGY AND NUCLEAR ENGINEERING

Master's Thesis

Development and validation of a Python-based model for an AEM electrolyser: performance and degradation analysis

Supervisor:

Prof. ANDREA LANZINI

Co-Supervisor:

FRANCESCO DEMETRIO MINUTO

ELENA ROZZI

Edison S.p.A. external supervisor:

MASSIMILIANO BINDI

Candidate:

CHRISTIAN SCAVELLI

A.A. 2024/2025

Sessione di Marzo/Aprile

Abstract

The transition to renewable energy sources requires efficient energy storage and conversion systems. Among these, AEM (Anion Exchange Membrane) electrolyzers have emerged as a promising technology for green hydrogen production due to their potential to combine the advantages of both alkaline and PEM electrolyzers. However, their long-term performance and degradation behaviour under real operating conditions remain crucial aspects for industrial-scale deployment.

This thesis project, developed in collaboration with Edison S.p.A., presents the modelling of a realistic AEM electrolyzer test bench. In particular, the aim of this Python-based simulation model is to simulate the dynamic behaviour of AEM electrolyzers, integrating both their electrical response and degradation over time. The model simulates hydrogen production based on variable energy inputs from renewable sources (RES), making it a valuable tool for assessing future operational scenarios integration with RES. The degradation mechanisms are evaluated based on experimental tests performed during this thesis in accordance with the Joint Research Center (JRC) protocols.

Various modelling techniques, including empirical, semi-empirical, and physics-based approaches, were examined in from the scientific literature. Based on this review, the most suitable formulations and equations were selected to accurately describe the polarization curves, thermal management, and degradation phenomena of the AEM electrolyzer.

The model was fine-tuned to reproduce the dynamics of a real AEM electrolyzer operating at the Officine Edison laboratories. The model takes into account the electrical configuration, layout and operational constraints of the test bench, allowing for a faithful reproduction of the system's behaviour within the simulation. By integrating these practical aspects, the model bridges the gap between theoretical formulations and real-world implementation.

The Python model receives as input the energy powering the AEM and calculates the corresponding hydrogen output over time, considering key electrochemical and thermal parameters. The results of the model are then validated by comparing them with experimental data, ensuring its reliability in real-world applications.

The validation results confirmed the model effectively predicts the electrolyzer's behaviour, with a low root mean squared error (RMSE) and mean absolute percentage error (MAPE), particularly for voltage and hydrogen production. Initially, a discrepancy in the temperature sensitivity was identified, attributed to the assumption of a constant polarization curve temperature in the model. Additionally, the analysis revealed a higher-than-expected current prediction, linked to an increased membrane humidification degree, which in turn affected conductivity and efficiency. This behaviour led to the identification of an operational fault in

the real electrolyzer, demonstrating the model's potential even as a diagnostic tool. Afterwards, the fault has been solved by substituting the stack of the electrolyser (a critical component) and the model has been validated.

The model successfully approximated hydrogen production, with the cumulative output aligning closely with experimental values. Its accuracy is supported by the statistical metrics results: RMSE of 0.1410 and MPE of 0.1685. This highlights the model's reliability in predicting AEM electrolyzer performance, making it a valuable tool for scenario analysis, operational optimization, and long-term performance assessment.

Table of contents

List of figures

List of tables

List of abbreviation

PEM	Proton Exchange Membrane
ALK	Alkaline
AEM	Anion Exchange Membrane
SOEC	Solid Oxide Electrolyzer
RES	Renewable Energy Source
PV	Photovoltaic
AEMEC	Anion Exchange Membrane Electrolyzer
DC	Direct Current
AC	Alternative Current
OOP	Object Oriented Programming
EIS	Electrochemical Impedance Spectroscopy
JRC	Joint Research Center
OCV	Open Circuit Voltage
TRL	Technology Readiness Level
OER	Oxygen Evolution Reaction
HER	Hydrogen Evolution Reaction
PTL	Porous Transport Layers
LHV	Lower Heating Value
HHV	Higher Heating Value
EC	Electrolyzer
GDL	Gas Diffusion Layers
BP	Bipolar Plate
PID	Proportional Integral Derivative
CFD	Computational Fluid Dynamics

SMR	Steam Methane Reforming
LCOH	Levelized Cost Of Hydrogen
BOT	Beginning Of Test
EOT	End Of Test
TIP	Test Input Parameter
TOP	Test Output Parameters
RWD	Real World Degradation
RMSE	Root Mean Square Error
MAPE	Mean Absolute Percentage Error

1. Introduction

1.1. Context and motivation

Since the end of the 20th century, reducing greenhouse gases (GHG) has been a priority. Consequently, a worldwide effort has been organised to reduce greenhouse emissions and restrict the world average temperature rise to 3°C over pre-industrial levels [1]. Renewables, including solar, wind, hydropower, biofuels and others, are at the centre of the transition to less carbon-intensive and more sustainable energy systems. Generation capacity has grown rapidly in recent years, driven by policy support and sharp cost reductions for solar photovoltaics and wind power in particular.

The European Union has set an ambitious target of achieving climate neutrality by 2050. Among the key objectives is the ambitious goal to triple global renewable energy capacity to over 11,000 GW by 2030, a critical step to address climate change and ensure the sustainability of energy systems worldwide [2].

An overview of the RES capacity goal is presented in Figure 1.

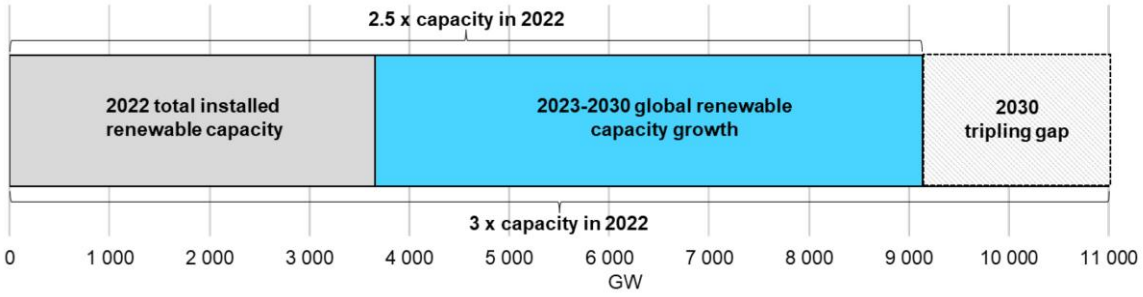

Figure 1 - Renewable capacity growth from 2022 to 2030 and the gap to global tripling renewables goal[2].

Moreover, an overview of the capacity growth is presented in Figure 2.

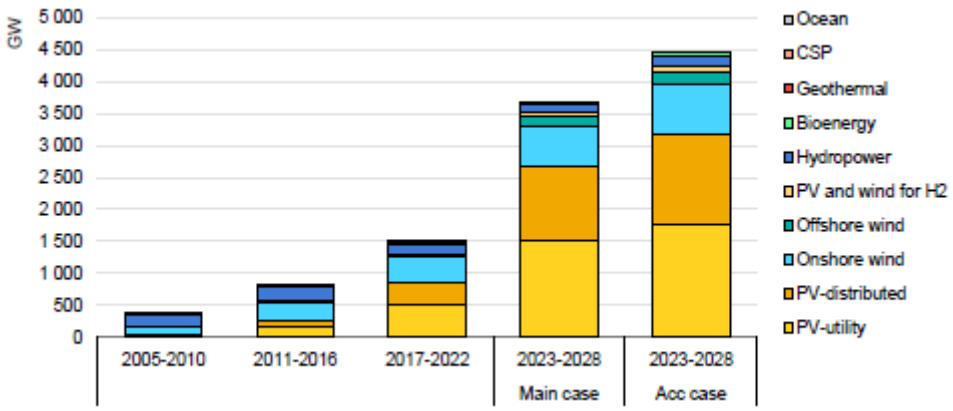

Figure 2 - Renewable capacity growth by technology, 2005-2028 [2].

Achieving this ambitious target requires a coordinated effort among governments, financial institutions, industries, and local communities to overcome significant challenges:

- Policy gaps and regulatory uncertainty: many countries lack clear targets and supportive frameworks to drive renewable energy deployment.
- Infrastructure barriers: insufficient transmission and distribution networks impede the integration of renewable sources into existing energy systems.
- Financial constraints in developing economies: high capital costs and limited private investment hinder progress in many emerging markets [2].

In this context, green hydrogen holds a crucial position, primarily due to its status as a carbon-neutral gas that can aid substantially in reducing emissions in sectors that are particularly challenging to decarbonize. Additionally, it has the potential to achieve cost competitiveness over time [3].

The interest of hydrogen in EU has been enlightened in the annual International Renewable Energy Agency (IRENA) report, as Figure 2 points out. The report highlights the expected growth of renewable energy capacity dedicated to hydrogen production, estimating an increase of 45 GW between 2023 and 2028 [2]. Furthermore, IRENA predicts that increasing renewable energy capacity and efficiency could reduce global emissions by 94%. However, despite exponential growth in renewable energy installations, these systems only account for 12% of global energy consumption, far short of the levels required to meet climate goals [2]. To bridge this gap, hydrogen is positioned as a critical catalyst for transitioning to a clean energy future, with several nations implementing strategies and roadmaps to integrate hydrogen into various sectors [1], [2].

Despite being a well-established technology for nearly 200 years, its use is often restricted to specialized, small-scale applications such as the electronics, food, and medical industries, as

well as in marine and aerospace contexts [2]. These limitations stem from the relatively high energy consumption and cost compared to other large-scale hydrogen production methods like natural gas reforming, coal and petroleum coke gasification, and the gasification or reforming of heavy oils, which dominate global production. As of 2006, water electrolysis contributed only about 4% of the global hydrogen supply [4] .

With growing concerns over rising energy costs, dwindling fossil fuel reserves, and the environmental impact of carbon dioxide (CO_2) emissions from fossil fuel combustion, hydrogen is gaining attention as a versatile and clean energy carrier. Indeed, it emits only water during use [4]. It can be produced from various sources, including (as previously stated) renewable energy, natural resources, and even industrial by-products like those from chlor-alkali processes. It has a lower transport cost than electricity, and can be stored reliably, safely and conveniently for long periods of time. It also favours 'sector coupling', i.e. integration between the electricity and gas sectors, which allows for greater flexibility and thus lower costs for the energy system as a whole [3]. The versatility enables hydrogen to enhance energy systems by aligning energy production with consumption patterns across time and locations. This hybrid approach allows energy to be stored and utilized in diverse ways. For example [1]:

- *Energy-to-energy:* converting energy into hydrogen for storage and later re-electrification.
- *Energy-to-gas:* using electrolysis to produce hydrogen, which can be stored or mixed with natural gas.
- *Energy-to-fuel:* creating hydrogen-based fuels for transportation or ammonia for maritime use.
- *Energy-to-feedstock:* utilizing hydrogen for chemical and synthetic fuel production.

The Energy-to-Gas approach using RES as input energy has gained significant attention because it unifies 2 key aspects of the energy transition, leading to reduce, even more, greenhouse gas emissions and create a sustainable energy system. This approach moves away from traditional fossil-fuel-based production methods to more environmentally friendly technologies, leveraging energy from solar, wind, geothermal, and biomass resources [1].

A review of the RES hydrogen production methods is shown in Figure 3.

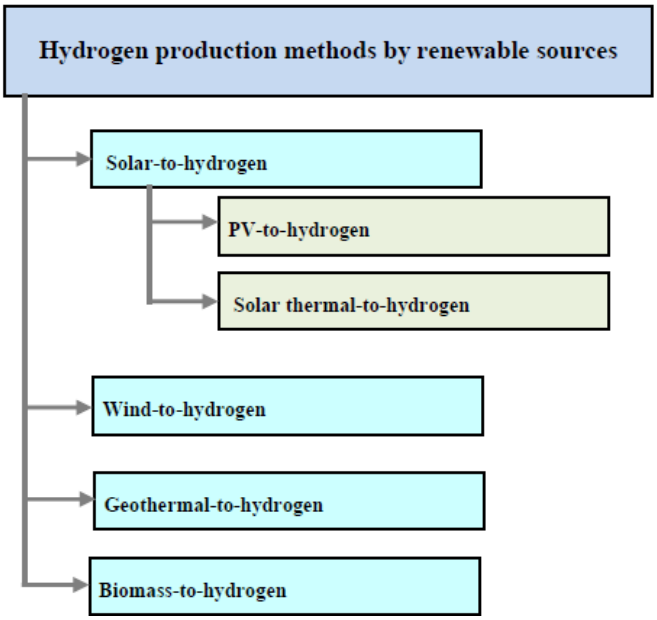

Figure 3 – Main hydrogen production methods by renewable sources [1].

The device which can produce Hydrogen exploiting the water electrolysis principle is named “Electrolyzer”, while the device which transform hydrogen into electricity and heat is called “Fuel Cell”, which is basically an inversed electrolyzer. These two technologies can work synergistically together, that is why they are seen as critical components of the "hydrogen economy", a concept which aims at creating sustainable energy systems [4].

The relevance of this concept is even highlighted in several different contexts. For instance, in small-scale applications and in distributed energy systems, particularly for remote communities where grid access is limited or impractical. Using renewable energy sources such as solar and wind, water electrolysis can convert surplus electricity into hydrogen, which serves as a clean fuel for heating and as an energy storage medium. Surplus electricity is the one not demanded by the grid and thus overproduced and not utilized. Stored hydrogen can later be utilized in fuel cells for electricity generation or as a direct fuel [4].

Moreover, for remote or isolated regions rich in renewable resources, water electrolysis can offer critical advantages. It provides mobility and flexibility, essential for powering households, telecommunication stations, small manufacturing industries, and off-grid systems. Examples include hydrogen-powered trial villages and renewable-powered communication stations where wind and solar energy, combined with hydrogen storage and fuel cells, provide reliable and sustainable energy solutions [4].

Figure 4 and Figure 5 enlighten what has just been discussed, ranging from the importance of RES powered electrolysis to the exploitation of hydrogen as flexible energy carrier.

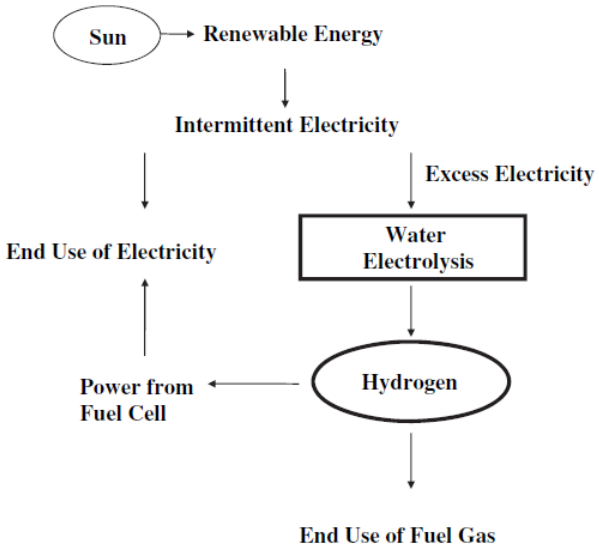

Figure 4 - A schematic illustration of a conceptual distributed energy system with water electrolysis as the principal engine of the process combining fuel cells and electrolyzers [4].

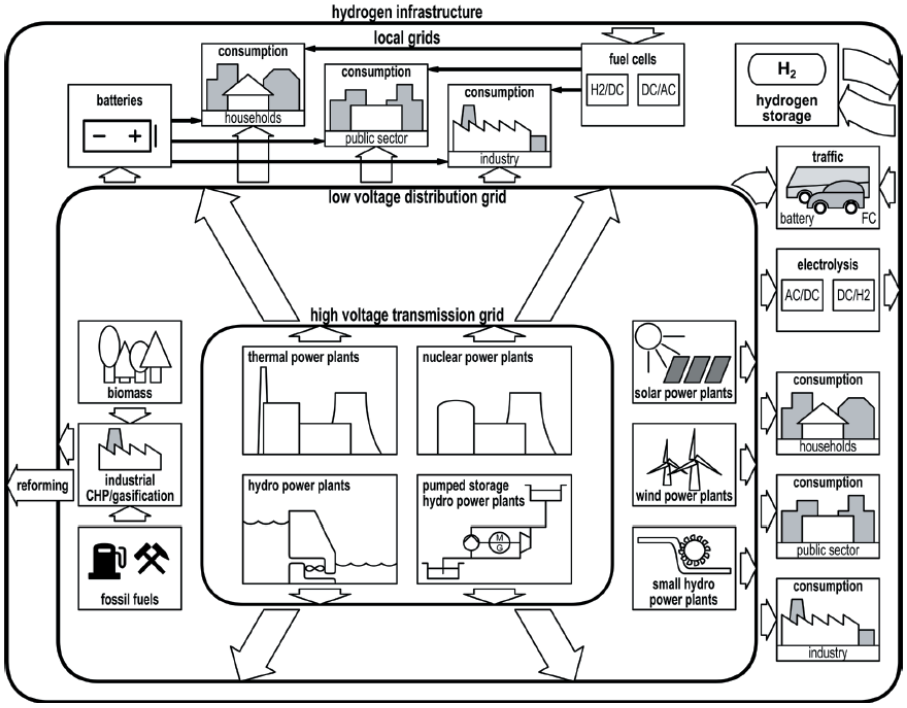

Figure 5 - The idea of hydrogen infrastructure integration into conventional power system [5].

1.2. Problem definition and objective of the thesis

To summarize the points previously discussed, the increasing global demand for clean and sustainable energy sources has underscored the critical importance of hydrogen as a versatile energy carrier. Among the various methods of hydrogen production, electrolysis powered by renewable energy sources (RES) has gained significant attention due to its potential to achieve zero-carbon emissions. A major challenge in this context is to realistically predict hydrogen production over time, considering both the intermittent nature of RES and the performance degradation of electrolyzers. Indeed, degradation threaten the electrolyzer durability and contemporary its hydrogen production capability.

Hydrogen production systems face two primary obstacles:

1. Intermittency of renewable energy sources: the availability of renewable energy, such as solar or wind power, fluctuates depending on environmental conditions. This variability makes it difficult to ensure a steady and predictable energy supply for the electrolyzers, thereby impacting hydrogen production rates.
2. Degradation of electrolyzer performance: over time, electrolyzers experience degradation in their performance due to various factors such as material wear, chemical reactions, and operational stresses. This degradation reduces efficiency, increases maintenance costs, and complicates the long-term planning of hydrogen production systems.

Accurately addressing these challenges is crucial for the effective integration of hydrogen production with renewable energy systems. Without a detailed understanding of these issues, stakeholders may struggle to design efficient systems, predict hydrogen output, or plan for the long-term sustainability of the infrastructure.
In this context, a significant gap exists in the current literature: the lack of a computational model that simulates the real-world operation of an electrolyzer while incorporating degradation as a relevant and configurable option. While various models have been developed to predict hydrogen production, they often:

- Focus on ideal or simplified scenarios, neglecting the impact of performance degradation.
- Fail to integrate energy input variability and electrolyzer wear in a cohesive framework.
- Lack the adaptability to explore different degradation scenarios or protocols.

This gap limits the ability to analyse long-term scenarios and hinders the development of robust, future-proof solutions. Examples of existing models and their limitations will be detailed later in the next chapters, providing context for the necessity of addressing this gap.

This problem is particularly significant for several reasons:

- Energy transition goals: the EU and global initiatives toward achieving carbon neutrality by mid-century require robust hydrogen production systems to support renewable energy storage and decarbonization efforts.
- Operational realism: many current models fail to account for the dual challenges of energy intermittency and electrolyzer degradation, limiting their applicability to real-world scenarios.
- Decision-making needs: stakeholders require reliable projections of hydrogen production to make informed decisions on investments, operational strategies, and energy policies.

In summary, the problem of realistically predicting hydrogen production from electrolyzers powered by renewable energy lies at the intersection of energy variability and system degradation. Addressing these challenges is critical for ensuring the scalability and sustainability of hydrogen as a key component of the global energy transition.

In the light of above, the objective of this thesis is to contribute to the advancement of hydrogen production systems by developing a Python flexible predictive model. This framework has the aim to simulate the operation of an AEM-type electrolyser in time, including its actual long-term degradation caused by both steady and intermittent power condition. The intermittent power condition is performed by simulating a PV panel as energy input source for the electrolyser.
The setting of the model is desired to be practical. Namely, input values should be present and known in the data sheets of a real purchasable electrolyser. At most, the model should require some variables that can be easily calculated starting from the ones inside the data sheet.
Moreover, the framework is designed to be scalable so that the simulations can adapt to each context. In particular, to the size of a case study electrolyser and to the variability and size of a RES farm that provides the input power.

The realization of this model has been possible thanks to an internship held in the R&D department at Edison S.p.A. , specifically at the “Officine Torino” , Energy Center. This activity was fundamental because it allowed to study and perform researching activity in the Edison laboratories over an AEM-type electrolyzer. By interfacing the design process of the framework with the study of the electrolyzer curve, the model achieves a better realism degree.

This thesis is structured as follow:

1. **Introduction:**
   defines the background over the concept of hydrogen importance, defines the research problem and its significance in the context of green hydrogen production.

2. **Literature review**:
   provides the theoretical and scientifical background over the electrolyzer technology. Defines the already created literature models, their structure, their electrochemical equations and their limits.
3. **Experimental setup and methodology:**
   defines the characterization of the AEM-kind experimental electrolyzer, starting from defining its layout test rig and ending to its characteristic curves such as the polarization or the degradation one. The methodology of the degradation calculation is finally described.
4. **Python model development:**
   defines all the followed steps that lead to the creation of the python model, starting from the objectives and framework definition to the equation parameterization and ending to the Python script composition.
5. **Results**:
   presents the validation results of the Python model by comparing its predicted output values with the actual data obtained from experimental research on the laboratory electrolyzer. Additionally, simulations are conducted to evaluate the impact of degradation on the electrolyzer's performances.
6. **Conclusions**:
   summarizes the key findings of the entire thesis, assesses whether the research objectives were met and defines the model limits and its potential improvements.

Through these objectives, this thesis seeks to bridge knowledge gaps and support the development of hydrogen production systems that are both practical and aligned with the broader goals of a carbon-neutral future.

2. Literature Review

2.1. Overview of hydrogen production technologies

Currently, the global annual production of hydrogen is approximately 0.1 gigatonnes, mainly consumed on-site for refining and metal treatment. This percentage is small compared to the rest of the fuel utilization due to the fact that hydrogen, unlike fossil fuels, is not naturally available in its pure form.
Production processes can be categorized into conventional methods, which rely on fossil fuels, and renewable technologies. Conventional methods include hydrocarbon reforming and pyrolysis, whereas renewable technologies involve the use of biomass or water splitting via electrolysis, thermolysis, or photo-electrolysis. An comprehensive overview of the possible methods is shown in Figure 6 [6].

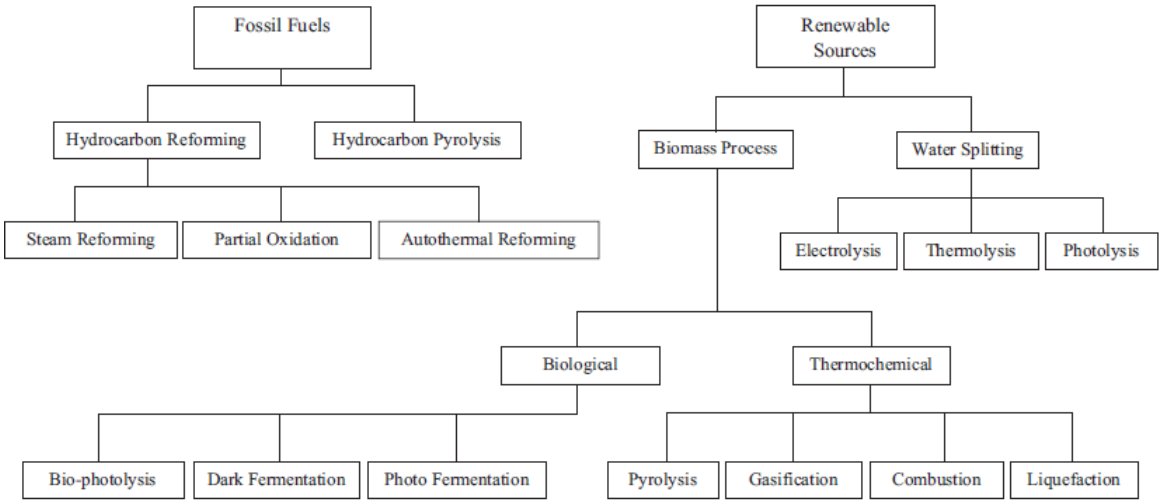

Figure 6 - Complete overview about the hydrogen possible production methods.

2.1.1. H2 production from fossil fuels

Hydrogen (H2) production from fossil fuels relies on well-established technologies, primarily hydrocarbon reforming and pyrolysis. These methods are among the most advanced and widely used, meeting the majority of global hydrogen demand. Currently, approximately 48% of the world's hydrogen is produced from natural gas, 30% from heavy oils and naphtha, and 18% from coal. Fossil fuels thus maintain their dominant role in hydrogen production due to their relatively stable costs and the existing infrastructure.

The main technologies for producing hydrogen from fossil fuels include:

1. **Hydrocarbon reforming**: this process converts hydrocarbon fuels into hydrogen using various reforming techniques:
    - *Steam reforming (SR):* a catalytic process where hydrocarbons react with steam to produce hydrogen and carbon oxides.
    - *Partial oxidation (POX):* converts hydrocarbons with oxygen at high temperatures to produce syngas (a mixture of CO and H2).
    - *Autothermal reforming (ATR):* combines the endothermic reactions of steam reforming with the exothermic reactions of partial oxidation to optimize hydrogen production.

    According to Chen, the levelized cost of H2 production using the SMR (steam methane reforming) process without CCUS (carbon capture, utilisation and storage) is $1.53/kg H2. The major cost comes from purchasing source material (natural gas) [7].

    In Figure 7 a classic membrane reactor for steam methane reforming is shown.

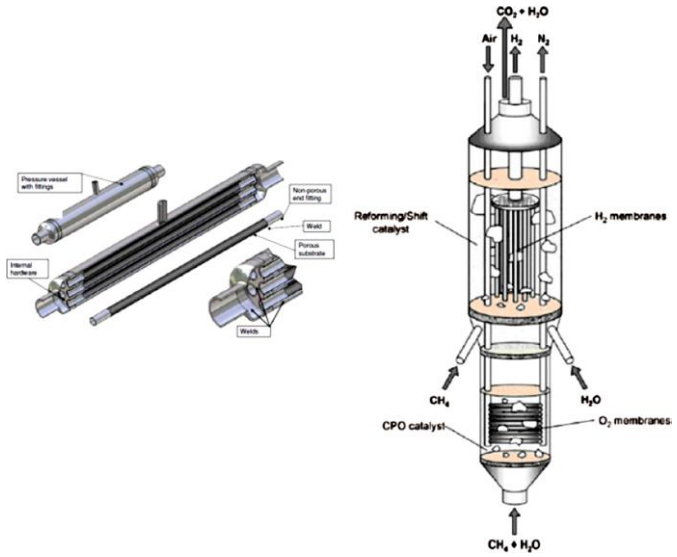

Figure 7 - Multiple membranes reactor for steam methane reforming [6].

2. **Hydrocarbon pyrolysis**: this process thermally decomposes hydrocarbons to produce hydrogen and solid carbon. Pyrolysis eliminates CO2 emissions by sequestering carbon in solid form, making it an environmentally attractive option.
3. **Coal gasification:** this process exploits high reactivity of coal combined to water or to both oxygen and water or to carbon dioxide and water. A syngas containing H2 is produced.

The levelized cost of H2 production using the Coal gasification process without CCUS is $2.62/kg H2. The major cost lies in purchasing source material (coal) [7].

While fossil fuel-based methods are highly developed and supported by extensive infrastructure, they face significant limitations, including dependency on fossil fuels and CO2 emissions. However, the adoption of advanced technologies such as membrane reactors and carbon capture and storage (CCS) can significantly mitigate their environmental impact, making these processes more sustainable [6].

2.1.2. H2 production from renewable sources

Hydrogen production from renewable sources, as previously stated, represents a vital approach for reducing dependence on fossil fuels and mitigating the environmental effects of climate change. As fossil fuel reserves decline and the urgency of addressing greenhouse gas emissions grows, renewable hydrogen technologies are poised to become increasingly significant, eventually surpassing conventional methods in prominence.

Hydrogen production from renewable sources analysis can be broken down into biomass based production, thermochemical processes, biological processes and last but not least water splitting technologies. Electrolyzers, obviously, are involved in the last method.

2.1.2.1. Biomass-based hydrogen production

Biomass, a renewable energy source derived from organic material like plants, agricultural residues, forestry byproducts, and waste, offers a sustainable feedstock for hydrogen production. Its use is considered carbon-neutral because the carbon dioxide released during energy production is balanced by the amount absorbed by plants during their growth cycle.

2.1.2.2. Thermochemical processes

Thermochemical methods use heat and chemical reactions to convert biomass into hydrogen-rich gases. Two prominent approaches are pyrolysis and gasification:

- **Pyrolysis** involves heating biomass at high temperatures without oxygen, breaking it down into a mixture of gases (including hydrogen), tar, and solid carbon. Further processes convert carbon monoxide into additional hydrogen by reacting it with steam, while advanced purification techniques ensure high-quality hydrogen.
- **Gasification** employs air, oxygen, or steam to decompose biomass at higher temperatures than pyrolysis. This process produces a gaseous mixture (syngas) that is

treated to extract hydrogen. Gasification achieves better hydrogen yields than pyrolysis, with efficiencies reaching nearly 50%.

In Figure 8, the flow diagram of the biomass process. Exiting the gasifier, the mix contains also other kind of products mixed together, so post treatments processes are needed. In Figure 9 an example of gasifier to produce H2, included in the gas product.

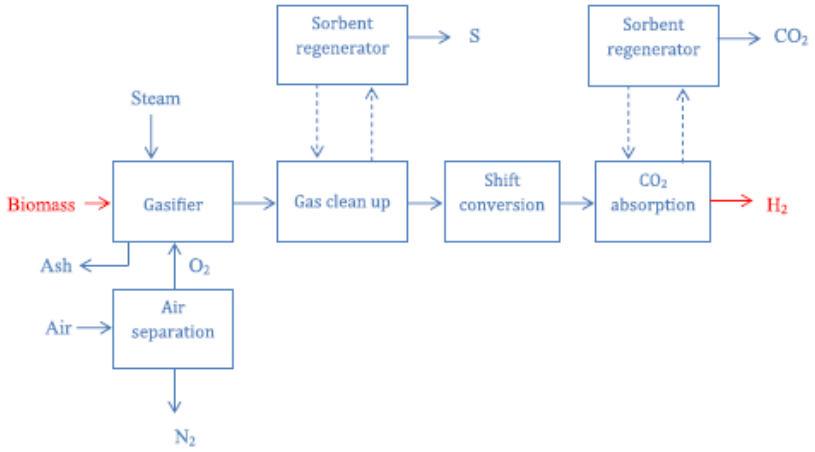

Figure 8 - Flow diagram of the biomass pyrolysis process [6].

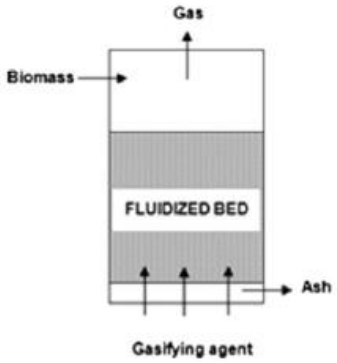

Figure 9 - Bubbling fluidized bed gasifier configuration [6].

2.1.2.3. Biological processes

Biological methods operate under mild conditions of temperature and pressure, making them more environmentally friendly but less efficient. These processes include:

- **Bio-photolysis**, where green or blue-green algae utilize sunlight to split water into hydrogen and oxygen. This method has the advantage of consuming carbon dioxide during the process but is limited by slow production rates and the need for extensive surface areas to collect light.

- **Dark fermentation**, in which anaerobic bacteria digest carbohydrate-rich organic matter in oxygen-free environments to produce hydrogen alongside organic acids. While glucose is a preferred substrate, agricultural and other organic waste can also be used.
- **Photo-fermentation**, where specific bacteria convert organic acids into hydrogen using sunlight. This process complements dark fermentation by utilizing the byproducts of the latter, achieving higher hydrogen yields but requiring significant light exposure and large bioreactors [6].

2.1.2.4. Water splitting technologies

Water splitting technologies is maybe the most promising way and offer one of the cleanest pathways for hydrogen production, as they rely on water as the primary raw material and generate only oxygen as a byproduct. Indeed, water is a free resource found almost everywhere in the world. Technological innovation has made it possible to create increasingly efficient plants capable of making the most of this resource. The three main approaches are:

1. **Electrolysis**: a mature and widely used method where water is split into hydrogen and oxygen using electricity. Technologies like alkaline and proton exchange membrane (PEM) electrolysis can achieve efficiencies of up to 73%. When powered by renewable energy sources, electrolysis becomes a completely clean process, although high electricity costs make it expensive compared to other methods. In Figure 10 a scheme of the process.
2. **Thermolysis**: this method involves heating water to extremely high temperatures to break it down into hydrogen and oxygen. Modern innovations use thermochemical cycles, such as the copper-chlorine (Cu-Cl) cycle, to reduce the required temperature and make the process more feasible. These cycles divide the overall reaction into smaller steps, using intermediate chemicals to enhance efficiency.
3. **Photo-electrolysis**: this process uses sunlight and specialized semiconductors to drive water splitting. Although it eliminates emissions entirely, current limitations in photocatalyst materials result in low efficiency, making it less competitive at this stage.

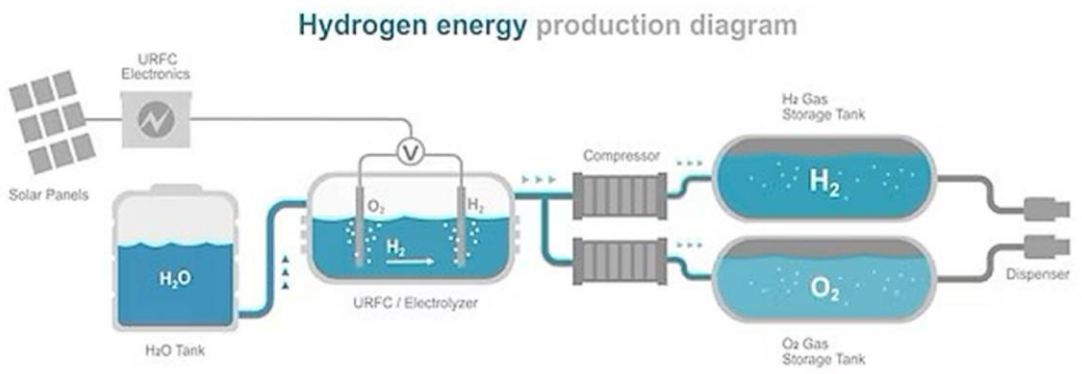

Figure 10 - Electrolysis general scheme powered by renewables [8].

In Figure 11 and Figure 12 a flow diagram of the thermolysis water splitting process and of the photo-electrolysis process are respectively shown [6].

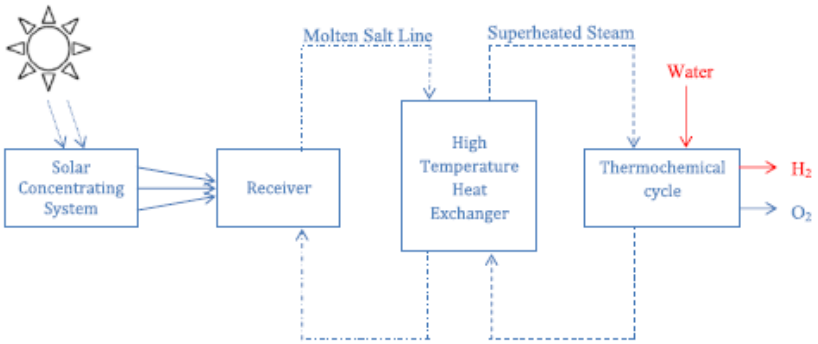

Figure 11 - Flow diagram of the solar-based thermochemical water splitting process [6].

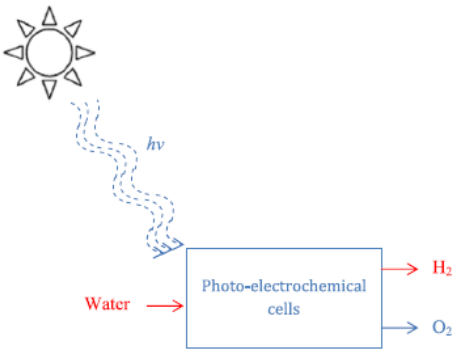

Figure 12 - Flow diagram of the photo-electrolysis process[6].

According to S. Baral and J. Sebo, the minimum cost of producing hydrogen using a combination of solar PV (with storage) and onshore wind turbines with alkaline water

electrolysis was $3.1 per kg in 2023 [9]. Notably, the cost with solar thermal (CSP) plants in the same year raises up to $15.6/kg [9].

Similarly, Díaz provides a LCOH (levelized cost of hydrogen) of 3.25 USD/kg with a system composed of PV powered electrolysis and storage system [10].

It is clear that currently all the renewable combinations have high production costs and cannot compete with hydrogen derived from fossil fuels. Still further researches are needed to make the H_2 renewable production competitive.

Among all the renewable possibilities, the main topic of this thesis is the water electrolysis process that will be better analysed in chapter 2.2.

2.2. Electrolyzers: principles and performance

2.2.1. Working principle

Electrolyzers are electrochemical devices that use electrical energy to split water molecules (H_2O) into their fundamental components: hydrogen (H_2) and oxygen (O_2). This process, known as electrolysis, is based on the principles of electrochemistry. When an electrical potential is applied across the system, water undergoes chemical reactions at the electrodes, resulting in the production of gases.
The process begins with the application of direct current from an external power source. This energy is needed to break the chemical bonds in water molecules.

An electrolyzer typically consists of two main components: the stack and the auxiliary systems. The stack is the core element where the water electrolysis process takes place. It is composed of multiple individual cells, arranged either in series or in parallel, depending on the design requirements (Figure 13). Cells connected in series increase the overall voltage of the stack, whereas cells connected in parallel enhance the current. This configuration is necessary because a single cell produces only a small amount of hydrogen; therefore, multiple cells are interconnected to generate a substantial output. The stack, along with its auxiliary systems, is typically housed within a cabinet, similar to the one shown in Figure 14.

Figure 13 - Example of a Hyter AEM electrolyzer stack [11].

Figure 14 - Hyter AEM electrolyzer cabinet [11].

Inside the stack, water is introduced into two separate compartments divided by a membrane or diaphragm. This membrane is essential, as it selectively allows ions to pass through while keeping the produced gases separate. At the anode, water molecules undergo an oxidation reaction, where electrons are removed, producing oxygen gas and charged ions either protons (H^+) in acidic systems or hydroxide ions (OH^-) in alkaline systems.
Simultaneously, at the cathode, a reduction reaction occurs. Here, the protons (or hydroxide ions) gain electrons to form hydrogen gas.

The overall reaction is the water electrolysis one:

$$H_2O \rightarrow H_2 + \frac{1}{2}O_2 \qquad \textit{Eq. 1}$$

The membrane or electrolyte ensures the proper flow of ions while maintaining the separation of gases. In acidic systems, protons (H^+) migrate through the membrane from the anode to the cathode, while in alkaline systems, hydroxide ions (OH^-) flow in the opposite direction. This selective ion movement ensures the overall efficiency and safety of the process.
In Figure 15, a scheme of the working principle.

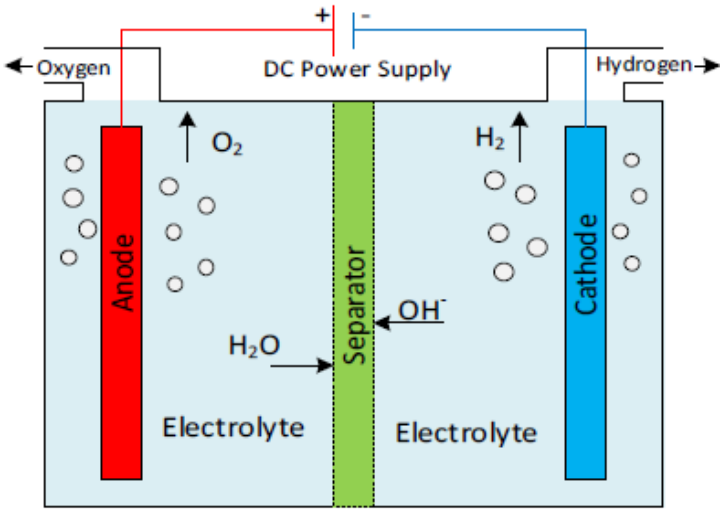

Figure 15 - Electrolysis process for hydrogen production [12].

2.2.2. Classification

There are multiple types of electrolyzer, each offering unique benefits and applications. These devices are typically classified into four main categories based on their type of electrolyte and operating temperature range. These distinctions greatly influence the choice of materials and components used in their construction. The four primary electrolyzer technologies are Alkaline (ALK), Proton Exchange Membrane (PEM), Anion Exchange Membrane (AEM), and Solid Oxide Electrolyzer Cells (SOEC). These categories are visually compared in terms of performance and features in available commercial electrolysis systems.

Two main groups of electrolysis' technologies can be distinguished among them, depending on the process temperature: low temperature and high temperature electrolysis. The former is already well developed and cost-competitive, while the latter is not currently mature enough to address the actual markets, but it may have applicability in the future [13].

Low temperature electrolysis is characterized by cell temperatures around 40-80 °C and it includes alkaline water electrolysis, proton exchange membrane electrolysis and anion exchange membrane electrolysis. All these technologies have the potential for further cost reductions and efficiency improvements, particularly ALK and PEM electrolyzers, which have been commercially available for many years and continue to advance. [13].

High temperature electrolysis, instead, is characterized by much higher operation temperatures, around 700-900 °C, and it includes solid oxide electrolysis (SOEC). It is a less mature technology, and its investment costs are still very high. However, SOEC is expected to have a greater efficiency compared to low temperature electrolyzers [14].

Because of the high working temperature, high temperature electrolysis needs for high-temperature sources of heat close, like concentrated solar power or high temperature geothermal. This might limit the long-term viability of SOEC [14].

Another possible classification can be carried out based on the electrolyte nature. In alkaline electrolyzers and AEM, a concentrated potassium hydroxide (KOH) solution typically serves as the electrolyte, enabling the transport of OH- anions. A porous diaphragm or separator, permeable to the KOH solution, ensures the physical separation of electrodes and gases produced during the process [8].
In contrast, PEM and SOEC systems utilize a solid electrolyte to separate the electrodes. This eliminates the need for a liquid electrolyte solution, as ion transport occurs within the solid modules of these systems. A comparative summary of the operational parameters and critical components of these four electrolyzer types highlights the variability among manufacturers and ongoing development, particularly in the AEM and SOEC categories, which are still in their nascent stages [8].

In this work of thesis, an AEM-kind electrolyzer will be studied as main topic. It is a technology which derives from PEM and ALK electrolyzers, thereby in the next chapters only these three kinds will be analysed.

2.2.2.1. Alkaline electrolyzer

Alkaline electrolyzers are among the most established and widely used hydrogen production technologies. They operate using a liquid electrolyte, typically composed of concentrated potassium hydroxide (KOH) or sodium hydroxide (NaOH) solutions [8].

The fundamental process of alkaline electrolysis occurs within a cell comprising an anode, a cathode, and a separator. The electrodes, often made of nickel or stainless steel, are immersed in the liquid electrolyte. The separator is, instead, made up by two gaskets and a diaphragm usually made of ZIRFON. The layers displacement is shown in Figure 16. When an electrical current is applied, water molecules at the anode undergo oxidation, producing oxygen gas, protons (H+) and electrons. These electrons flow through an external circuit to the cathode, where they reduce water molecules to generate hydrogen gas and hydroxide ions (OH^-). The hydroxide ions migrate back to the anode through the electrolyte, completing the electrochemical cycle. In Figure 17, both anode and cathode reaction are shown as well as the scheme of the process [8].

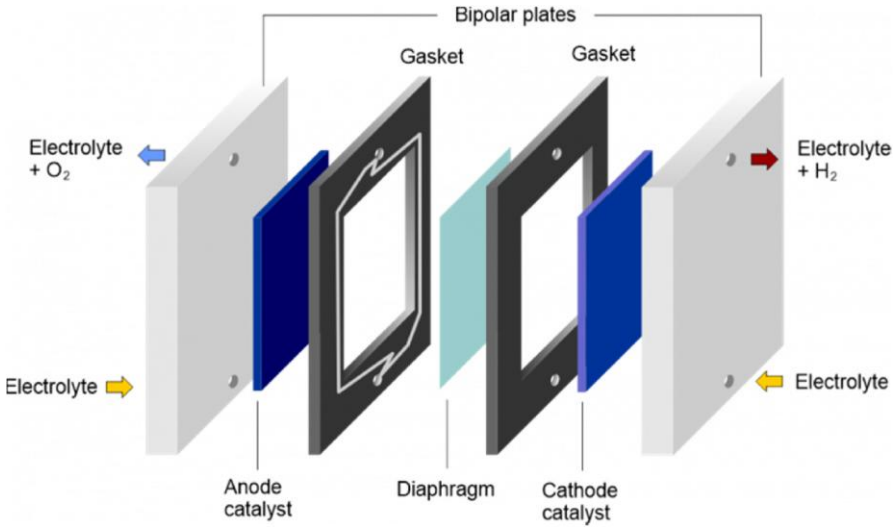

Figure 16 - Structure of an alkaline cell [8].

- **Anode Reaction:**

$$4OH^- \leftrightarrow 2H_2O + O_2 + 4e^-$$

- **Cathode Reaction:**

$$4H_2O + 4e^- \leftrightarrow 2H_2 + 4OH^-$$

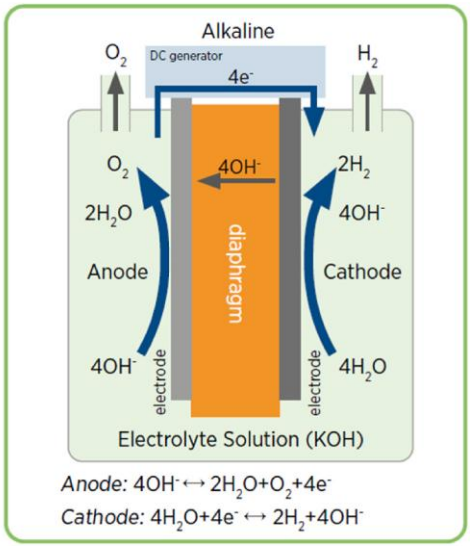

Figure 17 - Alkaline cell working principle and involved reactions [8].

2.2.2.2. Proton exchange membrane electrolyzer

Proton Exchange Membrane (PEM) electrolyzers utilizes a solid polymer electrolyte to conduct protons and separate the hydrogen and oxygen generated during water electrolysis. This design allows for a compact system with high efficiency and rapid response capabilities, making PEM electrolyzers particularly suitable for dynamic operations and integration with renewable energy sources [8].

The working principle of PEM begins with water being introduced into the anode side of the electrolyzer. Here, the water molecules are oxidized, releasing oxygen gas, protons (H^+), and

electrons. The oxygen gas is expelled, while the protons pass through the proton exchange membrane to the cathode. Electrons travel via an external circuit to the cathode, where they recombine with the protons to form hydrogen gas. In Figure 18, both anode and cathode reaction are shown as well as the scheme of the process [8].
The proton exchange membrane plays a critical role by allowing only protons to pass through, ensuring the separation of gases and preventing cross-contamination [8].

The proton exchange membrane is typically made from perfluorosulfonic acid polymers, such as Nafion®, which offer high proton conductivity and chemical stability. The electrodes are coated with precious metal catalysts: iridium or iridium oxide at the anode for the oxygen evolution reaction (OER) and platinum at the cathode for the hydrogen evolution reaction (HER). These catalysts facilitate the electrochemical reactions efficiently but contribute to the high cost of PEM electrolyzers. Additional key components include porous transport layers (PTLs) and bipolar plates. PTLs, often made from titanium or carbon-based materials, ensure effective distribution of water and gases while providing structural support for the membrane. Bipolar plates, typically composed of titanium with protective coatings, manage electrical conductivity and thermal regulation within the system [8]. The layer displacement is shown in Figure 19.

- **Anode Reaction:**

$$2H_2O \leftrightarrow O_2 + 4H^+ + 4e^-$$

- **Cathode Reaction:**

$$4H^+ + 4e^- \leftrightarrow 2H_2$$

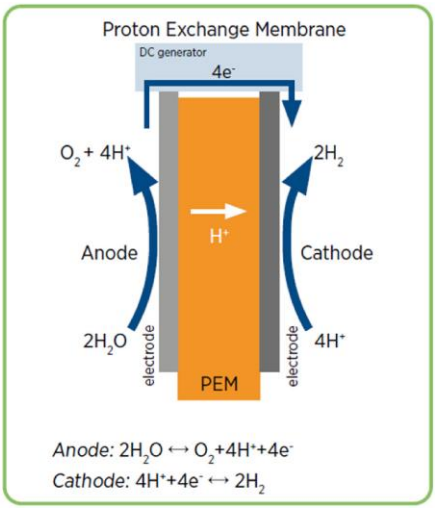

Figure 18 - PEM cell working principle and involved reactions [8].

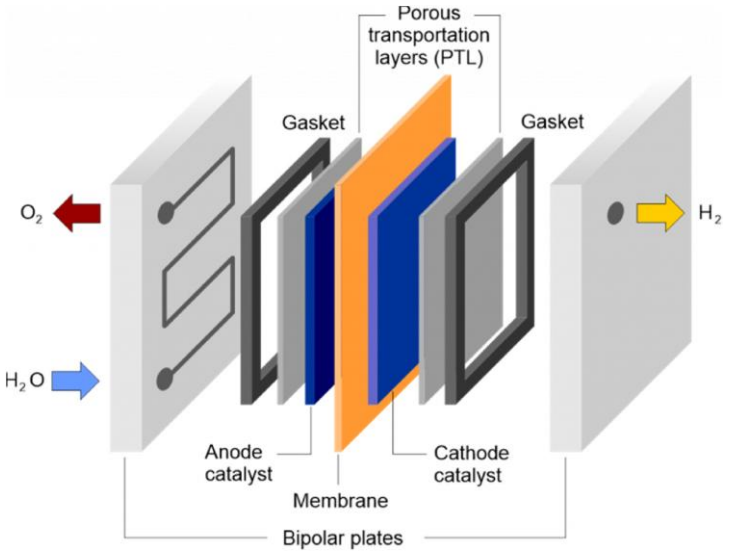

Figure 19 - Structure of a PEM cell [8].

2.2.2.3. Anion exchange membrane electrolyzer

Anion Exchange Membrane (AEM) electrolyzers are an innovative hydrogen production technology that operates under alkaline conditions. These systems utilize an alkaline polymer membrane that allows hydroxide ions (OH^-) to migrate from the cathode to the anode. This technology was born with the idea of solve problems of PEM and ALK and combine their advantages: it does not rely on expensive catalyst as PEM, reaches higher efficiency than ALK since higher current density, it can operate in high pH environments, it can produce pressurized hydrogen unlike ALK[15].
The AEM has a lower conductivity than PEM, mainly because of the lower mobility of hydroxyl ions compared to protons. Therefore, polymers with higher ion exchange capacity are usually used, which then typically take up more water and have reduced mechanical robustness under flooded conditions[13].

The operating mechanism of AEM electrolyzers begins at the cathode, where water molecules are reduced to form hydrogen gas and hydroxide ions. The hydroxide ions then travel through the anion exchange membrane to the anode, where they are oxidized to produce oxygen gas and water. The alkaline environment reduces the need for high-purity water, allowing these systems to utilize a wider range of water sources [8]. A graphic explanation of the process is shown in Figure 20.

- **Anode Reaction:**

$$4OH^- \leftrightarrow 2H_2O + O_2 + 4e^-$$

- **Cathode Reaction:**

$$4H_2O + 4e^- \leftrightarrow 2H_2 + 4OH^-$$

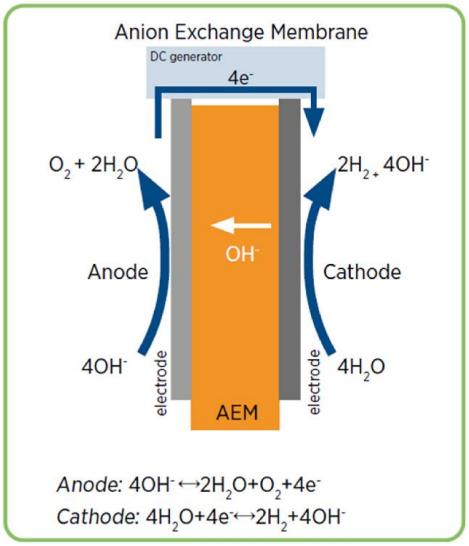

Figure 20 - AEM cell working principle and involved reactions [8].

The membrane typically is composed of quaternary ammonium-functionalized polymers to facilitate the selective transport of hydroxide ions while maintaining chemical stability in the alkaline environment. Non-precious metal catalysts, such as nickel, cobalt, and iron-based compounds, are employed at both the anode and cathode [8].
Currently, the most used OER catalysts are IrO2, Ni, Ni-Fe alloys, graphene, Pb2Ru2O6.5, and Cu0.7Co2.3O4, while Pt-black, CuCoOx, Ni-Mo, Ni/CeO2-La2O3/C, Ni, and graphene are used as HER catalysts [16].
Key structural components include porous electrodes and stainless steel or coated bipolar plates (in titanium or stainless steel as well), which ensure efficient gas distribution, electrical conductivity, and corrosion resistance [8].
Regarding the electrolytic solution, typically, a small percentage of electrolyte (HCO3-/CO32- or dilute KOH) is added to the water feed, in order to increase the cell performance. AEM electrolyzers can operate with water feed at both electrodes or in anode feed only [17].

The cell layer distribution is displaced in Figure 21.

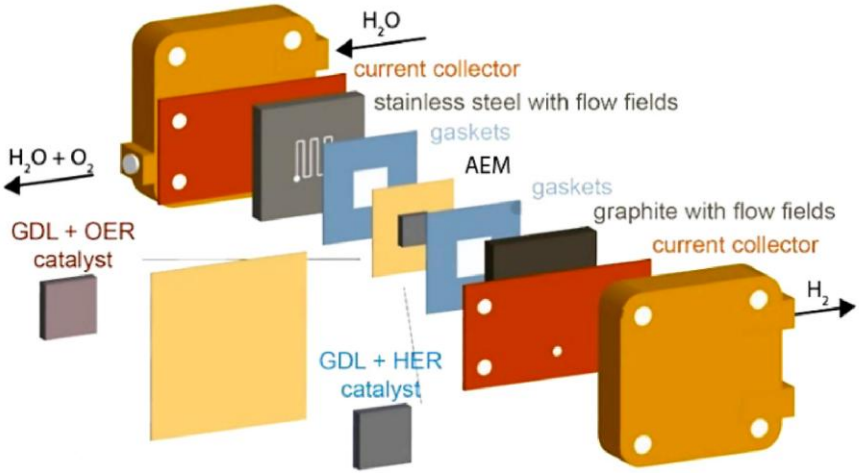

Figure 21 - Structure of a AEM cell [8].

2.2.3. Techno-economic comparison debate

Each of the described electrolyzer-type has its own benefits and drawbacks. Each one has its own application field depending on the cost, the size, the capability to work in not nominal conditions and the durability in time.
Alkaline electrolyzers has the advantage to use non-precious and cost-efficient materials, which significantly reduces the overall system cost, unlike PEM. Additionally, they are capable of producing high-purity hydrogen, making them suitable for a wide range of industrial applications [8]. On the other hand, their performance can be limited by the ionic conductivity of the electrolyte and the durability of the diaphragm or separator used to maintain gas separation. Advances in diaphragm materials, such as the development of reinforced microporous layers, have helped address these issues by enhancing ionic conductivity and reducing gas crossover [8].
Alkaline electrolyzers are particularly well-suited for large-scale industrial hydrogen production unlike PEM. They are commonly deployed in settings where stable and continuous operation is required, in case of intermittent conditions PEM perform much better [8].

PEM electrolyzers operate efficiently at temperatures ranging from 50°C to 80°C and can achieve high current densities higher than ALK, making them suitable for applications requiring high-purity hydrogen [8].

AEM electrolyzers are the newest technology. Currently, they face challenges, such as achieving high current densities and ensuring long-term durability, ongoing advancements in material science and system design are addressing these limitations. Their ability to produce hydrogen at lower costs and with greater flexibility makes them a promising option for sustainable energy applications [8].

Currently, Alkaline technology has a TRL equal to 9 and it is commercially used in industry, PEM, instead, is mainly used for medium and small applications (TRL = 6-8). The AEM technology, instead, is still in development and demonstration (TRL= 5-6) and it has started to be used in small commercial applications [18].

In the following Table a review of the cost of each EC electrolyzer.

Table 1 - Electrolyzer system investment costs (US dollars per kilowatt nominal power). Up to 2022 [19].

Present		2030	2050	Source
Alkaline				
700	2017	450	450	Fraunhofer, 2018
500 to 1,400	2019	400 to 850	200 to 700	IEA, 2019
500 to 1,000	2020			IRENA, 2020
540 to 900	2022			OIES, 2022
600 to 1,100	2022			Goldman Sachs, 2022
610	2022	344		DOE, 2022
Proton exchange membrane (PEM)				
1,460	2017	810	510	Fraunhofer, 2018
1,100 to 1,800	2019	650 to 1,800	200 to 900	IEA, 2019
700 to 1,400	2020			IRENA, 2020
667 to 1,450	2022			OIES, 2022
800 to 1,250	2022			Goldman Sachs, 2022
Solid oxide				
1,410	2017	800	500	Fraunhofer, 2018
2,800 to 5,600	2019	800 to 2,800	500 to 1,000	IEA, 2019
-	2020		<300	IRENA, 2020
2,300 to 6,667	2022			OIES, 2022
>1,850	2022			Goldman Sachs, 2022
Anion exchange (alkaline membrane)				
>931	2022			OIES, 2022

According to the U.S. Department of Energy, the uninstalled capital cost of PEM electrolyzer systems at today's manufacturing volumes is $700–$1,100/kW and the LCOH ranges from $6.00 to $7.20/kg H2 [20]. ALK capital cost ranges from $500/kW to more than $1,500/kW uninstalled cost achieving a LCOH of $5.00–$5.50/kg H2 [20].
AEM are not commercially available yet.

Knowing the price of each technology, as follows the overall electrolyzer efficiencies and the overall stack lifetime both up to 2022.

Table 2 - Electrolyzers' electrical efficiency. Up to 2022 [19].

Present		Source
Alkaline		
63% to 70%	LHV	IEA, 2019
50% to 68%	LHV	IRENA, 2020
68% to 77%	HHV	OIES, 2022
52% to 69%	LHV	Goldman Sachs, 2022
Proton exchange membrane (PEM)		
56% to 60%	LHV	IEA, 2019
50% to 68%	LHV	IRENA, 2020
70% to 80%	HHV	OIES, 2022
60% to 75%	LHV	Goldman Sachs, 2022
Solid oxide		
74% to 81%	LHV	IEA, 2019
75% to 85%	LHV	IRENA, 2020
80% to 90.8%	HHV	OIES, 2022
74% to 81%	LHV	Goldman Sachs, 2022
Anion exchange (alkaline membrane)		
52% to 67%	LHV	IRENA, 2020
<= 74%	HHV	OIES, 2022
40% to 70%	LHV	Goldman Sachs, 2022

Table 3 - Stack lifetime (hours). Up to 2022 [19].

Present	Long-term/2050	Source
Alkaline		
60,000 to 90,000	100,000 to 150,000	IEA, 2019
60,000	100,000	IRENA, 2020
60,000 to 100,000		OIES, 2022
60,000 to 90,000		Goldman Sachs, 2022
87,600		DOE, 2022
Proton exchange membrane (PEM)		
30,000 to 90,000	100,000 to 150,000	IEA, 2019
50,000 to 80,000	100,000 to 120,000	IRENA, 2020
50,000 to 90,000		OIES, 2022
30,000 to 80,000		Goldman Sachs, 2022
Solid oxide		
10,000 to 30,000	75,000 to 100,000	IEA, 2019
<20,000	80,000	IRENA, 2020
20,000 to 90,000		OIES, 2022
10,000 to 40,000		Goldman Sachs, 2022
Anion exchange (alkaline membrane)		
>5,000		IRENA, 2020
30,000	100,000	OIES, 2022
5,000 to 9,000		Goldman Sachs, 2022

2.3. Degradation mechanisms in electrolyzers

Electrolyzer technology is still in evolutionary stage. This is due to the high cost and mostly to the limitations of the hydrogen production. In this work the low temperature electrolyzer are only analysed (ALK, PEM, AEM). Each of these technologies presents specific advantages and unique challenges, particularly in terms of degradation and durability, which are critical aspects to ensure long-term performance and economic sustainability. The degradation effect is associated with the materials, working principles, working operation. Notably, the latter is one of the most critical aspects since does not depend on the technology effect but on how the electrolyzer is set to work. A steep variation of the operating range can badly influence the device lifetime, accelerating the aging effect. Therefore, the integration with a RES, which would lead to an intermittent operation, is an important aspect to be studied. The bad effect of a variability load affects differently each EC technology.

A common problem across all kind of electrolyzer which use metallic component is related to hydrogen embrittlement effect. This reduces the structural integrity of the electrodes enhancing the risk of stack breakdown [21].

2.3.1. Alkaline electrolyzers degradation

Alkaline electrolyzers use a liquid electrolyte solution of potassium hydroxide (KOH) or sodium hydroxide (NaOH) to transport OH^- ions between the electrodes. In nominal condition the following can be the problems associated to the technology.
A prolonged exposure to the highly alkaline electrolyte leads to the corrosion of electrode materials, such as nickel or its alloys. This is due to the formation of metal oxides and hydroxides during operation[22].
Over time, the diaphragm or separator that prevents mixing of hydrogen and oxygen deteriorates due to mechanical stress, chemical attack, or impurities in the electrolyte[23]. Since hydrogen is highly reactive this can even lead to explosion of the stack. A related problem is the gas bubbles accumulation over the electrode surface, reducing the effective area and thus slowing down the reactions[24].
For those reasons, traditionally ALK operate at low current densities. They are relatively inflexible, i.e. they have a relatively high minimum load (10–40 % of nominal load)[25]. Indeed, in the context of intermittent power resource, this technology is not really suitable. Frequent start-stop cycles induce thermal and mechanical stresses[26].
An important aspect is that ALK presents an anode degradation due to the generation of reverse current across the stack, each time that the electrolyzer shutdown occurs, so each time the input power is unavailable[26], [28].

2.3.2. Proton Exchange Membrane electrolyzers degradation

PEM electrolyzers use solid polymer membranes that conduct protons from the anode to the cathode. Just like the ALK technology, the crossover is an active problem that occurs with the time[24].
Free radicals, such as reactive oxygen species, generated during electrolysis and thermal and mechanical stress can compromise the integrity of the membrane [27]. This lead to increased gas crossover, reduced proton conductivity, and shorter operational lifespan.
PEM is a technology which requires noble metals due to the acid membrane. However, with the time the corrosion affects them badly, especially under high operating potentials and under dynamic conditions[28].
In the same way, a prolonged exposure to humid and acidic environments, coupled with compression stress from the stack reduce gas transport, increase mass transport losses, and lead to uneven current distribution[29].

Their ability to operate at high pressures and current densities makes them ideal for applications requiring a rapid response, such as coupling with renewable energy sources. They represents the best compromise in terms of input power variability among the electrolyzer technologies.
They generally are used for smaller scale application with respect to the alkaline ones[16].
Naturally, the intermittent operation would reduce its durability but not as much as the others types.

2.3.3. Anion Exchange Membrane electrolyzers degradation

AEM electrolyzers are an emerging technology that combines the advantages of ALK with those of PEM. AEMs use polymer membranes capable of conducting anions (OH^-), but their development is hindered by degradation vulnerabilities. Its TRL status is not high so it is still under research. Since combination of both PEM and ALK, AEM electrolyzers show same durability problems.

Firstly, AEM membranes presents chemical instabilities: loss of ion exchange capacity due to degradation of cationic functional groups and breakdown of the polymer backbone. Also because of nucleophilic attacks on functional groups, especially under high pH and elevated temperature conditions[31].
Electrochemical issues: electrochemical oxidation of electrode materials, including loss of catalytic activity and aggregation of catalyst particles. Local pH variation negatively impacts the stability of catalyst-electrolyte interfaces[30].
Then, certainly, physical and mechanical degradation: detachment of ionomers from catalyst surfaces due to excessive swelling of the membrane and accumulation of gas bubbles. Also, formation of mechanical defects such as pinholes or membrane rupture under differential

pressure conditions[30].
As it happens for PEM and ALK, corrosion of support materials: degradation of gas diffusion layers (GDLs) and bipolar plates (BPs), often due to the formation of metal oxides in alkaline conditions[30].
Gas bubbles generation and accumulation at the anode exchange surface, reducing mass transport and blocking catalytic interfaces as well[30].

About the intermittent conditions, there are still low numbers of papers which address its behaviour. Generally speaking this technology is still under development in nominal and even worse in intermittent conditions. However, there are some universal recognized degradation.
They experience reversal currents when shutting down the electrolyzers, such ALK[25].
Frequent rest periods without solution feeding lead to lower humidity levels inside the membrane, resulting in irreversible degradation of the membrane's ionic conductivity. The ohmic resistance (dominated by membrane resistance) increases significantly over time [31]. The solution feeding must continue to flow to avoid this problem.
Dynamic stress on materials: cyclic operations, such as frequent starting and stopping, impose mechanical and electrochemical stresses on the components. These stresses may lead to microstructural changes or weakening of the membrane and electrode interfaces[31].

2.4. Modelling approaches review for electrolyzers

Electrolyzer modelling is essential for predicting performance under various conditions. Existing approaches range from empirical to physics-based models, each with different complexity and accuracy levels. This section reviews key modelling techniques and examines if and how they incorporate degradation effects. The aim is to identify gaps in current methodologies and provide a basis for developing a more realistic model with degradation over time.

Below, some recurring parameters/constants.

Table 4 - Recurring values.

Name of the constant/parameter	Symbol
Operating pressure (bar)	P
Universal gas constant (J/mol*K)	R
Temperature (°C)	T
Faraday Constant (C/mol)	F
Current (A)	i
Current Density (A/m^2)	j

2.4.1. Electrical overview

An electrolyser cell can be modelled in different ways, to include all the exiting or entering energy flows. Rozzi and Grondin describe a possible approach in modelling the cell thanks to a mass balance, mass and charge transport, and electrochemical kinetics applied to the electrolysis cell [32], [33]. The connection between the operating cell voltage and the cell current is represented by the electrolyzer's characteristic curve, also known as the polarization curve [33]. The hydrogen production is related to the cell current (Eq. 10) which, in turn, is connected to the cell voltage. Therefore, to regulate the hydrogen production, operating voltage is modified. This modelling way is described by several authors such as Rozzi and Marangio [33], [34].
Rozzi together with Emam and Sood, then, state that the voltage ideally is the OCV (open circuit voltage), also known as Nernst voltage or reversible voltage but, due to non-faradaic losses, it is generally higher. Basically, the Nernst voltage represents the lowest voltage needed to power an electrolyzer [33], [35], [36]. The procedure follows the logic of the Gibbs free energy change of the reaction, defined as:

$$Erev = \frac{\Delta G}{zF} \qquad \textit{Eq. 2}$$

Being z the electrons transferred per reaction (in this case z=2). ΔG instead is the Gibbs free energy change of the occurring reaction and it depends on different factors, each model describes it in different ways. A recurring dependence is the temperature. Indeed, the general formula is:

$$E_{rev} = E_0 + \frac{RT}{2F} ln(C) \qquad \textit{Eq. 3}$$

E_0 is the reversible voltage at standard pressure (1 bar). According to Rozzi and Gomez Vidales it is a function of temperature as well [33], [37].
Gomez Vidales model states that *C* is a parameter that depends on the operating partial pressures (in bar) of the reactants (namely water) and of the products (namely hydrogen and oxygen). On the other hand, Titheridge modelling is more particular. It expresses that when electrolysis is carried out using KOH electrolytes (commonly employed in the anode and cathode chambers of AEM water electrolyzers), the activities of H_2, O_2, and H_2O are affected by the characteristics of the KOH electrolyte [38].
Detailed expression for C can be found in the appendix.

All the previously described models introduce an equation which rules the polarization curve. It is the following:

$$E_{cell} = E_{rev} + \eta_{act,an} + \eta_{act,cat} + \eta_{ohm} + \eta_{conc} \qquad \textit{Eq. 4}$$

E_{rev} is the reversible voltage, equal to 1.23V in standard condition. However, in real-world systems, the voltage is higher due to inefficiencies such as resistance in the system and additional energy losses at the electrodes. These inefficiencies are the overpotentials and increase the voltage needed to power the electrolysis. They represent three primary deviations from the ideal equilibrium conditions of the cell. Titheridge describes η_{act} as follow [38]:

- **Activation overpotential** (η_{act}) is related to charge transfer at the electrodes. Electrons must overcome an energy barrier to transfer from the reactants to the electrodes; without sufficient energy, electron recombination occurs.

The activation overvoltage η_{act} consists of both the cathode and anode effect. According to Gomez Vidales, it is expressed by the Butler-Volmer equation [37]:

$$\eta_{act} = \frac{RT}{\alpha_{a/c}\, F} arcsinh\left(\frac{j}{2j_{0,a/c}}\right) \qquad \textit{Eq. 5}$$

- $\alpha_{a/c}$ is the charge transfer coefficient of the electrodes (a and c represent anode and cathode respectively).

- $j_{0,a/c}$ is the exchange current density [$A\ m^{-2}$], namely the current at equilibrium in the absence of net electrolysis and at zero overpotential. This parameter strongly depends on the nature of the electrodes, taking factors such as their materials into consideration.

Some authors makes simplification of the equation. Titheridge states that in most electrochemical reactions $\alpha_a = \alpha_c = 0.5$ [38], some others author as Santistevan-Pineda use the logarithmic dependence in place of hyperbolic arcosine [39].

Again Gomez Vidales describes η_{ohm} as follow [37]:

- **Ohmic overpotential** (η_{ohm}) is associated with the resistance to charge flow within the cell. This resistance is caused by both ion transport through the membrane and electron flow through cell components such as electrodes, interconnectors, and current collectors. To overcome this resistance, an additional voltage is required.

The ohmic overvoltage η_{ohm} can be represented using Ohm's law. The total ohmic loss as a function of the voltage can be expressed as:

$$V_{ohm} = r * i \qquad \textit{Eq. 6}$$

- r consists of the total electrical stack resistance. Each component in the electrolytic cells contributes. Generally speaking, r is the sum of the contributions of electrolyte resistance and the resistance of the membrane separator.
  The former is related to some geometric and chemical parameters which are: the distances between the anode and cathode, respectively and the membrane, the anode and cathode cross-section areas , the ionic conductivity of the KOH. The latter, then, depends on the molar concentration of the electrolyte (which is known) and temperature of the cell.
  The resistance of the membrane separator depends on the AEM thickness, the total area of the membrane and its conductivity. The membrane conductivity, in turn, is related to the humidification degree and operating temperature. The membrane is considered fully hydrated.

The last contribution, namely η_{conc} is called concentration or diffusion overpotential. Gomez Vidales model defines it as a limitation in mass transport. Reactant molecules must diffuse within the electrodes and reach the active sites where the reaction takes place, introducing an additional voltage requirement [37].

Before analysing the model parameterizations, it is important to observe that the influence of this term on the operation of a AEM-type electrolyzer is often considered irrelevant. Santistevan-Pineda states that this depends on the geometry of the feed configuration system: in systems where the electrolyte is recirculated quickly the development of the concentration overvoltage is prevented, creating a constant temperature in all the electrolyte mass flow [39].

The integration of the diffusion overvoltage introduces new constants and a more complex system design. Indeed, the migration process is accurate and precise. From a water migration balance the exact concentrations of the products in the cathode and anode are calculated. The present analysis is based on the observations made by Gomez Vidales [37].

Figure 22 shows the list and direction of the species migrations.

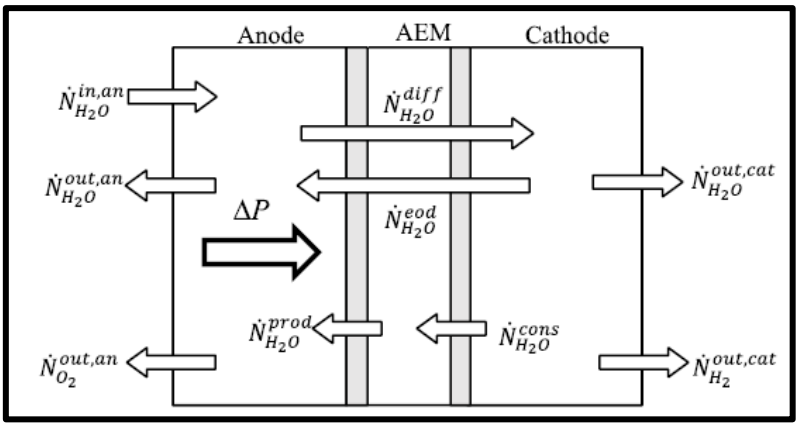

Figure 22 - Schematic representation of the water transport and mass flows in an AEM water electrolyzer (AEMWE) cell [37].

The net water flow through the membrane is the result of various processes that transport water across the anion exchange membrane. The model considers three primary phenomena:

- Diffusion-driven flow $\dot{N}_{H_2O}^{diff}$:
  water transport across the AEM, driven by diffusion from regions of higher concentration to lower concentration, can be modelled using Fick's law. For simplicity, the model assumes a linear concentration gradient across the membrane in accordance with Fick's principles. It depends on the active membrane area, the membrane water diffusion coefficient, the electrode thickness, the water concentrations at their respective membrane/electrode interface.

- Electro-osmotic drag $\dot{N}_{H_2O}^{eod}$:
  the phenomenon occurs when OH^- counter-anions transported across the AEM drag water molecules along with them. The molar flow associated with this process is determined by the electro-osmotic drag coefficient which represents the average number of water molecules carried by each hydroxide ion. This molar flow also depends on the total number of hydroxide ions traveling through the membrane.

- Pressure-induced flow $\dot{N}_{H_2O}^{pe}$:
  the water transport across the membrane caused by a pressure gradient is influenced by the membrane's permeability and can be calculated using Darcy's Law. It particularly depends on factors such as: the membrane permeability to water, the water viscosity, the active area of the membrane, the pressure gradient and the electrode thickness.

The total water across the membrane $\dot{N}_{H_2O}^{mem}$ is thus represented by the following equation:

$$\dot{N}_{H_2O}^{mem} = \dot{N}_{H_2O}^{diff} - \dot{N}_{H_2O}^{eod} - \dot{N}_{H_2O}^{pe} \qquad \textit{Eq. 7}$$

Further explanations of the equation of each term in the appendix.
The diffusion overvoltage equation is the following:

$$\eta_{diff} = \frac{RT}{4F} ln\left(\frac{C_{O_2mem}}{C_{O_2mem,0}}\right) + \frac{RT}{2F} ln\left(\frac{C_{H_2mem}}{C_{H_2mem,0}}\right) \qquad \textit{Eq. 8}$$

Here, C_{O_2mem} and C_{H_2mem} represent the concentrations of oxygen and hydrogen, respectively, at the membrane/electrolyte interface [$mol\ m^{-3}$]. The subscript 0 indicates reference values corresponding to a specific working condition. All the values are calculated with the Fick's Law. Notably, the process is described by the effective binary diffusion coefficient of transport for anode $D_{eff,a}$ and cathode $D_{eff,c}$. They describe respectively the diffusion at O2/H2O and H2/H2O interface. The expression is provided below:

$$D_{eff,A-B} = D_{A-B}\varepsilon\left(\frac{\varepsilon - \varepsilon_p}{1-\varepsilon}\right)^{\alpha} \qquad \textit{Eq. 9}$$

A-B stands for the arbitrary pair interface.
α is an empirical coefficient, ε is the electrode porosity, ε_p is the percolation threshold and D_{A-B} is the mixture diffusion coefficient and depends on the characteristics of the two species.
More details in the appendix.

Since the concentrations depends on what happens locally, they introduce also new variable dependences: the local anode pressure Pa, the cathode local pressure Pc, the local anode temperature Ta, the local cathode temperature Tc, the hydrogen production $\dot{n_{H_2}}$ and the oxygen production $\dot{n_{O_2}}$.

In Figure 23, Amores points out the effect of the sum of all overpotential contributions on the voltage growth, needed as input to power the electrolyzer [40]. A steeper curve indicates greater losses. Higher the losses, higher the required voltage to achieve the same current density output. For the reasons mentioned above, the green curve shows less losses compared to the red one.

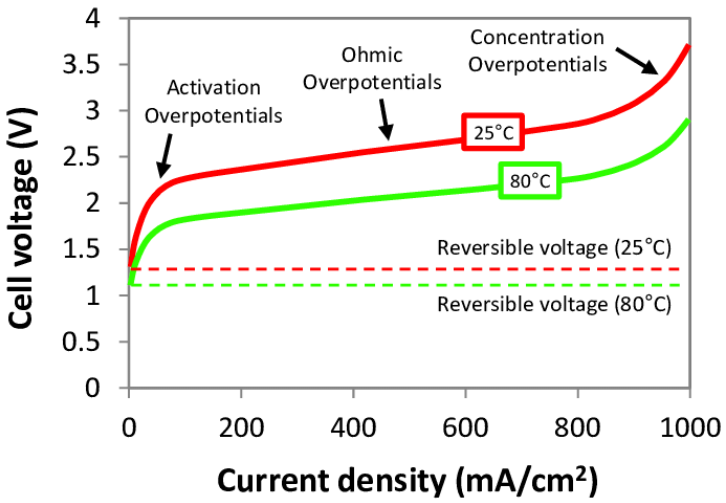

Figure 23 - Polarization curve: effect of overvoltages [40].

Furthermore, Rozzi states that the hydrogen production is proportional to the current density. It is defined by the Faraday law and expressed as follow [33]:

$$\dot{n}_{H2} = \frac{i * A * N_{cell}}{z * F} \qquad \textit{Eq. 10}$$

Being $\dot{n}_{H2}$ the hydrogen molar flow [mol/s], *i* the current density [A/cm2], N_{cell} the number of cells in the stack, A is the cell surface [cm2].

However, in actual electrolysis cells, the hydrogen production is lower than the theoretical value due to parasitic current losses in the gas pipelines and the cross-permeation of gaseous products. As a result, the actual production rate is determined by multiplying the theoretical rate by the Faraday efficiency. This is explained by Lamy [41].

A last analysis cares about the efficiency of the electrolyzer (η). There are different formulas which express this concept. From a theoretical perspective, the equation is, from Lamy [41]:

$$\eta = \frac{energy\ requirements\ under\ reversible\ condition}{energy\ requirements\ under\ irreversible} = \frac{W_{rev}}{W_{irrev}} \qquad \textit{Eq. 11}$$

Defined as the ratio of the minimum amount of energy W_{rev} (in J mol-1) required to split one mole of water under equilibrium (reversible) conditions to the real amount of energy W_{irrev} (in J mol-1) required to split that mole of water under constant (T, p) operating conditions.

From a more practical perspective instead, the equation could be, again from Lamy [41]:

$$\eta = \frac{energy\ content\ of\ the\ products}{total\ energy\ requirements} = \frac{W_{rev}}{W_{irrev}} \qquad \textit{Eq. 12}$$

This is a better approach since an electrolyzer is a physical device which receives some energy as input and transform it as chemical energy of the output products. So in a real test bench, this formula is preferable. In turn, the energy content of the products can be expressed as the product between the molar flow rate of the products and their corresponding lower heating value (LHV) or higher heating value (HHV). They both are measures of the energy content which is captured inside the products.

Another possibility to assess the performance of the electrolyzer is by using an even more practical parameter named specific consumption, which is no other than its reciprocal. Practically, it is the energy consumed to produce a certain amount of products.

2.4.2. Thermochemical modelling of electrolyzers

The majority of literature models does not have a self-evolution thermal management. Indeed, usually the electrochemical part is mainly analysed and the temperature is kept fixed for each sampled working condition. Models like this is, for instance, the one designed by Moradi Nafchi [42].

On the other hand, there are authors that use the CFD (Computational Fluid Dynamics) to understand the temperature trends. Most of them use a temperature gradient to know the temperature distribution across the cell structure, see Toghyani [43]. Others, moreover, consider the electrolyzer as a black box and thermal fluxes exit or enter the box. In these kind of models, the temperature of the electrolysis stack is determined using a quasi-steady-state thermal model, treating the device as a zero-dimensional system with lumped thermal capacitance. The heat balance is established by considering a constant rate of heat generation and heat transfer over a specified time interval. Thermal design like this are already present in literature, both Grondin[32] and Sood[35] use this kind of structure. However both of them do not consider the hot or cold effect related to the entering reactants and exiting products, unlike Rozzi does [33]. The Rozzi equation is the following:

$$C_{th}\frac{dT}{dt} = \Phi_{cell} - \Phi_{loss} - \Phi_{cool} - \sum_i h_i \dot{N}_i \qquad \textit{Eq. 13}$$

C_{th} is the overall thermal capacity of the stack [J/K]. It can be estimated experimentally or calculated as the sum of each component's thermal capacity, $\frac{dT}{dt}$ is the thermal coefficient which defines how the temperature evolves in time, Φ_{cell} is the heat generated in the stack, Φ_{loss} is the overall convective-radiative heat dissipated with the stack surrounding. The modelling of this loss should be specific according to each component of the electrolyzer. However, Rozzi provides a simplification of it. An overall average loss is considered with the classic equation [33]:

$$\Phi_{loss} = \frac{1}{R_{th}}(T - T_{amb}) \qquad \textit{Eq. 14}$$

- Where R_{th} is the thermal resistance of the stack [K/W] which can be described by means of the external surface of the stack (A) and the overall convective-radiative heat-transfer coefficient (h): R_{th}= 1/($h \cdot A$), T_{amb} is the ambient temperature.

- $\sum_i h_i \dot{N}_i$ is the net sum of the reactants and products fluxes. In particular, the sum of the heat removed by the deionized water, which enters the device, and that removed by hydrogen and oxygen leaving the stack. h is the heat-transfer coefficient [J/mol] and N the molar flow rate [mol/s].

Moreover, Qi model states that an electrochemical cell exchanges electrical and thermal power with the environment [44]: the thermal behaviour of the cell, the heat ϕ_{cell} is governed by two contributions: thermodynamics, the heat generated due to the electrochemical reaction ϕ_{react}; transport processes, the heat generation related to the irreversibilities of the transition process ϕ_{irr}. They are linked through the following equation:

$$\Phi_{cell} = \Phi_{react} - \Phi_{irr} \qquad \textit{Eq. 15}$$

By substituting values of both terms:

$$\Phi_{\text{cell}} = \left(\frac{\Delta\bar{h}}{zF} - V_c\right) I \qquad \textit{Eq. 16}$$

z and F have already been described, I is the current flowing across the cell, $\Delta\bar{h}$ is the enthalpy variation of the reaction. It comes from the heat generated by the reaction itself, V_c is the real cell voltage. It comes from the irreversibility term, indeed it is higher than the reversible voltage.

According to Mori, the first term inside the brackets $\frac{\Delta\bar{h}}{zF}$ is named thermoneutral voltage (U_{TN}). It defines the thermal operability of the cell, namely whether the thermal energy is absorbed by the cell or is dissipated towards the ambient (see Figure 24). If the cell voltage is equal to U_{TN} the cell neither absorb or dissipate heat, it is in thermal equilibrium, so thermally neutral. U_{TN} is 1.482V in standard condition [5].

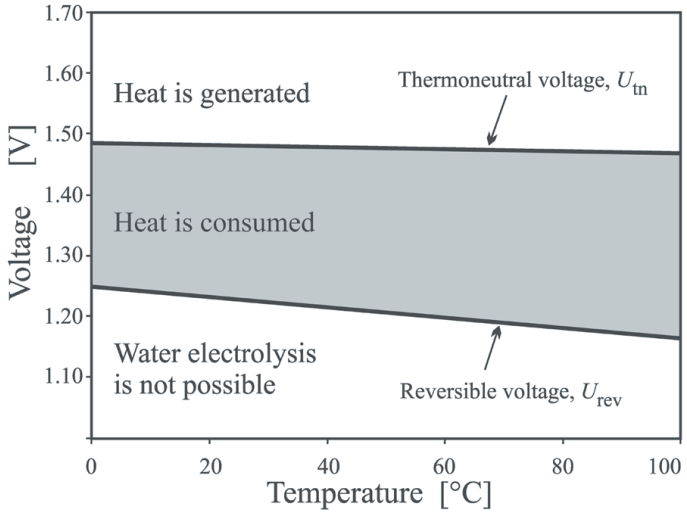

Figure 24 - Reversible and thermo-neutral voltage for water electrolysis as a function of temperature at a pressure of 1 bar [5].

There are three possible thermal working condition. With regard to Figure 24, the upper zone is the exothermicity one which is below limited by the thermoneutral voltage U_{TN}. The next area is the endothermicity one which is limited above by the thermoneutral voltage and below by the reversible voltage. As already stated, the latter represents the minimum voltage required to make the reaction happen, that is why the third zone, delimited by the reversible voltage, is the one where the electrolysis cannot happen. Temperature influences the limit values between the zones.

2.4.3. Degradation mathematical formulation

The electrolyzer degradation is universally addressed to the voltage degradation in terms of nominal voltage increase. This because the cell or short stack voltage under reference operating conditions generally increases over time, the degradation rate, indicated by the voltage rate, is positive. This parameter is composed of reversible and irreversible contributions.

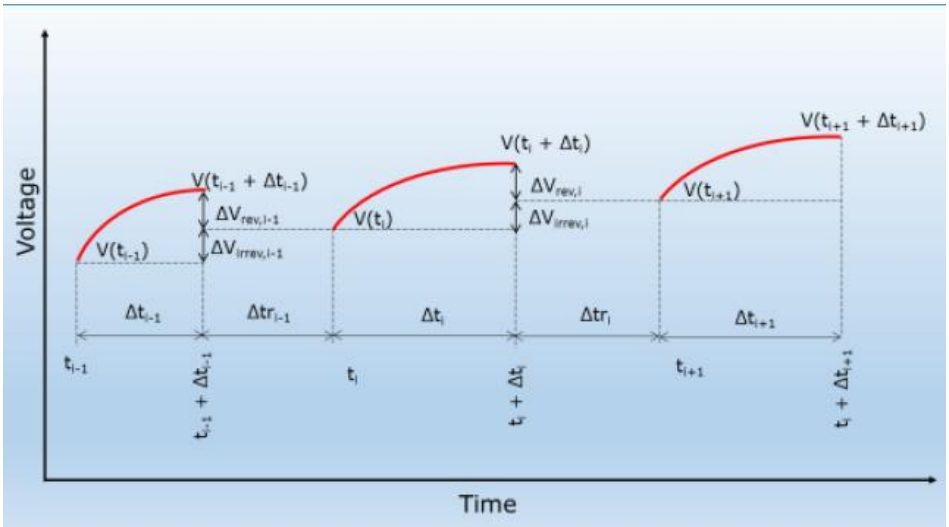

Figure 25 - Graphical representation of the reversible and irreversible increase in degradation rate [32].

A cycle is the period of time that lies between the turning on and the turning off of the electrolyzer.
The reversible degradation represents a portion of the continuous voltage increment that occurs during each cycle of the simulation. It affects the operation of the stack just temporary until the end of the cycle. When restarting a new simulation, the nominal voltage drops back to the initial value. Eq. 17 represents the single reversible voltage increase while equation Eq. 18 represents the total reversible increase of all the performed cycles.

$$\Delta U_{\mathrm{rev},i} = U(t_i + \Delta t_i) - U(t_{i+1}) \qquad \textit{Eq. 17}$$

$$\Delta U_{\mathrm{rev},1-N} = \sum_{i=1}^{N} \Delta U_{\mathrm{rev},i} \qquad \textit{Eq. 18}$$

Those values can be easily identified in Figure 25.
The total reversible degradation rate represents the reversible time degradation, defined by equation Eq. 19:

$$\dot{U}_{\mathrm{rev},1-N} = \frac{\Delta U_{\mathrm{rev},1-N}}{\sum_{i=1}^{N} \Delta t_i} \qquad \textit{Eq. 19}$$

Δt_i is the duration time of each single cycle.
The irreversible degradation, instead, represents that portion of voltage increments that does not nullify at the end of the simulation. Indeed, when restarting a new cycle the initial operating

voltage is not the same as the one of the first simulation. It is always increased by a factor which represents none other than the irreversibility of the process. The equation of the single cycle degradation is:

$$\Delta U_{\text{irrev},i} = U(t_{i+1}) - U(t_i) \qquad \textit{Eq. 20}$$

In the same way the irreversible degradation rate is the following:

$$\dot{U}_{\text{irrev},1-N} = \frac{\Delta U_{\text{irrev},1-N}}{\sum_{i=1}^{N} \Delta t_i} \qquad \textit{Eq. 21}$$

In Figure 25 the graphical explanation.
In the light of above, the total degradation rate of an electrolyzer is the sum of both contributions:

$$\dot{U} = \dot{U_{\text{rev}}} + \dot{U_{\text{irrev}}} \qquad \textit{Eq. 22}$$

As expected, the voltage degradation according to dynamic conditions is generally higher than steady state conditions one (Figure 26).

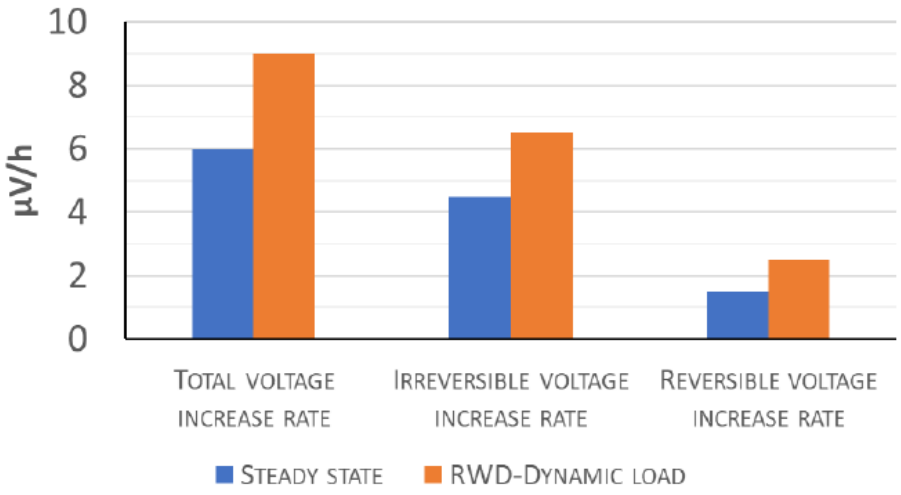

Figure 26 - Bar chart illustrating degradation indicators for PEMWE under steady-state conditions and with a single load profile [32].

3. Experimental Setup and Methodology

3.1. Objectives

The experimental activity carried out concerns an electrolyzer test bench based on AEM technology, located in the laboratory of 'Officine Edison Torino'.

The objective of the experimental activity was to analyze the working principle of the electrolyzer, its characteristic curves, its durability (and its degradation). Moreover, the EC test rig is examined and improved with new devices useful to reach a complete observation of the electrolyzer response. Notably, a RES generator.

3.2. Description of the AEM electrolyzer

The Edison owned AEM electrolyser comprises an electrolytic stack, a power supply generator, a hydrogen pressure regulation system, a water and electrolyte recirculation management system, and a cooling mechanism. The electrolyser was provided by "HYTER" , an Italian company founded in 2011 that nowadays stands out as one of the leading electrolyser manufacturers in Italy. The device was ordered in June 2019 but due to the covid was commissioned from March 2021. It aimed to be tested for research purposes. The held activity, instead, dates back from October 2024 to February 2025, the time shift is relevant. It is expected a pre-existent degradation on the electrolyser when performing the test. It will be analysed later.

"The AEMWE electrolyser cell, the heart of Hyter's AEMWE electrolysers, utilises a patented polymeric anion exchange membrane that operates in an alkaline environment with a 3-5% alkaline potassium hydroxide (KOH) solution. This configuration reduces the aggressiveness of the solution and promotes efficient transport of the OH- ion from the cathode to the anode of the cell, through the polymer membrane" taken from the Hyter official website [45]. Currently, the company produces AEMEC with a size that ranges from 10 kW to 120 kW of the machine and a nominal hydrogen production of up to 24 Nm3/h (referred to nominal conditions at the beginning of life and an external temperature of 20°C) [45]. However, as previously stated, the analysed device is an old one, with a rated power of around 2.5 kW power and a maximum hydrogen production of about 500 Nl/h.

Each single component is analyzed in the next sections.

3.2.1. Electrolytic stack

The electrolytic stack serves as the core component of the electrolyzer. It consists of 54 cells, organized into two stacks connected electrically in parallel, with each stack comprising 27 cells arranged in series. Each cell has the geometry of a cylinder whose surface area is 50 cm^2 .
As already stated, each cell is composed of:

- A cathode, where the reduction reaction takes place, producing hydrogen gas.
- An anode, where the oxidation reaction occurs, releasing oxygen gas.
- A solid membrane, which allows the passage of water and hydroxyl ions while being impermeable to hydrogen and oxygen gases.

Cathodic Electrode:
The cathode is made of platinum-cerium oxide, a material that ensures high electronic conductivity and catalytic activity to facilitate the reduction reaction. The cathode's porous structure allows the passage of hydrogen gas produced during the reaction.

Anodic Electrode:
The anode is constructed from a Ni-Fe alloy, chosen for its excellent electronic conductivity and catalytic effectiveness in oxidation reactions. Its porous design enables water molecules to move toward the membrane and oxygen molecules to escape as they are formed.

Anion Exchange Membrane:
The anion exchange membrane plays a critical role by permitting the transport of hydroxyl ions and water while blocking hydrogen and oxygen gases. Additionally, it acts as an electronic insulator to prevent short circuits within the cell.

Electrolytic Solution:
The electrolyte is a solution consisting of water and about 3 wt% potassium hydroxide (KOH), which facilitates the ionic transport necessary for the electrolysis process.

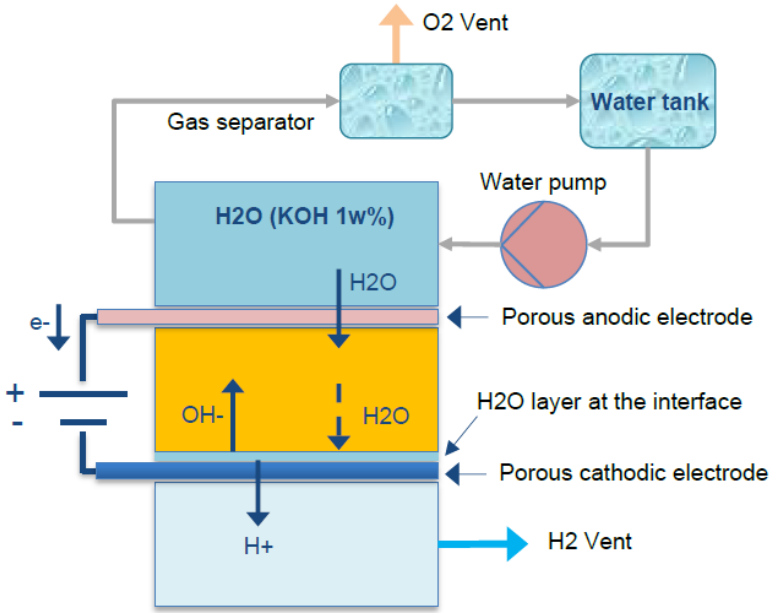

Figure 27 - Scheme of the electrolytic cell.

The electrolytic solution circulates within the anode compartment. Some of the water passes through the membrane and reaches the cathodic surface, while another portion exits the cell along with the oxygen produced during the reaction.
The solid membrane facilitates the diffusion of hydroxyl ions from the cathode to the anode and enables water to migrate in the opposite direction.
Notably, in the cathodic compartment, there is no fluid recirculation. Instead, it becomes fully saturated with hydrogen gas until a maximum pressure of 20 bar is achieved.

In Table 5, an overview of the technical specifications of the studied electrolyzer.

Table 5 - Principal technical parameter of the case study electrolyzer.

Description	Value	Unit
Maximum working temperature	Up to 45	°C
Recommended working temperature	40	°C
H2 pressure	1-20	absolute bar
Production rate	0 – 0.5	Nm3/h
Electrolyzer generator power	0 – 2.6	kW
Current density	400	mA/cm2
Stack specific energy consumption at BOL	3.9	kWh/Nm3

3.2.2. Auxiliaries

The electrolytic cell cannot work without a proper auxiliar design system. The original test rig has the following auxiliar devices.

***Power supply generator**:*
the electric energy required for hydrogen production is supplied by the grid. The stack is equipped with a DC current generator. Based on the desired hydrogen production rate, the necessary current is calculated by the electrolyzer's management software using Faraday's law (This current is then delivered to the stack to enable operation.

***Hydrogen pressure regulation**:*
the tested electrolyzer operates with an unbalanced pressure system. While the anodic compartment is always kept at atmospheric pressure, the pressure on the cathodic side can be increased up to 20 bar using a back-pressure valve.
The back-pressure regulator is designed to maintain a specified pressure upstream. When the gas pressure at the valve inlet exceeds the set point, the valve opens to release the excess pressure [46]. The valve remains closed until the pressure reaches the defined set point. Once the pressure exceeds this value, the valve opens, allowing hydrogen gas to flow out. If the pressure drops too low, the valve closes again. Consequently, the hydrogen exits the cathodic compartment intermittently rather than in a continuous flow.

***Electrolytic solution recirculation management**:*
Figure 28 illustrates the process of managing the recirculation of the water and KOH solution required by the stack. When the water level in the H2O tank falls below a specific threshold, fresh water is supplied from the grid. Before entering the tank, the water passes through a series of filters designed to remove minerals, ions, and impurities. This process is included in the block named “Water treatment”.
After filtration, the water reaches a KOH tank. Once mixed, the electrolytic solution, 4 wt%, is pumped to the anodic compartment of the stack.
The liquid solution, along with the oxygen gas produced during electrolysis, exits the stack and enters a gas separator. In this separator, oxygen is vented into the atmosphere, while the remaining water passes through a cooling system and then returns to the tank. Additionally, a suction system operates every 10 minutes to remove moisture from the hydrogen line, ensuring high hydrogen purity. The extracted water is returned to the H2O + KOH tank for recirculation.

***Cooling system**:*
the electrolysis process generates heat, causing the water exiting the stack to be warmer than the water entering it. Although higher operating temperatures can enhance hydrogen production, an excessively high temperature must be avoided to preserve the integrity of the cell materials and increase the durability. According to Table 5, the optimal operating

temperature is around 40°C, with a maximum limit of 45°C set by the manufacturer.
For these reasons, a cooling system is essential. The electrolyzer includes a basic cooling system that maintains the temperature within a range, rather than at a constant value set by the manufacturer or user. The system consists of a heat exchanger and a thermometer both inside the device named "Cooler" in Figure 28. It activates only when the water temperature exceeds 41°C and remains operational until the temperature drops below 36°C.
It is worth noting that at lower water temperatures, the absence of a temperature control system capable of increasing the temperature to optimal levels results in suboptimal electrolyzer performance. This vacancy in the system design makes the system not perfect for intermittent operation, indeed when working from 0 to rated condition the electrolyser cell takes time to be heated [47].

In Figure 28, a scheme of the linkages between cell and auxiliar devices.

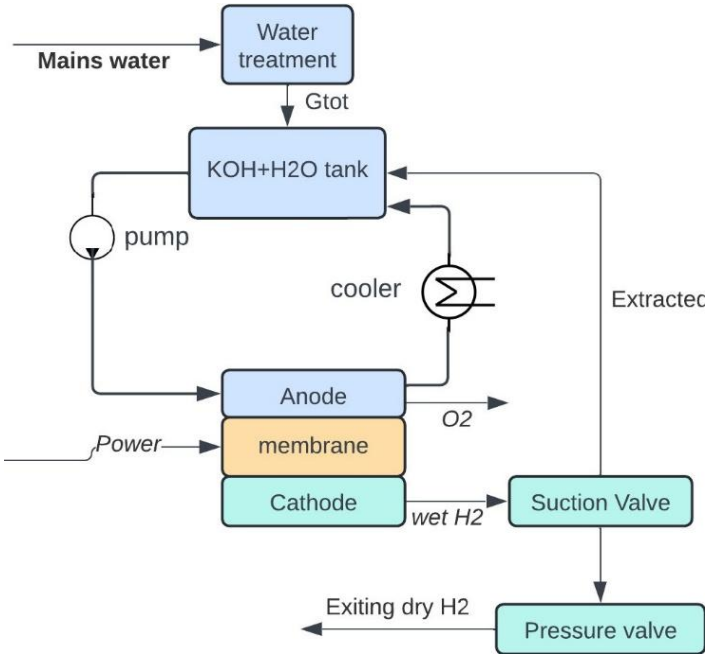

Figure 28 - Auxiliaries illustration and how they are linked to the cell.

3.3. Description of the test bench system

To test the case study electrolyser under real intermittent conditions a new system has been designed. The layout of the components is shown in Figure 29.

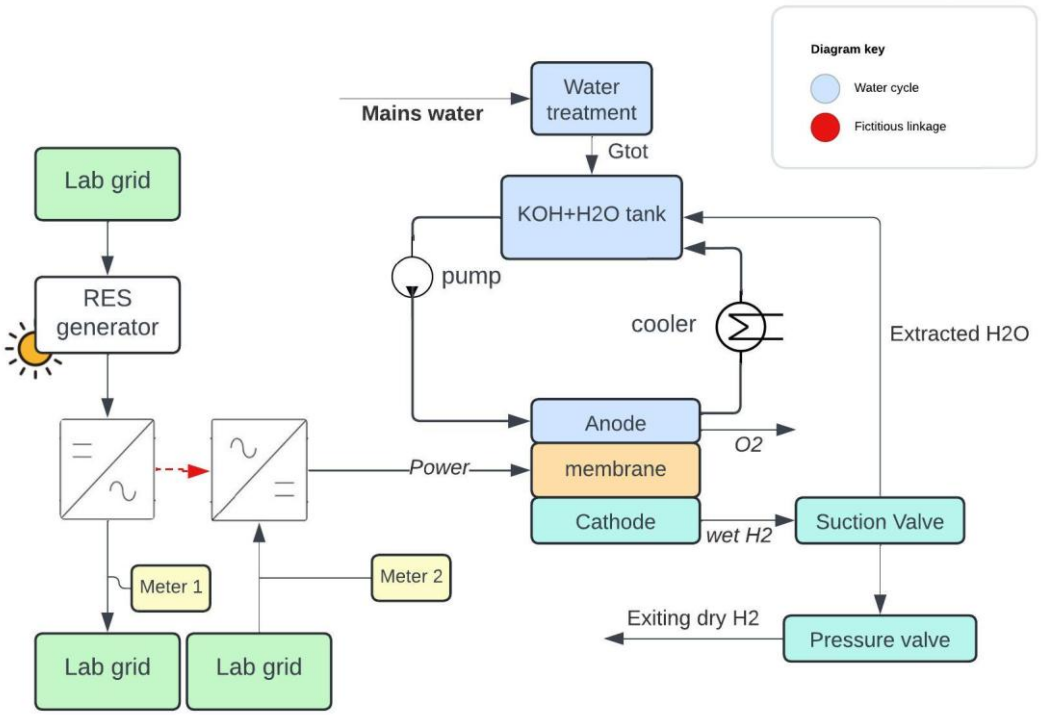

Figure 29 - Layout of the analysed test bench system.

The system has been designed to simulate the input energy coming from a RES, namely a PV energy system. Therefore a new device has been added to the bench layout. It is a controllable power generator (RES generator in Figure 29) which is powered by the AC lab grid and provides DC power just like a PV source.

Now, although the EC (electrolyzer) work with DC current, energy from RES generator cannot be directly exploited since it must be modified and transformed under the EC optimal conditions. Plus, the electrolzyer includes in the inside of their cabinet an integrated inverter that converts energy normally from AC to DC (from the grid to the EC). Therefore, a first inverter is needed and should be placed between the RES and the second inverter so that it can transform the energy from DC to AC.

This supplementation has been added later, so the connection between the new inverter and the integrated one was not directly possible due to technical reason. An undirect connection so has been installed: the laboratory (lab grid) powers the RES generator that simulates the use of a PV, the energy flow enters the first inverter which injects that energy inside the lab grid again. This flow is measured by a smart meter and produced again from the lab grid to the second inverter (integrated AEMEC inverter) thanks to a second meter that is placed at the inlet energy flow of the electrolyser cabinet. Doing so, the energy flow was correctly designed and the electrolyser was ready to be tested.

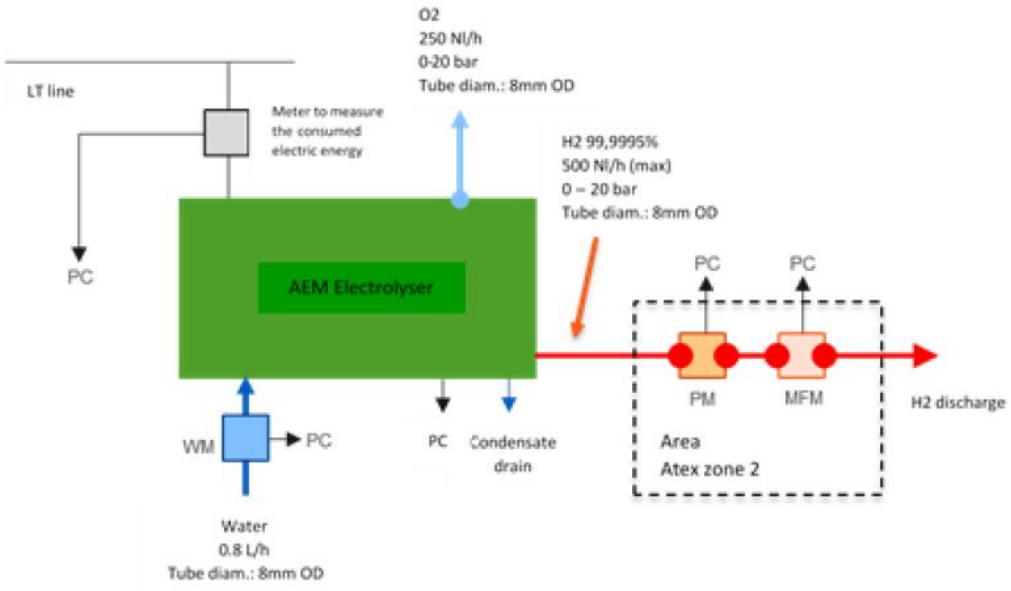

Figure 30 - Sensor, data acquisition and processing layout system.

The test station was designed to monitor and correlate various operational variables, ensuring accurate data acquisition. These variables include:

- Current [A] and voltage [V] supplied to the stack: these are recorded using a programmable logic controller (PLC).
- Electric energy consumption [kWh]: measured using both the energy meters. In Figure 30 it is simply represented the one that provides the energy to the cabinet.
- Water consumption flow rate [g/h]: determined by a water flow meter (indicated as WM in Figure 30).
- Hydrogen outlet pressure [bar]: measured at the cathodic side through a pressure meter integrated into the back pressure valve.
- Water temperature [°C]: monitored via a thermometer placed upstream the heat exchanger.
- Hydrogen flow rate [Nl/h]: measured using a flow meter. The produced hydrogen is conveyed through a small-diameter pipe into a protective box, where the mass flow meter (MFM) is located (see Figure 30).

Additionally, a controller software developed by Edison simplifies both test management and data acquisition. This software enables several adjustable parameters, some to test the electrolyzer powered by the grid and some when powered by the RES generator. They are:

1) Grid energy supply: the hydrogen volumetric flow rate and the hydrogen outlet pressure. The hydrogen flow rate can be set between 1 and 500 L/h, while the outlet pressure can

be adjusted from 1 to 20 bar. Once these parameters are configured, the current required to achieve the desired hydrogen production is supplied to the stack, and the back pressure valve is automatically regulated.

2) RES energy supply: the previous two parameter plus a power profile set at the input of the RES generator. The profile consists of different power steps, representing the energy that powers the electrolyzer in real time, and the time duration of each of them. It has the aim to understand the partial and intermittent behaviour of the electrolyzer. Notably, the AEMEC can be tested to understand how it performs in front of a rapid input energy variation or in front of a non-predicted partial input energy condition.

The software provides real-time access to the measurements gathered by the aforementioned sensors, ensuring seamless integration and efficient operation.
Finally, the test sampling time is 10 seconds. It cannot be more precise than that because of system limitations. Furthermore, less sampling time requires a higher computational power and this would be a problem when studying the operability of the electrolyzer because of higher calculation time.
The sampling time is important when studying the intermittence of the energy source. Indeed, if the rate of change of the input energy source is in the order of seconds and the one of the instruments is higher, most of the variations would not be captured by the acquisition system. Making the measurements almost useless.

In the following picture the entire test bench is displayed, ranging from the instrumentations data collection to the sensors to the electroyser.

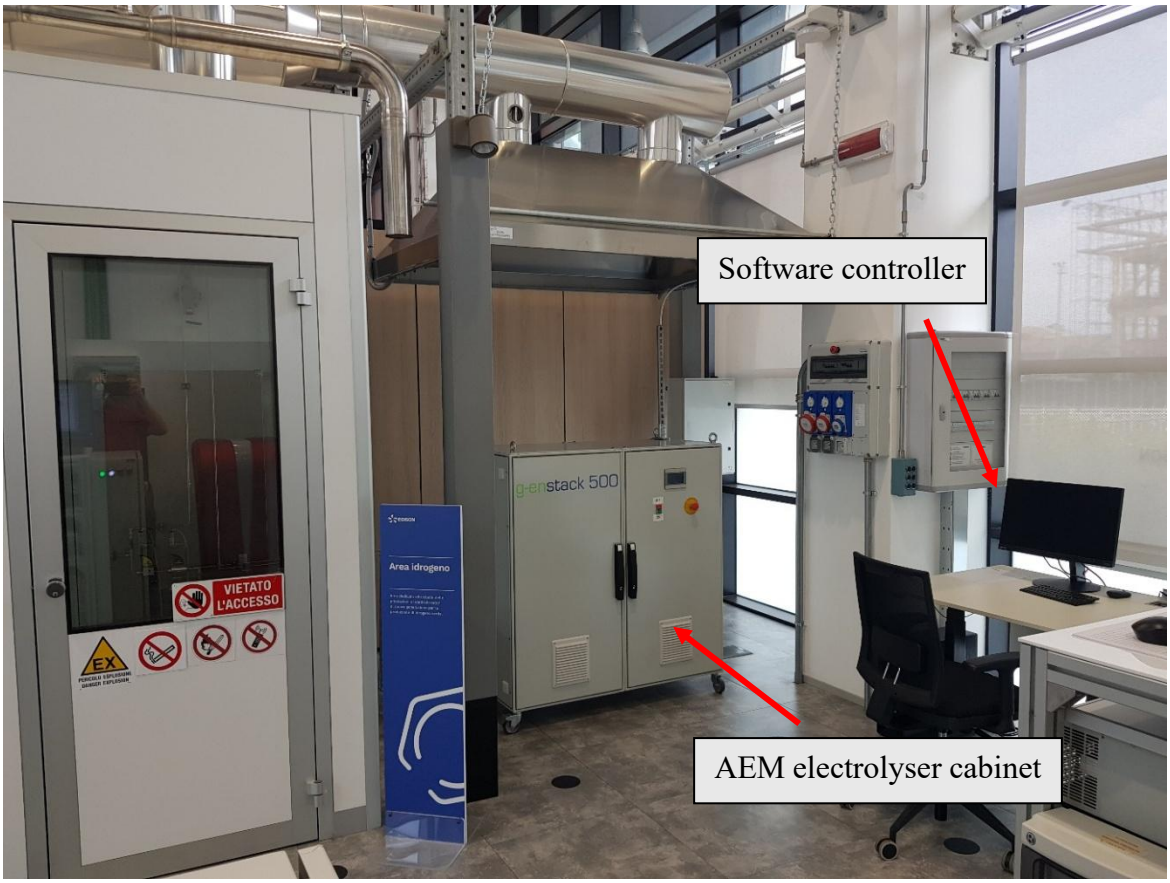

Figure 31 - Edison owned case study electrolyzer test bench.

3.4. Experimental evaluation of the polarization curve

When analysing an electrolyser the first step is always to compute the characteristic polarization curve. It is what it has been done first, over the AEMEC case study electrolyser. The device has already been studied. The previous activity were performed with the concern from the production point of view. It means that the characteristic curves regarding the electrochemistry of the EC, such as the polarization curve, were not calculated.
The calculation of the polarization curve is crucial to understand the general behaviour of the electrolyzer. Notably, to validate the model through a comparison with real data.

The followed procedure is the one provided by the JRC EU harmonization protocols [48]. The objective of the used testing protocol is to evaluate the performance of a low-temperature water electrolyzer cell or stack through a polarization curve under specified operating conditions. The procedure is designed to be general and applicable for testing low-temperature EC across various applications, whether for individual cells or stacks. For tests conducted at ambient pressure, performance is assessed by measuring from the lowest to the highest current density (ascending portion of the polarization curve), followed by measurements in reverse order, from the highest to the lowest current density (descending portion), in line with the manufacturer's

specifications and the test objectives. When operating, instead, under pressure, the performance assessment begins with measurements from the highest to the lowest current density (descending portion of the polarization curve), followed by a reverse measurement from the lowest to the highest current density (ascending portion).
The electrolyzer set-up allows to create these ascending or descending path by changing the input power, doable due to the power profile settings described in the previous section. Simultaneously, the H2 pressure and production settings are kept constant so as not to change the behaviour of the EC. In the process, voltage and current are measured and sampled together. The polarization curve is built by linking all the points in a Voltage-Current V-I diagram. In most of the cases, current is usually substituted with the current density, knowing the active area of the cell/stack, useful to make the plot independent from the electrolyzer size.

3.4.1. First attempt evaluation

The test bench layout modification, described in Section 3.3, leads to the possibility of changing the input power of the Hyter electrolyzer by power steps. A first attempt to evaluate the polarisation curve has been performed in November 2024.
The input power steps are listed in Table 6.

Table 6 - Complete list of the Power steps with the relative time duration. In green, ascending portion. In red, descending portion.

Time duration of each step (s)	Power of each time steps (W)	Time duration of each step (s)	Power of each time steps (W)
480	600	180	2500
180	0	180	2400
180	100	180	2300
180	200	180	2200
180	300	180	2100
180	400	180	2000
180	500	180	1900
180	600	180	1800
180	700	180	1700
180	800	180	1600
180	900	180	1500
180	1000	180	1400
180	1100	180	1300
180	1200	180	1200
180	1300	180	1100
180	1400	180	1000
180	1500	180	900

180	1600	180	800
180	1700	180	700
180	1800	180	600
180	1900	180	500
180	2000	180	400
180	2100	180	300
180	2200	180	200
180	2300	180	100
180	2400	180	0
180	2500		

Ascending and descending portion have almost the same number of steps. The former achieves one more with respect to the latter: a power step of 600W which lasts 480 seconds. This first step is necessary to initialize the EC: electrodes are stabilised in their correct oxidation state and the membrane is activated for OH^- ion transport [49]. The descending part does not need a preconditioning step since it comes exactly after the ascending one. The time duration of all the other steps is equal and it has been chosen purposely to allow the electrolyzer to measure stabilized values at each step. Indeed, previous tests show that the EC takes about 30 seconds to stabilize the values. The maximum set step power is equal to 2500W because it has been noticed that the power consumed in nominal condition (20bar, 500Nl/h) is around that value. The result have been collected and plotted in Figure 32.

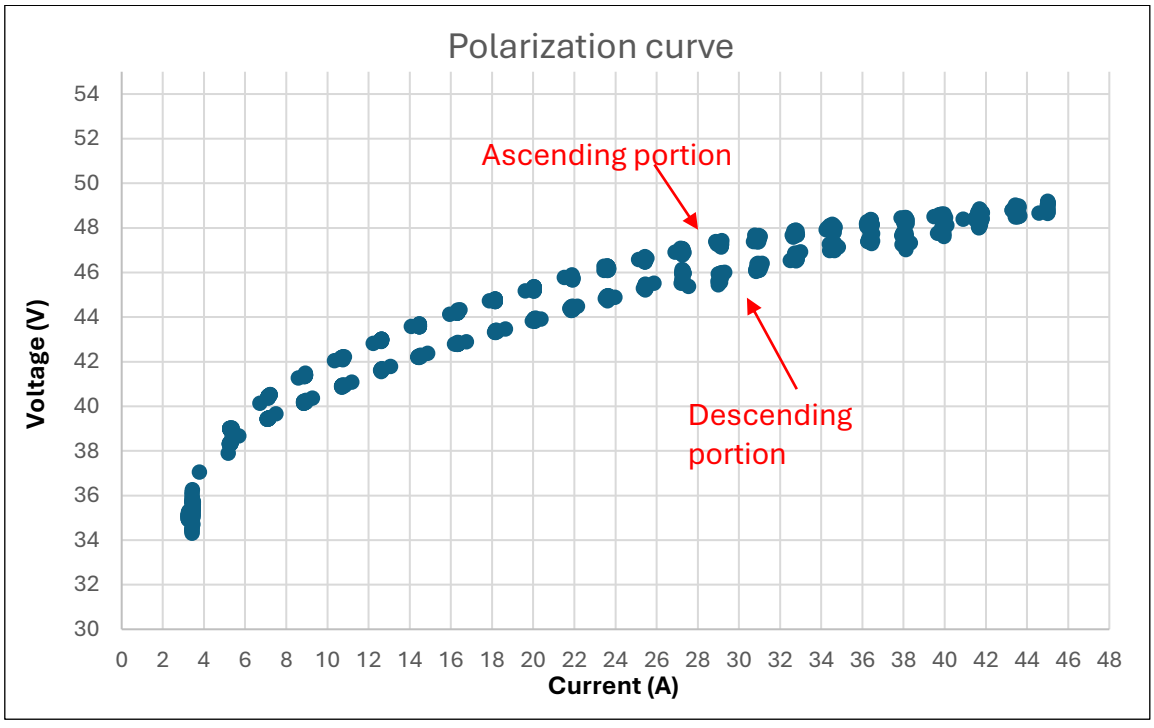

Figure 32 - Calculated first attempt polarization curve for both the portions.

The ascending and descending portion of curve are not coincident. This is due to the fact that when starting the simulation the stack is cold, progressively heats up. Since the descending portion comes just after the ascending one, without turning off the electrolyzer, it results that the stack has already been heated up. An higher temperature positively affects the operability of the stack, resulting in a lower voltage requirement at same current and same targeted production [50].

The temperature trend is displayed in Figure 33. The curve results discrete due to the fact that the power steps duration is about 180 seconds each. It is important to notice that at OCV the current should be around 0. Due to an error occurred during the data acquisition process, the activation overvoltage part results shifted towards right of 3A (cut in the curves comparison in Section 3.4.4).

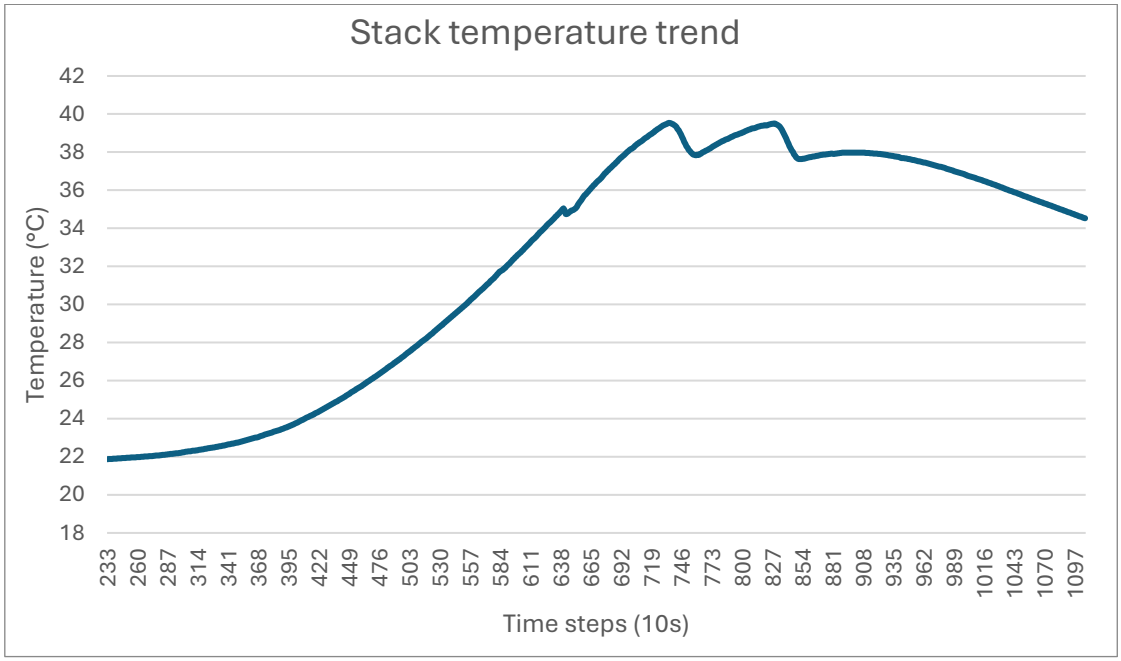

Figure 33 - Measured temperature trend while sampling the first attempt polarization curve.

The timesteps axis starts the counter from 233 and not from 0 due to the initial necessary preconditioning of the electrodes, namely the first power step sample is cut off [49], [51].

3.4.2. Second attempt evaluation

A second attempt to evaluate the polarisation curve has been performed on the 5th of February 2025. The input power steps are listed in Table 7.

Table 7 - Complete list of the Power steps with the relative time duration. In red, ascending portion. In green, descending portion.

Time duration of each step (s)	Power of each time steps (W)	Time duration of each step (s)	Power of each time steps (W)
3000	1200	360	50
360	1150	360	100
360	1100	360	150
360	1050	360	200
360	1000	360	250
360	950	360	300
360	900	360	350
360	850	360	400
360	800	360	450
360	750	360	500
360	700	360	550
360	650	360	600
360	600	360	650
360	550	360	700
360	500	360	750
360	450	360	800
360	400	360	850
360	350	360	900
360	300	360	950
360	250	360	1000
360	200	360	1050
360	150	360	1100
360	100	360	1150
360	50	360	1200
360	0		

As will be explained in the Section 5.1, the first attempt lead to the substitution of one of the two stacks composing the electrolyser. Indeed, one of them was damaged and compromised the first attempt evaluation. Due to thesis deadline the electrolyser was modified and set up to be tested with only one stack.. That is why, in Table 7, the maximum input power step is set to be around half the total electrolyser nominal one.

This time, aiming to keep the temperature constant, the descending part is performed first. Furthermore, according to JRC protocols, systems which produce pressurized hydrogen require sampling the descending part before the ascending one. The first step is the nominal power and it is kept for a long time so as to heat up the EC to a standard temperature (Figure 35). It is then

gradually decreased by 50 Watt each 360 seconds down to 0W. The ascending part comes immediately after, again up to 1200W.

Unfortunately, the testing set up was not definitive, it was just temporarily to allow the polarisation curve calculation of at least one stack. Indeed, theoretically the two stacks are perfectly coincident and the complete polarisation curve could have been calculated by just doubling the resulting current (the voltage is the same since parallel connection). The results are shown in Figure 34 and Figure 35.

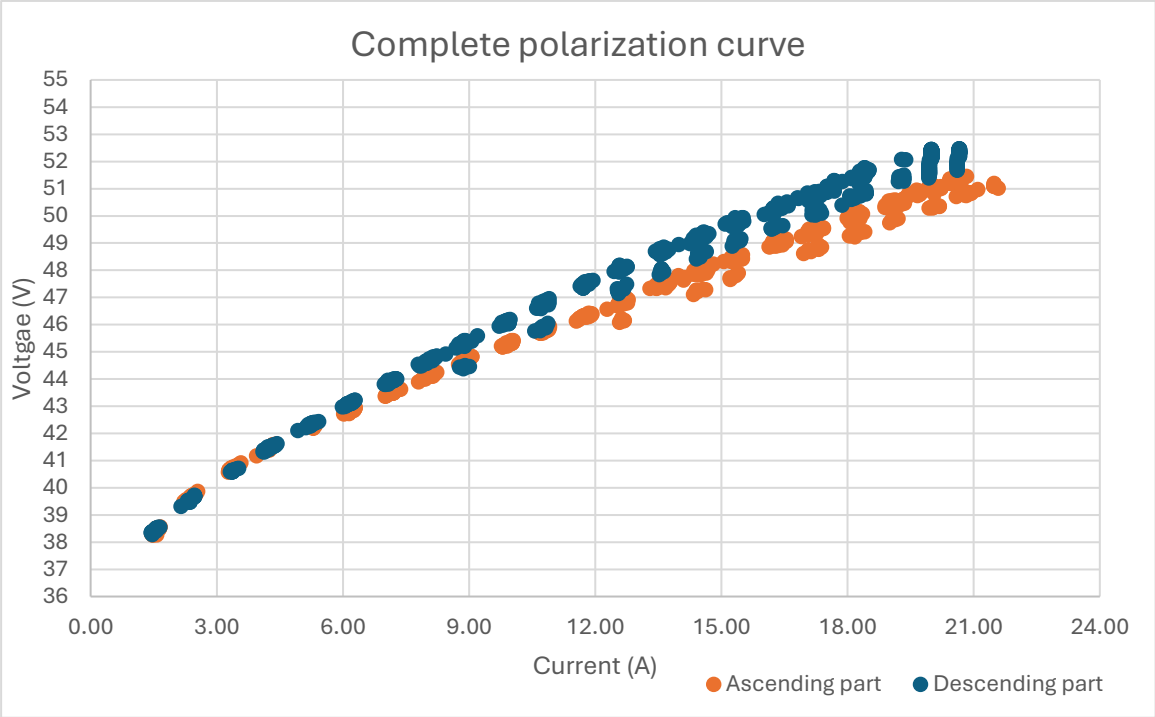

Figure 34 - Calculated second attempt polarization curve for both the portions.

As previously explained, the set up was temporarily, a test bench error occurred while switching from the descending to the ascending part of the power steps. This lead to a not complete sampling of the activation overvoltage part (see Figure 34 and the drop of Figure 35) of the blue curve.

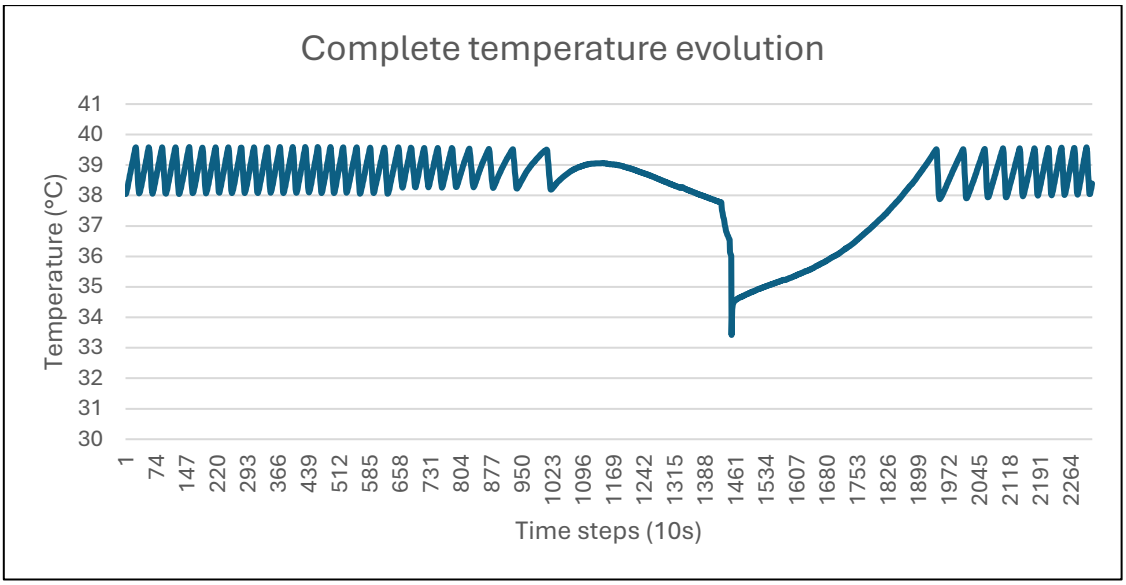

Figure 35 - Temperature trend measured while sampling the second attempt polarization curve.

3.4.3. Third attempt evaluation

A third attempt to evaluate the polarisation curve has been performed on the 6th of February 2025. The input power steps are again the ones in Table 7.

Only the descending part has been calculated for an error occurred during the simulation. The following picture shows the polarisation curve.

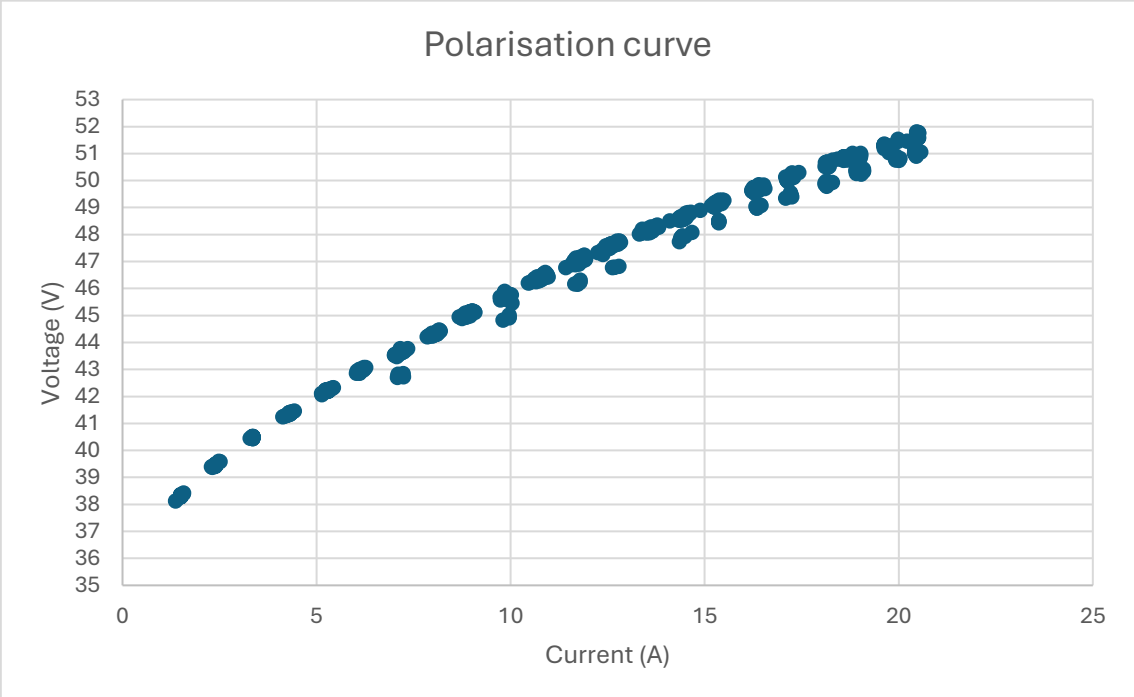

Figure 36 - Third attempt polarization curve for both the portions.

The curve appears to be correctly linear, the temperature is kept constant again thanks to the first step duration.

3.4.4. Curves comparison

In this section a comparison of all the calculated polarisation curves is provided, see the following Figure.

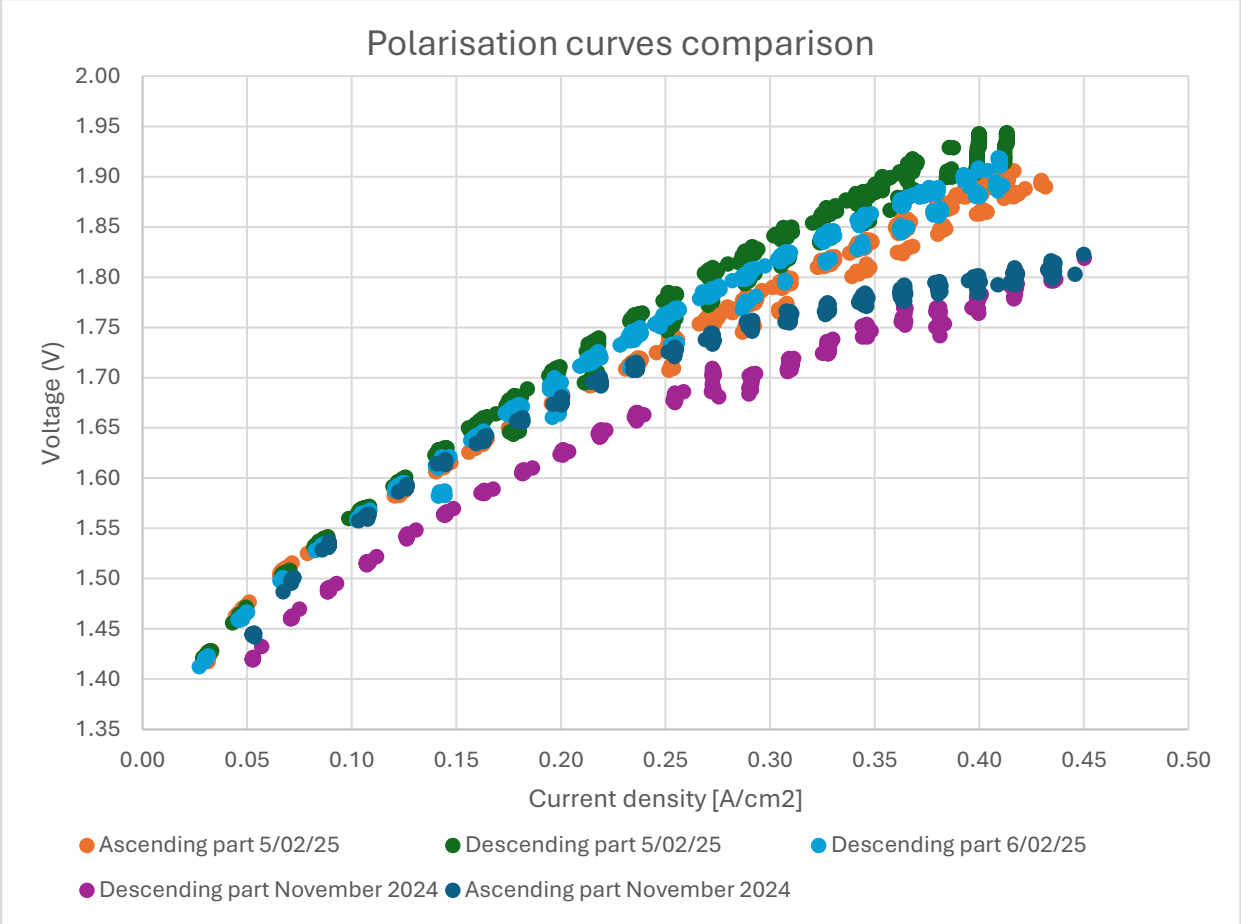

Figure 37 - Comparison of all the cell polarisation curves attempts

To compare all the polarisation curves the attempts held in February 2025 needed to be modified because of the unavailability of the second stack. Notably, the current has been doubled, the second hypothetic stack was considered exactly equal to the first.
Furthermore, the comparison has been provided under the form of the single cells and current density to make the polarisation curve comparable with the literature data.

Comparing all the polarisation curves the following statements can be appreciated:

- Ascending and descending polarisation curve trends of both 5th and 6th February are more linear with respect to November 2024 attempt. It is how the ohmic part should

behave properly. This enhancement is due to the ensured constant temperature condition kept for almost the whole tests duration.

- Ascending and descending polarisation curve trends of both 5th and 6th February show the highest voltage trend at constant current density. The data shift with respect to the November 2024 points out how one of the two polarisation curves is not correct. As explained in Section 3.4.2, the first attempt was regarded as wrong.

- November 2024 tests show a maximum current density higher than the February 2025 tests. This behaviour is due to an higher power reached related to the presence of both the stacks and due to the electrolyser experienced fault.

- All the activation overvoltages are not shown because of an initial sampling error occurred in the acquisition process. Indeed, all the attempts are affected by an initial current shift of about 0.3A/cm2. It has been cut.

To conclude, it has been appreciated that the correct polarisation curves to be used as benchmarks for the model future simulation are the February ones. In particular, as will be explained in Section 5.2, among them the 5 February descending part has been regarded as the best one. It will represent the reference point for the next simulations.

3.5. Experimental procedure for efficiency degradation

Over time, operational factors such as current density, temperature, and energy input, alongside material properties, contribute to the degradation of electrolyzer components, impacting efficiency and output. This chapter delves into the methodology employed to quantify and model the degradation of the experimental AEM electrolyzer.
This comprehensive approach provides a robust framework for analyzing future scenarios of hydrogen production, aligning with the thesis's goal of bridging experimental data with computational modelling. The following procedures has been extracted by the EU harmonised protocol [51].

As a first definition, the tests performed (in-situ tests) need to be compatible with the real operational environment that the materials are expected to experience during the stack operating life. The testing conditions encompass both static and dynamic scenarios, with dynamic conditions defined by a specific load-versus-time profile applied by the test hardware to a single cell or a short stack. To ensure comprehensiveness, testing should include normal and out-of-normal, or "stressor," operating conditions for the components of the cell or stack.

Consequently, in-situ testing conditions can be categorized into four dimensions: static, dynamic, normal, and stressor. The latter are meant to reduce the time required to monitor durability through performance degradation. They are load profiles modified to accelerate the degradation process. The latter is assumed to remain consistent with the actual service conditions, despite the faster rate of degradation. Therefore, validating this assumption and ensuring the transferability of results from accelerated tests to real-life scenarios demands extensive research and validation. An overview of all the possible tests is shown in Figure 38.

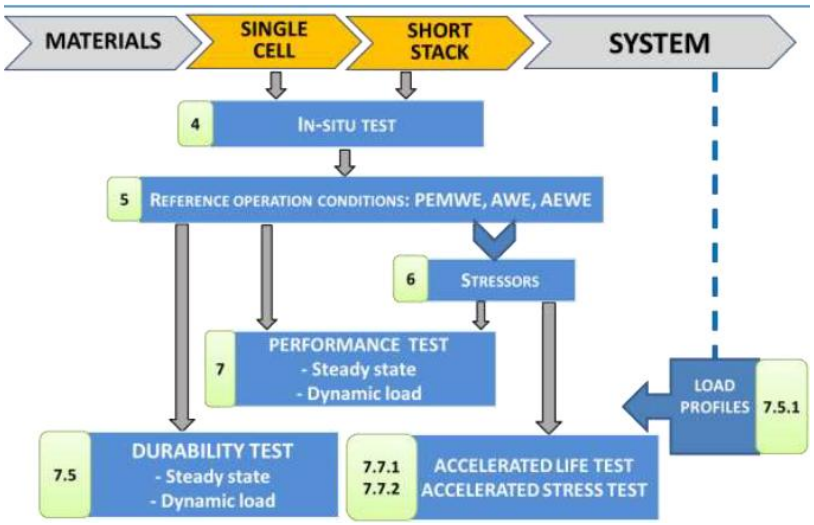

Figure 38 - Overview of all the EU harmonised in-situ tests [51].

The degradation threatens the nominal operation of the electrolyzer by reducing its efficiency and so its hydrogen production capability. This means a higher power to produce the nominal same amount of outputs or, alternatively, at same input power a reduced amount of outputs with respect to the nominal condition.
Durability refers to the ability of a single cell or a short stack to sustain its performance over time. Typically, the observed performance is evaluated in relation to the baseline established at the beginning of testing (BoT). The device's lifespan is quantified by its total operating hours, regardless of the operational mode. Addressing the electrolyzer degradation to the whole system level.
To evaluate durability a measurable parameter is required. This parameter is the degradation rate, which represents the rate at which performance declines over time from its initial value, based on a selected performance indicator. The most commonly used indicator in practice is the cell or short stack voltage increase, described in Section 2.4.3.

The rate of cell or stack voltage increase is determined experimentally by monitoring voltage changes across multiple test blocks, which include intermittent rest periods. To ensure a meaningful assessment of voltage increase, the loading profile applied in each test block must

remain consistent. Moreover, tests should only start after appropriate cell/stack activation and conditioning according to the manufacturer's instructions has been performed. This is valid both in dynamic and steady load.

To replicate real-world service operating conditions in controlled in-situ tests, it is necessary to convert the power input of an electrolyzer system into an equivalent electrical current density. A reference maximum current density j_{max} is needed to state when the test should end. Specifically, j_{max} corresponds to the current density at which the cell or stack reaches a particular voltage at BoT. During testing, degradation is assessed by observing voltage changes at this same current density. As performance degrades, the voltage at j_{max} increases, marking the End of Test (EoT) when it reaches a predefined higher value. This procedure is shown in Figure 39.

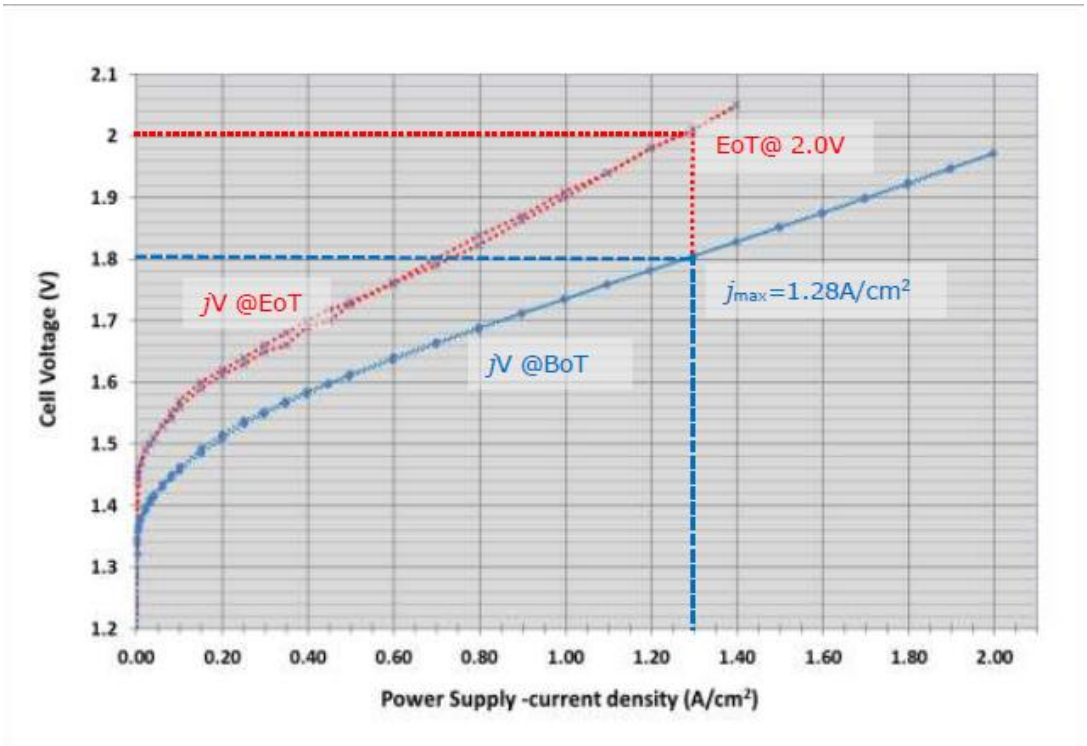

Figure 39 - Diagram showing the identification of j_{max} and the End of Test (EoT) criterion for PEMWE [51].

When performing both steady or dynamic state tests, it is important to distinguish between test input parameters (TIPs) and test output parameters (TOPs). The former are the parameters the EC can modify to be regulated, the latter are the output measured test parameters.

3.5.1. Steady state degradation test protocol

The EU agreed protocol meant to assess the steady state degradation rate and the durability is shown in Table 8.

Table 8 - Agreed Protocol for assessing steady state degradation rate for in-situ cell and short stack testing of PEMWE, ALK and AEMWE [51].

STEADY STATE DEGRADATION TEST PROTOCOL	
Step	Description
1	Initiate the process by activating and conditioning the cell or stack in accordance with the manufacturer's guidelines. If such specifications are unavailable, adopt standard laboratory procedures.
2	Define and set the test input conditions (TIPs)
3	Conduct a polarization curve at the beginning of test (BoT) and record the voltage of the cell or stack at the corresponding current density j.
4	Maintain continuous operation of the cell or stack under constant TIPs for a duration of 1,000 hours.
5	After the 1,000-hour period, perform another polarization curve and measure the voltage at the same current density j. This process should be repeated for subsequent test intervals if necessary.
6	Switch off the current supply and leave the setup under open circuit voltage(OCV) conditions for 60 minutes. During this time, ensure that the water recirculation flow rate and test temperature are maintained.
7	Reactivate the TIPs used in Step 1-2 and allow the cell or stack voltage to stabilize over 120 minutes. If the observed change in voltage over time ($\Delta U/\Delta t$) is zero or positive, proceed to the next step. If the change is negative, extend the stabilization period by an additional 60 minutes and repeat the process until a positive $\Delta U/\Delta t$ is achieved.
8	Perform another polarization curve and record the voltage of the cell or stack at the same current density j.
9	Repeat steps 3 to 7 until the test concludes, either after completing step 8 following 3,000 hours of continuous operation under steady-state conditions or upon reaching the end of test (EoT) criterion.

A graphical representation of the degradation protocol is shown in Figure 40.

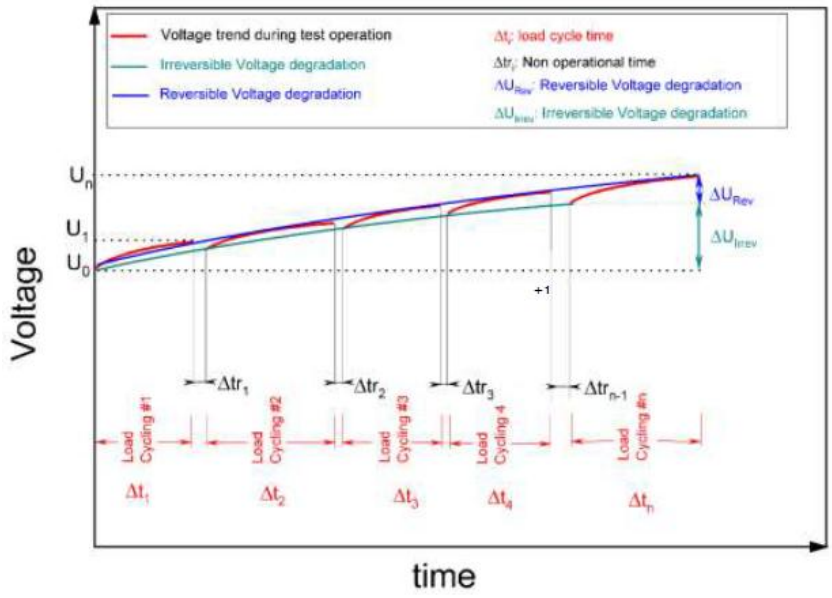

Figure 40 - Voltage increase broken down into reversible and irreversible contributions in different loading cycle [51].

3.5.2. Dynamic load degradation test protocol

The EU agreed protocol meant to assess the dynamic degradation rate and the durability is shown in Table 9.

Table 9 - Agreed protocol for assessing dynamic load degradation rate for in-situ cell and short stack testing of PEMWE, ALK and AEMWE[51].

DYNAMIC LOAD DEGRADATION TEST PROTOCOL	
Step	Description
1	Begin by activating and conditioning the cell or stack as per the manufacturer's specifications. If no specific guidance is provided, follow standard laboratory procedures.
2	Define and set the test input conditions (TIPs)
3	Conduct a polarization curve at the beginning of test (BoT) and record the voltage of the cell or stack at the corresponding current density j.
4	Operate the cell or stack using the selected load versus time profile for a number of cycles equivalent to 160 hours of operation. Round the number of cycles to the nearest integer.
5	Conduct another polarization curve and measure the of the cell or stack at the same current density (j) as before. Repeat for subsequent intervals if needed.
6	Switch off the current supply and leave the setup under open circuit voltage(OCV) conditions for 60 minutes. During this time, ensure that the water recirculation flow rate and test temperature are maintained.

7	Reactivate the TIPs used in Step 1-2 and allow the cell or stack voltage to stabilize over 120 minutes. If the observed change in voltage over time (ΔU/Δt) is zero or positive, proceed to the next step. If the change is negative, extend the stabilization period by an additional 60 minutes and repeat the process until a positive ΔU/Δt is achieved.
8	Perform another polarization curve and record the voltage of the cell or stack at the same current density j.
9	Repeat steps 4 to 8 for 10 loops, corresponding to a total duration of 1,600 hours. The test concludes either at this point or earlier if an end of test (EoT) criterion is met.

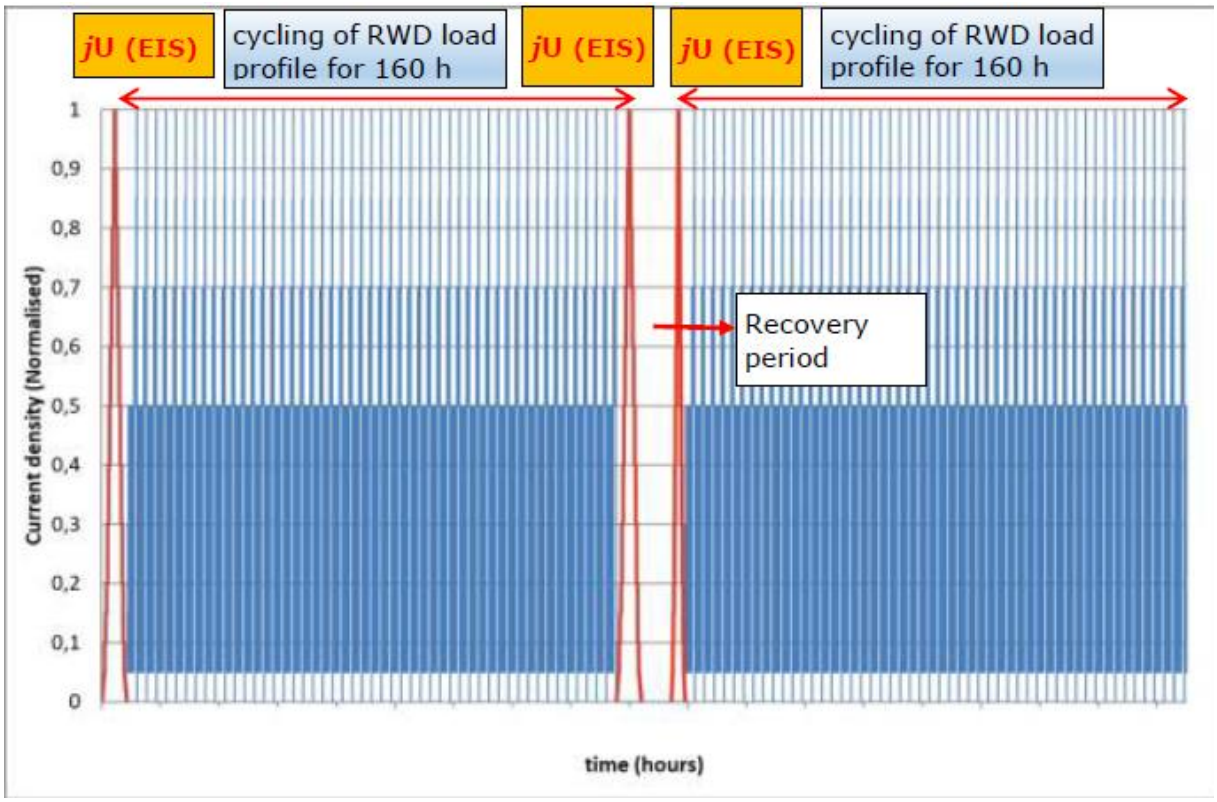

Figure 41 - Example of dynamic load degradation test protocol[51].

RWD stands for Real-World Degradation: load versus time profile based upon actual operating conditions experienced in different electrolysis systems applications.

Given that an electrolyzer system's lifespan can span several years, it is essential to evaluate degradation over a shorter timeframe when selecting new or improved materials or assessing durability. To achieve this, "accelerated testing" is employed. This approach involves subjecting materials and components to operating conditions beyond the typical operational range,

inducing similar degradation processes to those that would occur during normal use but at an accelerated pace, thereby reducing the testing duration.

The identification of specific stressor types and their corresponding settings to selectively induce degradation of particular materials under conditions that accurately represent actual service remains an unresolved research challenge. The lack of scientific agreement on load profiles and stressors capable of specifically targeting the degradation of materials within individual cell components necessitates adopting a distinct methodology for each kind of desired simulation. An example of suck kind of testing condition is the flexibility load profile, in Figure 42.

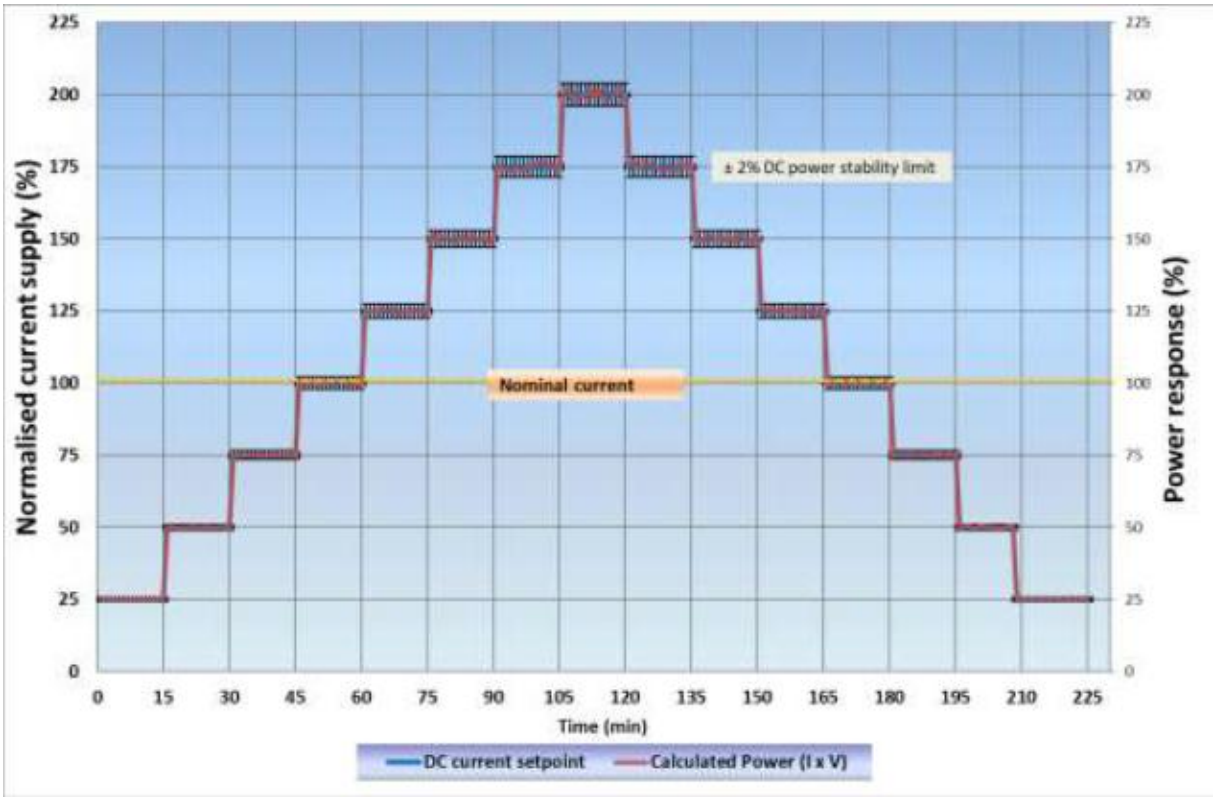

Figure 42 - Flexibility load profile test at 200 % of nominal current flexibility profile[51]

The testing condition reflects the idea of stressing the electrolyzer by powering it with 200% of the nominal current. This is done by progressively incrementing the current from 0, by current steps. Once reached the target, current is decreased by steps, down to 0. This cycle is repeated several times meanwhile power response is measured to check the degradation rate.

3.5.3. Attempt to evaluate degradation experimentally

Provided the basis for assessing the electrolyzer degradation, an attempt to evaluate the long run degradation of the case study electrolyser was held. It is defined as an attempt, because it has been calculated by analysing already taken data. There was no possibility to perform new analysis due to thesis deadlines. Reference has been made to the only long run analysis dated back to 2021, lasted around 900 hours of nominal steady state operation. The test is shown in Figure 43 (represented up to 700 hours).

Figure 43 - Steady state nominal condition long run analysis. Dated back to 2021. In blue the original data shift. In orange the average value trend.

The test has been devised to point out the reversible degradation of the case study electrolyser. However, an error occurred while sampling the data and brought the electrolyser to turn off. It will be turned on manually later on.

This event, which can be regarded as unlucky, actually gave the possibility to calculate a possible idea of the irreversible degradation. Indeed, having two long run cycles is what is needed to apply a possible test protocol to assess the voltage increase under each of its forms.

The two curves were separated and their initial and final voltage level recorded. Both are shown in Figure 44 and Figure 45.

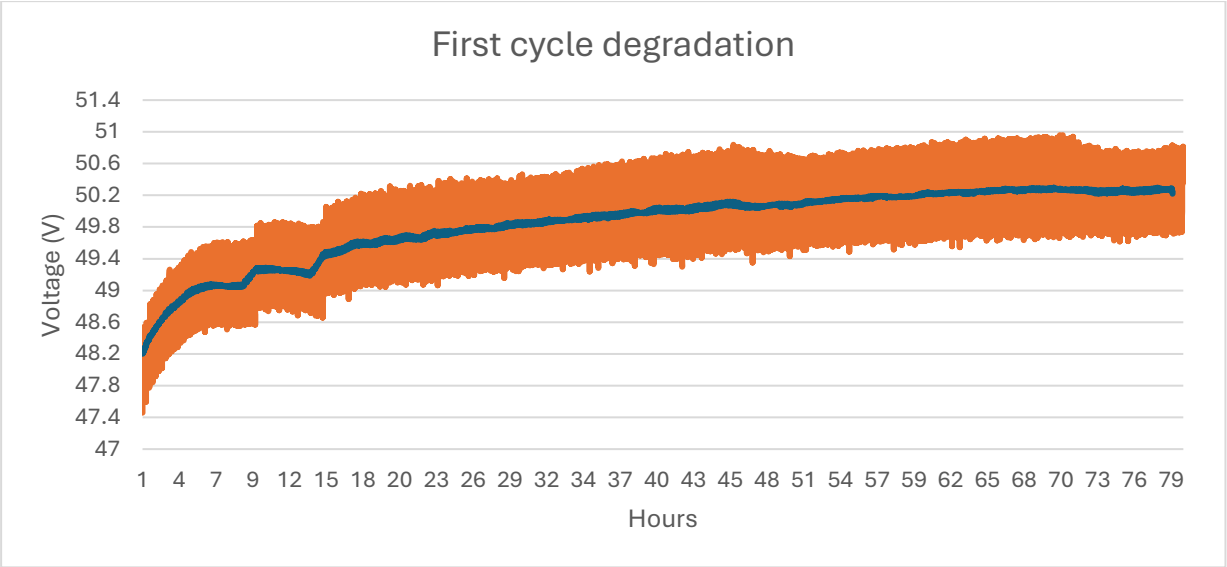

Figure 44 - First 80 hours of the long run analysis. In orange the original data shift. In blue the average value trend.

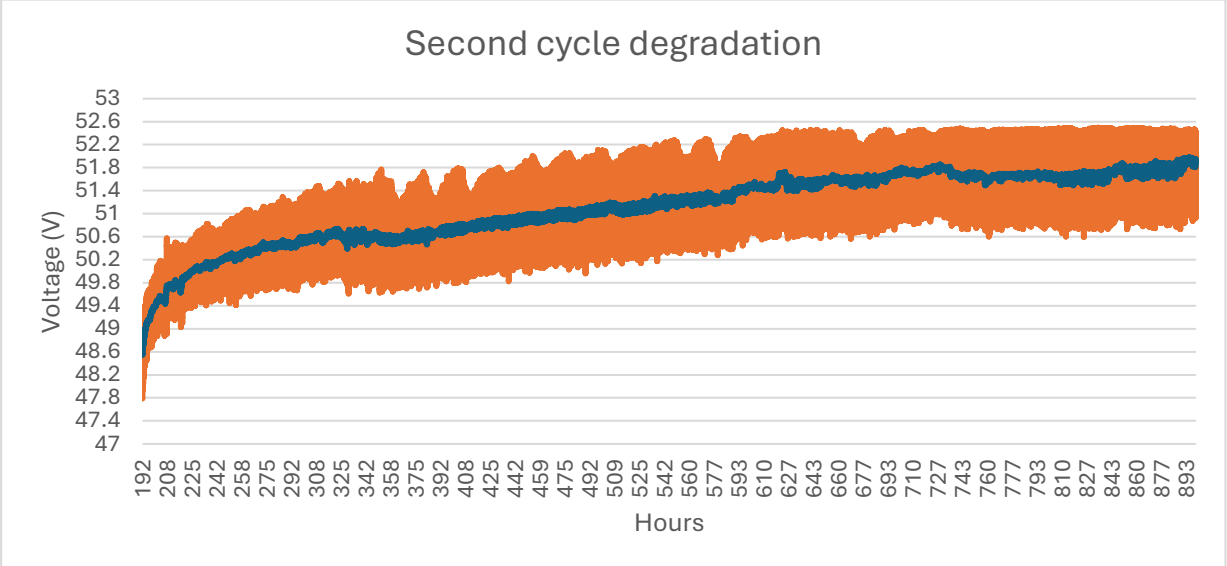

Figure 45 - Second cycle degradation lasted about 700 hours. In orange the original data shift. In blue the average value trend.

The reversible voltage increase has been calculated according to Eq. 17 and accounted for 0,028310735 V/h. On the other hand, the irreversible voltage has been calculated with Eq. 18 and accounted for 0,004772903 V/cycle.

3.6. Statistical metrics

Statistical methods are essential for assessing the accuracy and reliability of numerical analyses by quantifying deviations and evaluating consistency. Metrics such as the coefficient of determination (R^2), root mean squared error (RMSE), and mean absolute percentage error (MAPE) are commonly employed to measure the agreement between predicted and observed values. Each of these indicators provides a different perspective on the precision and variability of data, contributing to a comprehensive evaluation of performance. By applying these statistical tools, it is possible to systematically validate results and enhance the robustness of analytical approaches. All these metrics are utilised for the analyses held in Chapter 5.

The **coefficient of determination** (R^2) measures how well the model's predictions explain the variance in the experimental data. It is calculated as [33]:

$$R^2 = 1 - \frac{\sum(y_i - \hat{y}_i)^2}{\sum(y_i - \bar{y})^2} \qquad \textit{Eq. 23}$$

Where, $\boldsymbol{y_i}$ are the experimental values, $\boldsymbol{\hat{y}_i}$ are the predicted values from the model, $\boldsymbol{\bar{y}}$ is the mean of the experimental values.
Interpretation:

- $R^2 = 1$ means a perfect fit.
- $R^2 = 0$ indicates the model does not explain any of the variance.
- A negative R^2 suggests that the model performs worse than a simple mean-based prediction.

The **root mean squared error (RMSE)** measures the average magnitude of the error between model and experimental values. It is given by:

$$\mathrm{RMSE} = \sqrt{\frac{1}{\mathrm{n}}\sum(\mathrm{y_i} - \hat{\mathrm{y}}_\mathrm{i})^2} \qquad \textit{Eq. 24}$$

where n is the number of data points.
Interpretation:

- RMSE has the same unit as the measured variable.
- A lower RMSE indicates better model accuracy.
- Unlike R^2, RMSE is sensitive to large errors due to squaring.

The **mean absolute percentage error (MAPE)** is a relative error metric that expresses the prediction error as a percentage of the model values:

$$MAPE = \frac{1}{n}\sum \left|\frac{y_i - \hat{y}_i}{y_i}\right| \times 100 \qquad \textit{Eq. 25}$$

Interpretation:

- MAPE provides an intuitive percentage error.
- Lower values indicate better predictive accuracy.
- It is useful when comparing errors across different datasets or units.
- A drawback is that MAPE can be undefined or misleading when model values are close to zero.

Table 10 - Recap of the metrics differences.

Metric	Type	Sensitivity to large errors	Scale	Best value
$\boldsymbol{R^2}$	Goodness of fit	Less sensitive	Dimensionless (0 to 1)	1
RMSE	Absolute error	Sensitive	Same as data units	0
MAPE	Relative error	Less sensitive	Percentage (%)	0

4. Python Model development

4.1. Model structure and assumptions

The main activity performed in the laboratory of 'Officine Edison Torino' was to design a python model which has the aim to simulate the operation of an AEM-type electrolyser in time, including its actual degradation caused by both steady and intermittent power condition. The intermittent power condition is performed by simulating a PV panel as energy input source for the electrolyser, as discussed in Section 3.3.

The setting of the model is built in such a way that it requires as input values only the ones inside a data sheets of a real purchasable electrolyser, without requiring very specific data. At most, the model should require some variables that can be easily calculated starting from the one inside the data sheet.

The structure of the model follows the logic of *Object-oriented programming (OOP),* a programming paradigm that is based on the concept of "objects." These objects are instances of classes, which are templates or blueprints that define both the data structure and the behaviours associated with the data. OOP emphasizes the organization of code into reusable, modular components, making it easier to manage, scale, and maintain.

In Figure 46, the key aspects of a such type of programming language.

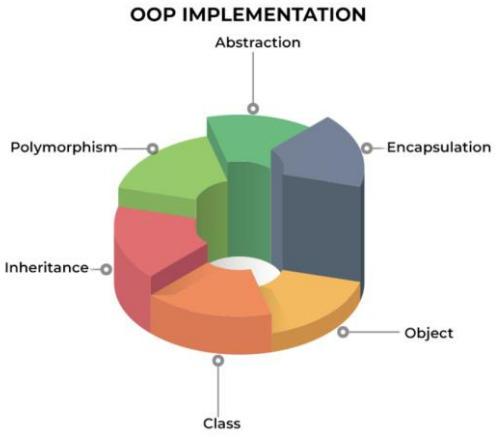

Figure 46 - Key aspects of the OOP [52].

Nowadays, AEM technology is not universally developed, it is still in its nascent stage as stated in Section 2.2.3. The possibility to own a AEM electrolyzer type is crucial, so that it can be used as sample to create the model structure basis. Currently, the majority of the AEM models are purely theoretic ones, entirely based just on formulas without caring of the internal real structure of a real electrolyzer. Therefore, the system structure described in Section 3.3 was seen as the foundation the code has been built on, for both the electrolytic stack and the auxiliary part. Finally, the integration of the degradation rate contributes to make this model innovative.

4.1.1. State-space problem: definition of inputs and outputs

The state-space problem refers to the analysis and representation of the dynamics of a system through state variables, using state-space representation. This approach allows for describing the behaviour of dynamic systems, which can be either continuous-time or discrete-time. Two fundamental properties in this context are reachability and controllability, which define how much it is possible to influence the state of the system through inputs.

In the context of the state-space problem, the first step was to define the model state input variables: as already assessed, the model must be realistic both in the input required variables and in the output ones. The operation of the laboratory AEM electrolyzer was analysed and studied to make the model as realistic as possible.
The set parameters are:

- The hydrogen output pressure which can be regulated arbitrarily up to 20 bar
- The hourly hydrogen volumetric flow rate expressed in Nl/h

By analysing the data sheet of the working AEMEC a list of available constants are given. They have already been listed in Section 3.3. All the other parameters are just measured during the operations.

In the context of electrolyzers, state variables and electric operative variables blend together. In particular, to define the system status four parameters are needed: two state variables that are pressure and temperature, two electric variables that are current (or current density) and voltage. Thanks to the electrochemical equations (described in Section 4.2), it is necessary to know just three of these to define the others.
Unfortunately, the temperature cannot be set at will as input parameter, it changes in time freely during the operation. It was already clear that a thermal balance was necessary to define the temperature evolution.
In the same way, hourly hydrogen volumetric flow rate has not been chosen as input variable because of two reasons:

1) The model was meant to be deterministic and not a design one. So, normally the volumetric flow rate is a output parameter since it states whether the system is performant or not. It is what the most matters of an electrolyzer alongside the efficiency.

2) The hydrogen production is energy dependent, it relies on the available input energy resource. The PV energy, indeed, is not a constant energy vector.

For the same reasons, instead, the available RES power has been chosen as input parameter. It already includes the information of both voltage and current.

The hydrogen pressure, likewise, must be chosen at the beginning of each real simulation because it changes the behaviour of the electrolyzer. This initial regulation is possible due to the nature of the device, which is an AEM technology. So, also the pressure is chosen as input parameter.

There was the need of one more parameter that cannot be addressed to one of the four system status parameters anymore. The choice fell on the polarization curve that, along with the available energy, is not a pure input parameter but a derived one. By combining them, both voltage and current are represented. The polarization curve can be calculated by measuring contemporary voltage and current. In particular, one of the two is regulated and the other is measured.

About the output variables, as just stated, the hydrogen production and the system efficiency are the most important. The reasons have been given by explaining why the hydrogen production cannot be an input parameter. The system efficiency, likewise, is a performance indicator. The last output is addressed to the water consumption and consequently the water flow rate required by the stack to make the system work. Indeed, as stated earlier, the electrolyzer has a particular management of the cooling and feeding system. They are combined together in one single system, the water that feeds the cells also cools them down.

In Table 11, a recap of what has just been assessed.

Table 11 - Input and output variables of the model.

Input variables	Output variables
Hydrogen pressure	Hydrogen production
Polarization curve (to be found)	System efficiency
Net available power	Water consumption

The input parameters enter the operative setting of the electrolyzer, than they are processed and transformed into some other intermediate and output flows. The former, in the same way, are then transformed into output ones by combining other information available in the model that

are going to be described. The model geometry in form of a process diagram is shown in Figure 47.

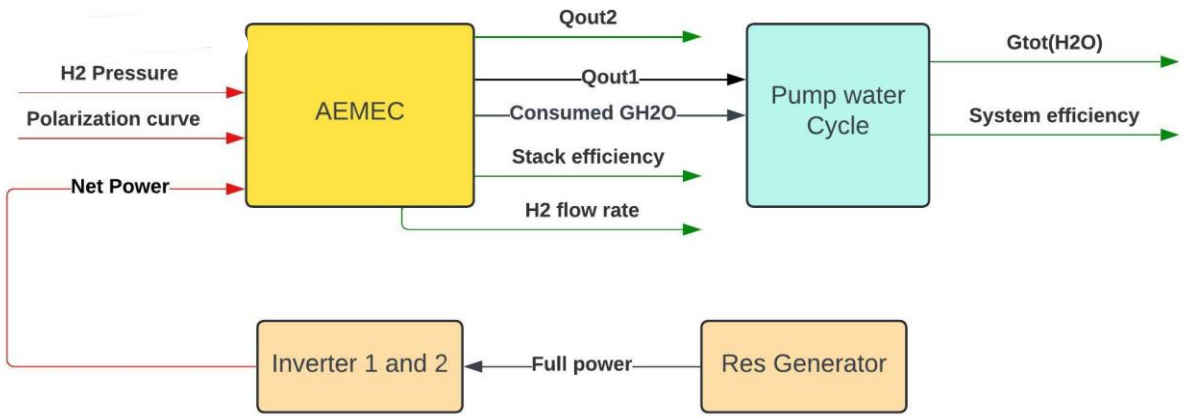

Figure 47 - Process diagram of the entire model. Red streams are input parameters, black streams are intermediate parameters, green streams are output parameters.

Starting from the beginning of the model structure, a RES generator produce some energy in DC form. The power flow is processed by the combination of two inverters that adjusts the flow with respect to the electrolyzer characteristics. It reduces a bit the available full power because of the inefficiencies of the conversion processes. The net power stream, along with the polarization curve and the hydrogen set outlet pressure, represent the input parameters of the AEMEC (Anion Exchange Membrane Electrolyzer).
This process produces both some intermediate streams and already output streams. Intermediate ones are:

1) Q_{out1}*:* the thermal energy which is subtracted from the EC by the cooling system.
2) $Consumed\ G_{H_2O}$: the water flow rate that is required to the cooling system to only power the electrolysis.

The output streams are the following:

1) H_2 *flow rate*: hydrogen production flow rate in time.
2) *Stack efficiency*: efficiency of the only stack part in time without auxiliaries.
3) Q_{out2}: thermal energy dissipated towards the ambient. It is not regarded as output variable in Table 11 because in the actual model it is not exploited as a useful stream. However, ideally It could be. That is why it is regarded as output one in Figure 47.

The intermediate streams enter, in the end, the last process block, namely the "Pump water cycle". The final two outlet streams are:

1) *System efficiency:* includes the stack efficiency and all the other auxiliaries efficiencies.

2) G_{tot}: the total water required from the mains which stands for all the water needs of the system. Notably, it is represented in Figure 28, Section 3.2.2.

4.2. Electrochemical parameterization and assumptions

This chapter outlines the parameterization choices and assumptions adopted in the mathematical formulation of the electrolyzer model. While Section 2.4 focused on theoretical modelling, here the selection of key model parameters is justified.
The parameterization considers various factors influencing system behaviour, while specific adjustments improve the accuracy of the model. By clarifying these aspects, this chapter strengthens the connection between theoretical modelling and practical application.

4.2.1. Overvoltages

At the core of the analysis there is the parameterization of the polarization curve. As explained in Eq. 4, it consists of the sum of the reversible voltage E_{rev} and the overvoltages associated to the inefficiencies of the process η_i. Starting from the first parameter, E_{rev} modelling is addressed to Titheridge model. The relative formulation is Eq. 3. It is constituted by two terms:

- E_0, the reversible voltage at standard pressure (1 bar), is calculated by using the NIST (National Institute of Standards and Technology) WebBook tables thermochemistry data [53]. The procedure follows the logic of the Gibbs free energy change of the reaction.

- C is a parameter that depends on the operating pressure (in bar), the water vapor pressure, and the water activity in the KOH electrolyte: the activities of H_2, O_2, and H_2O are affected by the characteristics of the KOH electrolyte [38].

The activation overvoltage η_{act} is modelled according to the Butler-Volmer equation, Eq. 5, defined in Gomez Vidales model [37]. Although the several simplification carried out by several models, in this parameterization none of them are performed to make it as much real as possible. The ohmic overvoltage η_{ohm} modelling is performed according to Gomez Vidales, in Eq. 6 [37]. The formula depends on a series of cell geometric characteristics described in the relative Section. The only known parameters are the molar concentration of the electrolyte and the net active area of the cell. All the others constants are unknown and need to be calculated.

Lastly, the concentration overvoltage η_{conc} . It is important to observe that although the influence of this term on the operation of a AEM-type electrolyzer is often considered irrelevant (as explained in Section 2.4.1), in the present model it is considered. Indeed, in a system like the analyzed case study electrolyzer , the electrolyte mix has the aim to feed, to cool and to make the electrolyte recirculate. The latter helps prevent the development of the concentration

overvoltage, creating a constant temperature in all the electrolyte mass flow. In this way, the polarization curve is complete.

The integration of the diffusion overvoltage is based on the observations made by Vidales [37]. It introduces new constants and a more complex system design. Indeed, the migration process is accurate and precise. The exact concentrations of the products in the cathode and anode are calculated from a water migration balance.

The net water flow through the membrane is the result of various processes that transport water across the anion exchange membrane. The model considers three already described primary phenomena:

- Diffusion-driven flow $\dot{N}_{H_2O}^{diff}$: it can be modelled using Fick's law. For simplicity, the model assumes a linear concentration gradient across the membrane in accordance with Fick's principles.
- Electro-osmotic drag $\dot{N}_{H_2O}^{eod}$
- Pressure-induced flow $\dot{N}_{H_2O}^{pe}$

The total water across the membrane $\dot{N}_{H_2O}^{mem}$ is represented by Eq. **7**. The diffusion overvoltage equation has been defined in Eq. 8.

Since the concentrations depends on what happens locally, they introduce also new variable dependences in the model: the local anode pressure Pa, the cathode local pressure Pc, the local anode temperature Ta, the local cathode temperature Tc, the hydrogen production $\dot{n_{H_2}}$ and the oxygen production $\dot{n_{O_2}}$.
Both values are determined using the Faraday's Law described in Eq. 10. In particular, using $z = 2$ for the hydrogen and $z = 4$ for the oxygen.
Moreover, to simplify the calculation, the temperature is considered equal in the stack of cell so $T_a = T_c = T$. The anode pressure P_a has been considered equal to the pressure of the mixture water-electrolyte entering the stack. The cathode pressure P_c, instead, is the hydrogen output pressure.

Most of the described model variables are too specific. In a realistic context they are not provided with the electrolyzer. In the absence of an EIS (Electrochemical Impedance Spectroscopy), it is not possible to define the characteristics of anode, cathode and separator precisely. The way they are obtained is described in Section 4.3.

In Table 12, the list of the unknown parameters.

Table 12 - Characteristics of the AEM cell to be determined.

Name of the parameter	Units of measurements
Anodic exchange current $i_{0,a}$	A
Cathodic exchange current $i_{0,c}$	A
Membrane humidification degree	-
Electrode porosity ε	Adimensional
Percolation thresold ε_p	Adimensional
Anode thickness	m
Cathode thickness	m
Membrane water permeability K_{darcy}	cm^2
Osmotic drag coefficient	$mol_{H2O}\ (mol_{OH^-})^{-1}$
Diffusion coefficient	$m^2 s^{-1}$
Membrane thickness	m
Membrane active area	m
Distance between cathode and membrane	m
Distance between anode and membrane	m
Anode cross-section area	m^2
Cathode cross-section area	m^2

What is known, instead, about the technical parameter is indicated in the following Table.

Table 13 - Known characteristics of the AEM cell.

Name of the parameter	Units of measurements
Active surface area	cm2
Electrolyte concentration	%wt
Number of series cells	Adimensional
Number of parallel strings of cells	Adimensional

The electrolyte concentration and its type is generally written in the data sheet of the electrolyte producer. The number of series and parallel cells alongside the active surface area are averagely provided, alternatively they can be defined by some easy calculations with the given data. These last parameters are fundamental to scale the model up or down according to the size of the owned AEM electrolyzer.

4.2.2. Model thermal management

The thermal management of the model was designed considering both the actual system structure of the electrolyzer owned by Edison and the models already present in the literature.

The model considers the electrolyzer as a black box and thermal fluxes exit or enter the box. Indeed, the present work needs to be flexible and adaptable in as many areas as possible. The temperature of the electrolysis stack is determined using a quasi-steady-state thermal model, treating the device as a zero-dimensional system with lumped thermal capacitance. The heat balance is established by considering a constant rate of heat generation and heat transfer over a specified time interval. The thermal management has been defined according to Rozzi [33].
In Figure 48 the scheme of the thermal fluxes.

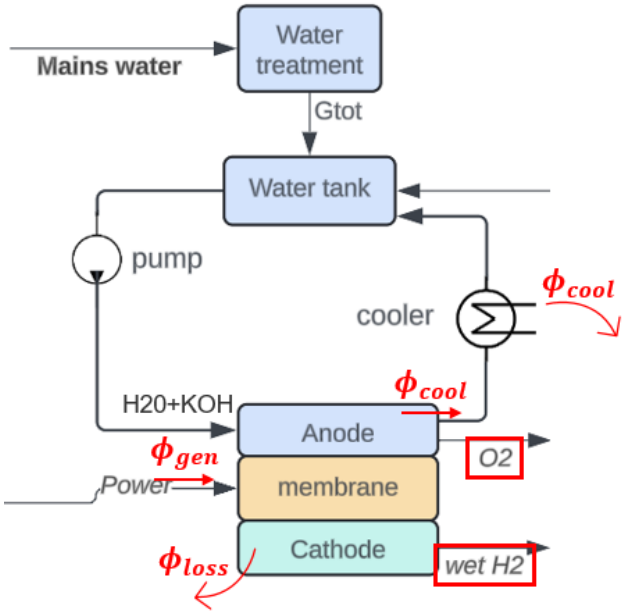

Figure 48 - Thermal fluxes entering and exiting the system.

The thermal fluxes balance equation has been chosen to be defined by Eq. 13. Some parameters are known some others need to be calculated.

C_{th}, the overall thermal capacity of the stack, can be estimated experimentally or calculated as the sum of each component's thermal capacity. In this model it has been calculated, further details in the next section. Φ_{cell} , the heat generated in the stack already been described by Eq. 15, is considered as a hot flux entering the electrolyzer (Figure 48). Φ_{loss} , the overall convective-radiative heat dissipated with the stack surrounding, generally should be specific according to each component of the electrolyzer. It was not possible for obvious reasons. An overall average loss is considered with Eq. 14.

Φ_{loss} is absorbed by the circulating electrolyte-water mixture and then, thanks to the pumping circuit, is transmitted to the cooler where it is dissipated. Electrolysers usually work above the thermoneutral voltage so, heat is generated, and cooling is required. Therefore, in this model, an auxiliary power, Φ_{loss}, is considered and removed. To calculate the amount of cooling necessary to the stack, a maximum temperature must be fixed. Indeed, although higher temperature gives better performance, AEMECs have poor thermal stability. Notably, the stack would ruin and the durability would be reduced [50].
The maximum temperature is chosen by the user according to the owned technology or according to the setting parameters. In particular, once the maximum value is reached, the temperature is kept constant thanks to the cooling system.

- $\sum_i h_i \dot{N}_i$, once again, is the net sum of the reactants and products fluxes where h is the molar enthalpy [J/mol] and N the molar flow rate [mol/s]. The first is calculated thanks to the NIST chemistry tables [53]. The second is calculated thanks to the Faraday law, described in Eq. 10.
  In Figure 48, the direction of the inlet and outlet described streams are represented, both input and output with the notations “H2O + KOH”, “O2”, “Wet H2” .

Most of the described parameters can be calculated by the model except two: the convective-radiative heat-transfer coefficient h and the overall thermal capacity of the stack C_{th}.

4.2.3. Calculation of h and C_{th}

Others scientific papers have experienced the same problem. Rozzi[33], for instance, refers to some tabulated literature values. However, the proposed thermal model is meant to be precise. Done by looking at the Edison AEMEC structure. Therefore, to determine h and C_{th} a practical approach has been carried out. Reference was made to the results of some previous experimental tests which had the aim to verify the operation and performance of the laboratory AEM electrolyser.

The thermal balance equation is a differential equation and a state-space problem. Therefore, there would be several solutions according to the boundary conditions, namely the initial conditions of the system. This procedure has the aim to define both the heat transfer coefficient and the overall thermal capacity. To achieve this, an evolution temperature plot (Figure 49) was needed in such a way as to provide the basis for the present analysis. Examining the type of problem, one of the two parameters between h and C_{th} must be kept fixed to understand the other one. Meanwhile, all the other terms of the equation must be kept fixed. Not merely that, the differential term must not vary along the temperature curve, in actual fact transforming the differential equation into a linear one.

The chosen parameter to be fixed is h. This by means of a specific equation found in literature [44]:

$$h = 2.51 \times 0.52 \left(\frac{T_{\text{stack}} - T_{\text{amb}}}{\varphi_{\text{stack}}} \right)^{0.25} \qquad \textit{Eq. 26}$$

- T_{stack} is the stack temperature
- T_{amb} is the ambient temperature
- φ_{stack} is the stack diameter. It can be calculated simply by knowing the active area and the geometry of the stack/cell (cylindric). However, in the present case the value was measured directly inside the cabinet of the AEMEC to have more accurate values and calculate precisely h and C_{th}.

The equation describes the natural convection heat transfer coefficient obtained from well-known correlations for natural convection on horizontal cylinders. In the majority of models h is kept constant neglecting its change with the temperature rises. An example is the model by Rozzi [33]. However, although h depends on different aspects, the most relevant (in static configurations) is exactly the temperature variations.

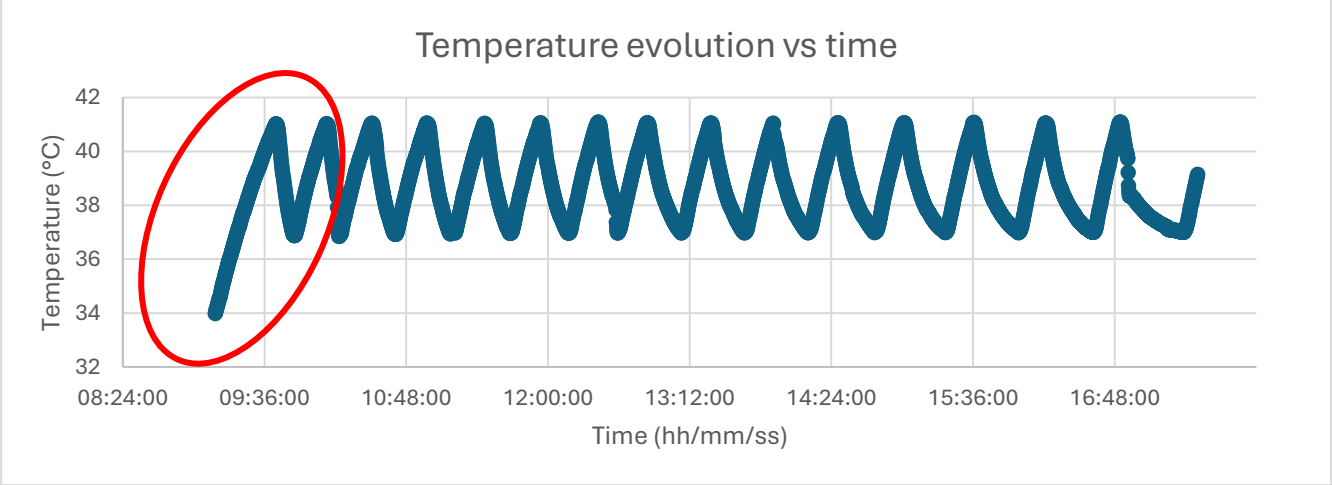

Figure 49 - Experimental test held at 20 bar and 400Nl/h: temperature vs time. The highlighted part of the curve is the section used as basis for the analysis.

The curve results saw-toothed because each time the temperature reaches 41°C the cooler turns on, cooling down the entire system.
In accordance with the purpose of the analysis, the differential equation should be transformed into a linear one. Therefore, the temperature plot has been synthesised into the first section of the curve. The zoomed part is displayed in Figure 50, where the curve linearization has been highlighted through the linear equation in overlay.

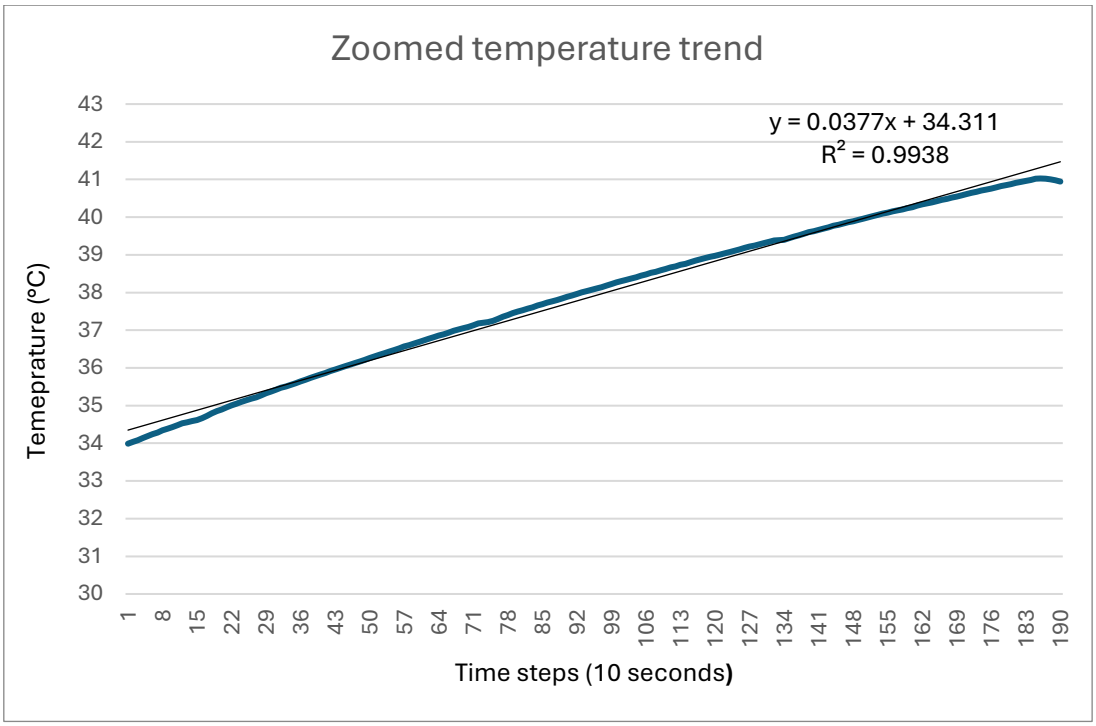

Figure 50 - A detail view of the highlighted section, provided in Figure 49 .

So, the thermal balance equation includes some constants which, as already stated, need to be fixed for an accurate measurements. Some of them were known, some others were not. The unknown ones are included in the heat transfer area of the stacks, important to understand the thermal losses towards the ambient. Indeed, the total geometric area requires more parameters to be known. They were measured experimentally inside the cabinet of the electrolyser. In particular:

1. φ_{stack}: the diameter of the two stacks
2. The length of each single cell, and so the total length of the stacks

Indeed, the total heat transfer area breaks down into two cylinders which are the two stacks of the electrolyzer. They have both the lateral surfaces and the base surfaces per two times.
The temperature ranges analyzed was between 35°C and 40°C. The thermal capacity was determined starting from one of the temperature values of the curve. Later on, more points of the curve were investigated to verify if the changing of the operation point would lead to different C_{th} values. The refrigerating effect of the cooler was not considered because it only turns on when temperature reaches 41°C, ambient temperature was measured and fixed. The thermoneutral voltage was calculated according to the temperature change and according to the NIST chemistry tables [53]. The number of cells were known while current and voltage were available from the experimental test data. The last parameter not yet considered is the refrigerating effect of the reactants and products inside the cell. They are all calculated thanks to the Faraday Law (Eq. 10) by simply changing the charge number.

At this point h and C_{th} were calculated. It resulted that:

1. $h \approx$ 4.2 J/m2*K
2. $C_{th} \approx 160000$ J/K

Then, both values were calculated for other points of the curve. Indeed, with the time the temperature increases and the boundary conditions changes. Both h and C_{th} need to be as constant as possible since they represent intrinsic characteristics of the cell. They resulted almost constant:

1. h ranges from 4 to 4.3 J/m2*K
2. C_{th} ranges from 150000 to 170000 J/K

At this stage, all the values of the thermal balance equation were calculated and ready to test the model. To make the model scalable, the thermal capacity was adimensionalized with the geometric dimensions of the laboratory electrolyzer stack and with the number of cells (both in series or in parallel). The redimensioning is then performed inside the part of the python code which cares of the temperature changes. It is done by utilising the net active area of the cell which is required as an input of the model.
The heat transfer coefficient, instead, is calculated at each iteration of the model. It varies with the time due to the temperature changes.

4.3. Model implementation in python

The implementation of the AEM electrolyzer simulation model is accomplished using Python, leveraging several well-established libraries to perform numerical calculations, data processing, and curve fitting. This section details the structure of the code, the libraries used, and the execution of the model for simulating the electrolyzer's performance over time.

4.3.1. Overview of the code structure

The code has been structured to achieve modularity, ease of debugging, and scalability for future adaptations. The code has been written in Pyhton because of its high-level, versatile programming language and its simplicity and readability. Its extensive standard library and rich ecosystem of third-party packages make it ideal to this model. Many libraries and tools have been used, as it will be explained later.
The modularity, reusability and Scalability of the model is given by the Object-oriented programming (OOP). Indeed, the code is arranged in classes and methods to make it as readable as possible (see Figure 51).

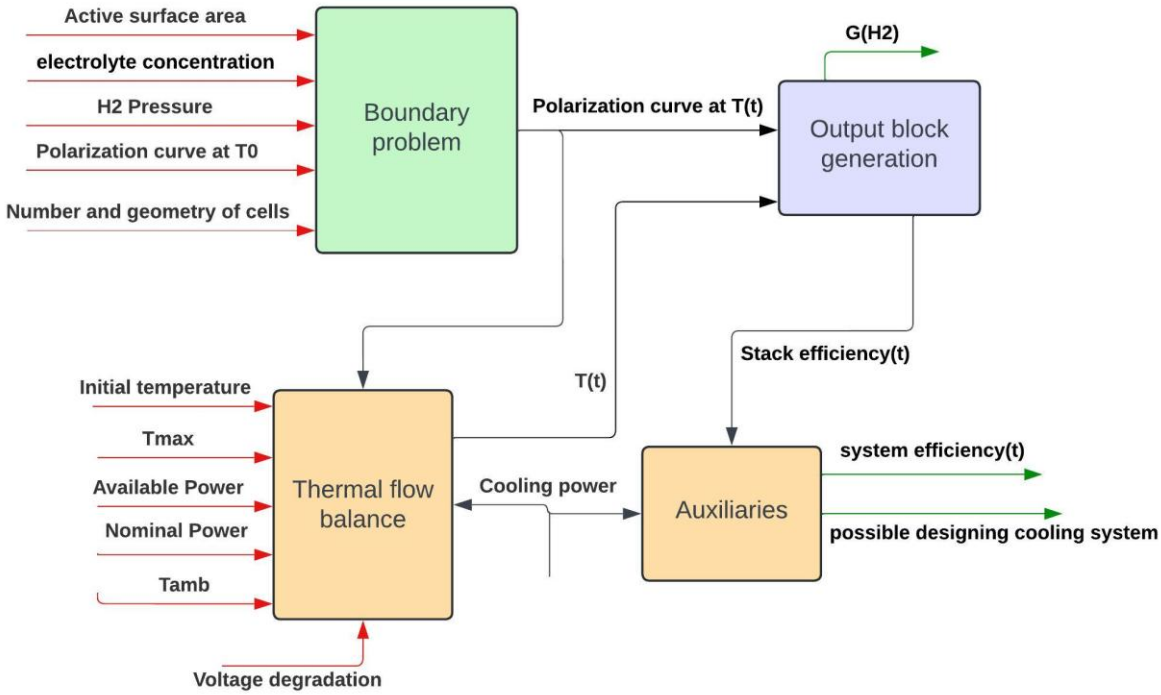

Figure 51 - Code Object diagram.

The main two classes are “Boundary problem” and “Thermal flow balance”. The other two provided blocks are graphically separated from the former classes just for the sake of simplicity and to make the plot as clear as possible. In reality, they are included.

4.3.1.1. Boundary Problem class

The aim of this class is to understand all the unknown parameters of the case study electrolyzer. This is achieved thanks to a combination of both the polarization curve as input parameter and the parameterization of the equations and variables, described in Section 4.2. The way used to calculate the unknown variables is a fitting process, namely fitting the parameters of the polarization curve given by the equations. It refers to the process of determining a mathematical function that closely matches a set of data points. It involves applying algorithms that adjust the parameters of a chosen function (e.g., linear, polynomial, exponential) to minimize the error between the actual data points and the predicted values from the function. In the present case, the unknown constants composing the polarization curve equation (Eq. 4) are varied to reduce the error from the real polarization curve described in Section 3.4. It is performed by using the SciPy library. The output of the class is the parameterized polarization curve so that the influence of its parameters (such as pressure, temperature, electrolyte concentration, active surface area) is performed.

The class framework is shown in Figure 52.

```
class BoundaryProblem:
    def __init__(self, conc_koh1, p, t_c, np, ns, active_area, pol_curve):···

    def lettura_csv(self):···

    def calcolo_g(self, A, B, C, D, E, F, G, H):···

    def calcola_valori_termodinamici(self):···

    def calcolo_Erev0 (self): #calcolo primo termine dell'ocv···

    def calcolo_ocv(self): #calcolo secondo termine ocv + ocv totale···

    def calcolo_Vact(self, i, i0_a, i0_c): #calcolo activation overvoltage···

    def calcolo_Vact1(self, i, i0_a, i0_c): #modifica activation overvoltage per maggiroe sensibilità alla temperatura···

    def calcolo_Vohm(self, i, lambd, d_mem, k_koh):···

    def calcolo_condizioni_riferimento(self, k_porosity, i, delta_a, delta_c, k_mem, n_d, k_darcy):···

    def restituisci_C_H2_mem_0(self, k_porosity, i, delta_a, delta_c, k_mem, n_d, k_darcy ):···

    def restituisci_C_O2_mem_0(self, k_porosity, i, delta_a, delta_c, k_mem, n_d, k_darcy):···

    def calcolo_Vdiff(self, k_porosity, i, delta_a, delta_c, k_mem, n_d, k_darcy):···

    def calcolo_curva_polarizzazione(self, i, i0_a, i0_c, lambd, k_porosity, delta_a, delta_c, n_d, k_darcy, k_mem, k_koh, d_mem):

    def calcolo_curva_polarizzazione1(self, i, i0_a, i0_c, lambd, k_porosity, delta_a, delta_c, n_d, k_darcy, k_mem, k_koh, d_mem):

    def fit_polarization_curve(self, I_asse, V_asse):···

    def Calcolo_Cth_h(self):···
```

Figure 52 - Boundary problem class: structure of the methods.

The input variables are shown as parameters of the "__init__" constructor method and coincide with the ones shown in Figure 51.

Now, the variables that the code fits are not all pure ones. Some of them enclose different unknown constants. This was made to reduce a possible error given by the iteration process and to reduce the runtime of the simulations. In reality, the unknowns are 16 (see Table 12), they have been reduced to 11 to let the program converging to a solution. Too many variables can cause an overparameterization or overfitting. They are all displayed in the following Table.

Table 14 - Complete overview of the fitting parameters (highlighted in blue) and their values. In white the parameters they come from.

Name of the parameter	Range of values from literature
Anodic exchange current $i_{0,a}$	$10^{-5} < i < 1\ A/cm^2$ [54], [55]
Cathodic exchange current $i_{0,c}$	$10^{-5} < i < 1\ A/cm^2$ [54], [55]
Membrane humidification degree λ	$14\text{-}21\ [\ mol_{H2O}\ (mol_{SO3})^{-1}]$ [37]
Electrode porosity ε	-
Percolation threshold ε_p	-

$\varepsilon\left(\frac{\varepsilon-\varepsilon_p}{1-\varepsilon}\right)^{\alpha}$	0-1 [41]
Anode thickness t_a	$10^{-6} < t < 10^{-2}$ m [56], [57]
Cathode thickness t_b	$10^{-6} < t < 10^{-2}$ m [56], [57]
Osmotic drag coefficient n_d	Around 3 $mol_{H2O}\ (mol_{OH^-})^{-1}$ [37]
Diffusion coefficient of water D_w	-
Membrane thickness $delta_{mem}$	$10^{-6} < t < 10^{-3}$ m [56]
$k_{mem} = \frac{D_w}{delta_{mem}}$	$10^2 < k_{mem} < 10^5\ m\ s^{-1}$
Membrane water permeability K_{darcy}	-
$k_{darcy} = \frac{K_{darcy}}{delta_{mem}}$	$10^{-18} < k_{darcy} < 10^{-10}\ cm$
Membrane active area A_{mem}	-
$d_{mem} = \frac{delta_{mem}}{A_{mem}}$	$1 < d_{mem} < 10^3\ m^{-1}$
Distance between cathode and membrane d_{cm}	-
Distance between anode and membrane d_{am}	-
Anode cross-section area S_a	-
Cathode cross-section area S_c	-
$k_{koh} = \left(\frac{d_{\mathrm{am}}}{S_a} + \frac{d_{\mathrm{cm}}}{S_c}\right)$	$10^{-2} < k_{koh} < 10^2\ m^{-1}$

The range of values from literature are shown to then compare the output results. The derived parameters ranges cannot have a precise range, an order of magnitude is given.

4.3.1.2. Thermal Flow Balance class

This class has different aims:

1. To make the code a time iterable process.
2. To calculate step by step the temperature changes in time.
3. To create the mathematical structure to integrate the reversible and irreversible degradation rate.
4. To read the input power provided by the RES source.
5. To calculate all the outputs of the simulation: so the hydrogen production over time, the system efficiency, the specific consumption and the needed water feeds.

The class framework is shown in Figure 53.

```
469  class ThermalFlowBalance():
470      def __init__(self, boundary_problem, Tamb, Tmax, Wnom, Tin, Power_csv, timestep, sim_duration, rev_deg_rate, irr_deg_rate)
499
500      '''metodo che caclola la pol curve per tutti gli step di temperatura definiti dalla funzione del boundary condition'''
501      def calcola_curve(self, I_asse, *popt): ···
518
519      '''metodo che definisce quale è la temperatura campionata più vicina a quella reale dello stack, infatti riceve in input i
520      def get_curve_for_temp(self): ···
547
548      def lettura_potenza(self): ···
581
582      '''metodo per calcolare la coppia V,I tale che il loro prodotto sia molto vicino ad uno presente sulla curva della PvsI'''
583      def calcola_coppia(self): ···
611
612      '''funzione che calcola l'aumento di temperatura partendo dalla coppia V,I stabilita, eseguendo gli scambi termici dello s
613      def Andamento_temperatura (self): ···
674
675      '''metodo che calcola la produzione di idrogeno ad ogni iterazione'''
676      def calcola_outputs(self): ···
684
685      def esegui_simulazione(self): ···
717
718      '''ho creato questa funzione per plottare le curve campionate a temperatura diversa e verificare se il codice funziona'''
719      def plot_curve(self, I_asse, *popt): ···
733
```

Figure 53 – Thermal flow balance class: structure of the methods.

The input variables are shown as parameters of the "__init__" constructor method and coincide with the ones shown in Figure 51.
The class is set to iterate until the chosen end of simulation. There are two parameters designed to set up the simulation, the timestep duration and the duration of the simulation. The first is important to assess how much sensitive should be each timestep by changing its duration. It is fundamental to coordinate it with the timestep of the input RES power to accomplish sufficiently precise results. The duration of the simulation is set according to type of results needed.

The loop cycle is shown in Figure 54.

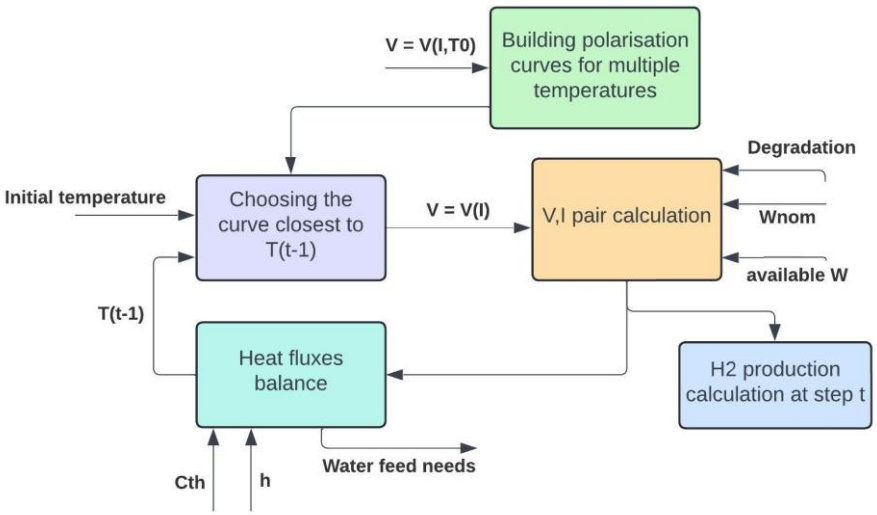

Figure 54 - Scheme of the iteration loop of the class.

The class receives the parameterised polarization curve from the "BoundaryProblem" class. Varying the temperature, several sampled polarisation curves are created and stored in a dictionary. Each cycle iteration, the algorithm will search for the right curve on the basis of the temperature evolution. At this point, the V-I voltage current working pair is calculated. This is done by receiving as inputs the RES available power and the nominal power of the electrolyzer. The exploitable electrolyser power is the minimum between the two. The V-I pair is chosen so that its product is nearest to the exploitable power.
Thanks to the current, the hydrogen production is assessed by the Faraday Law (Eq. 10). The V-I pair, alongside the thermal capacity and heat exchange coefficient, is fundamental to allow the balance calculation of the heat fluxes entering or exiting the electrolyzer. In this way, the temperature is performed together with the water feed needs to the cell, allowing the loop to start again.

4.3.1.3. Libraries, tools and features

The development of the Python model for simulating the operation of the AEM electrolyzer relies on several key libraries. Each library plays a crucial role in ensuring the functionality, accuracy, and usability of the model. An overview of the main libraries and their importance in the context of the implementation below (Figure 55).

```
import math
from Costanti import *

import pandas as pd #per importare il file csv
from scipy.optimize import curve_fit #per eseguire il fitting
import matplotlib.pyplot as plt #per costruire il grafico
import numpy as np #necessario per calcolare un sistema di equazioni in particolare per calcolare il Cth
```

Figure 55 - Libraries implementation in the code.

NumPy is a library for numerical computations and matrix operations in Python. It provides efficient tools for handling arrays and performing mathematical operations on large datasets. In the present code, NumPy is used to manage the numerical calculations required to simulate the system.

SciPy extends the capabilities of NumPy by offering a suite of advanced mathematical functions. It is particularly useful for tasks such as optimization, interpolation, and curve fitting. In this project, SciPy is utilised for fitting the polarization curve from the experimental data using optimization techniques.

The **pandas** library is designed for data manipulation and analysis. It is particularly effective in handling structured data, such as CSV files. Its role in this project includes reading and processing input files containing the experimental polarization curve and the renewable energy source (RES) data.

Matplotlib visualization library is a critical library for understanding model outputs. It enables the creation of detailed and customizable plots for the time evolution of the variables.

4.4. Integration of cell degradation

The cell degradation is assessed in terms of voltage degradation, namely voltage increase. It is composed by the reversible and irreversible voltage increase, in time.
The first one is a degradation that occurs at each second of the simulation, measured in V/s. Therefore, a counter is integrated inside the thermal flow balance class. At each timestep, it is updated, increased and summed to the operating V-I point. In particular, it shifts the polarization curve upwards keeping the current constant. The raised voltage at constant power makes the current lower and thus production efficiency is reduced.
The irreversible voltage degradation is performed in terms of V/cycle, as stated in the EU harmonised protocol [51]. With cycle, it is intended each time the input power drops to 0. Indeed, the irreversibilities arise each time the electrolyser turns off, when the electrodes electrochemistry is slowed down and a preconditioning of them is required again. Also here, a counter considers the increments of irreversibilities and the overall voltage increase which reduces the stack efficiency.
A third degradation element is represented by the initial voltage increase, at the start of the simulation. If there is the need to simulate the working electrolyser already degraded, a constant voltage factor is displaced to continuously increase the voltage utilization from the start of the simulation.

It is fundamental to state that, currently, there is not a universally recognized method to assess the intermittent degradation of electrolyzer. The one described is a possibility that fits better for a steady state degradation integration. Theoretically the intermittent degradation should consider parameters such as: rest time of EC due to unavailable RES power, variation speed of input RES power, time in which supplied power is higher than nominal one. None of them are considered in this model.

5. Results and Analysis

This section focuses on several key aspects: validating the Python model by comparing its outputs with experimental data obtained from the AEM electrolyzer tests, determining the appropriate polarization curve to be used as a benchmark for future simulations, and conducting a long-term analysis to understand the impact of degradation on electrolyzer performance.

By comparing simulation results with experimental data, the model's accuracy and reliability can be assessed, ensuring that it correctly represents the behaviour of the real system. The selection of the correct polarization curve is crucial, as it serves as the baseline for evaluating the electrolyzer's efficiency and performance under varying operating conditions. Furthermore, the long-run analysis will provide valuable insights into the degradation effects, quantifying its influence on hydrogen production and overall system efficiency over time.

Through these evaluations, this section aims to offer a comprehensive understanding of the electrolyzer's operational behaviour, supporting the optimization of its performance and long-term deployment in renewable energy applications.

The validation follows two steps: validation of the first class "Boundary problem" and validation of the second class "Thermal Flow Balance". The former cares about validating the fitted polarization curve, the latter cares about the validation of the outputs of the model. To compute these purposes, new parts of code have been introduced in the model.

5.1. Validation on November 2024

5.1.1. Boundary Problem validation

The validation of this class has been performed trial and error. The fitting method requires an initial list of guessed parameters, shown in Table 14 with the relative values range. The class would iterate to reach the perfect values to match the real polarisation curve with the equation parameterization. The approach is carried out by looking at the graphical comparison between the parameterized polarization curve and the real one. However, since the parameters to be fitted are several, the combinations are infinite. That is why the correct values range need to be implemented in the code, to obtain feasible fitted values. Concerning the derived parameters boundaries, they are chosen on the basis of the right order of magnitude without justifying with literature references.

The input polarization curve is the one experimentally calculated in November 2024, obtained and described in Section 3.4. However, before putting it as the input of the class, the curve has been modified so as to remove the current shift described in the same section. Indeed, it was just a residual value given by an instrumentation error.

The result is shown in the following picture.

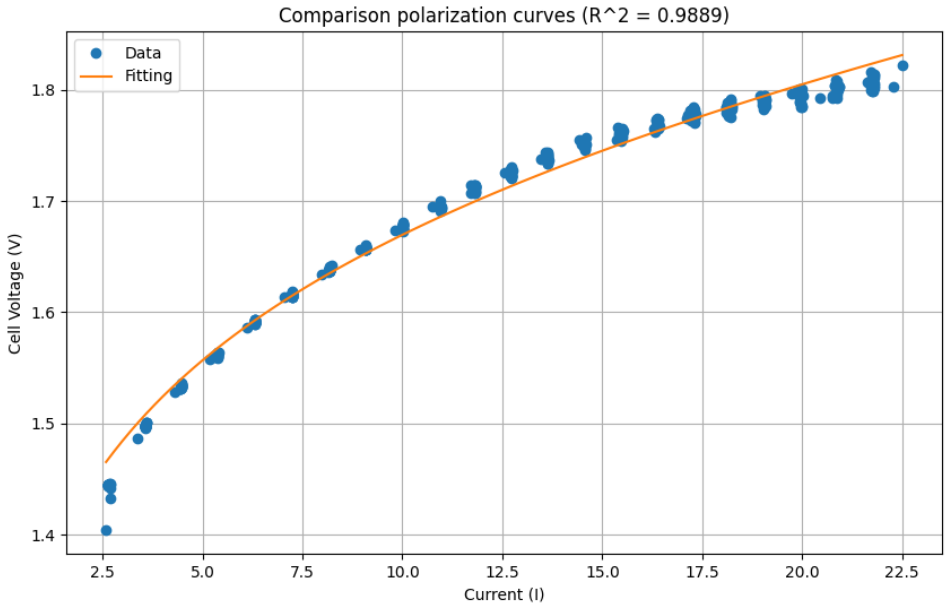

Figure 56 - Comparison between the experimental cell polarization curve, dated on November 2024, and the model parameterized one.

The polarization curve refers to a single cell of the stack which can be observed by the voltage and current magnitude.
The utilised statistical metrics for the fitting analysis is the coefficient of determination. $R^2 = 0.9889$ which is a good approximation.

5.1.2. Thermal Flow Balance validation

The validation of this class is carried out by comparing the trend of the model parameters: voltage evolution, current evolution, efficiency evolution, cumulative hydrogen production and temperature evolution. To compute this analysis, reference was made to the results of previous experimental tests of the case study electrolyzer, the one described in Section 4.2.3, dated back to 2021. The comparison has been carried out setting the input parameters of the simulation equal to the one of the experimental test. Namely, same active surface area, same electrolyte concentration, same hydrogen output pressure, same stack geometry, same initial simulation temperature, same maximum operating temperature, same nominal and available power, same ambient temperature, same total duration equal to 30 minutes.
To validate the model outputs, a new part of code has been written (Figure 57). It receives as inputs the model outputs trends, described above, and a CSV containing the experimental

values. The comparison metrics is based on the root mean square error and on the mean percentage error.

```
827   class ValidatingModel():
828
829 >     def __init__(self, thermal_flow, real_data_path):···
833
834 >     def import_real_data(self):···
854
855 >     def calculate_r_squared(self, real_values, model_values):···
867
868 >     def calculate_rmse(self, real_values, model_values):···
880
881 >     def calculate_mpe(self, real_values, model_values):···
894
895 >     def validate_model(self):···
922
923 >     def plots(self):···
```

Figure 57 - Written part of the Python code aiming to validate the model results.

By analysing all the parameters evolution in time of the predicted model and comparing it to the experimental values, an interesting assessment can be performed. The set input power was taken from the experimental test and was about 1650 Watt. Thanks to the plotted polarisation curve, the model deduces the V-I pair and compare it to the real one. Both comparison are shown in Figure 58 and Figure 60.

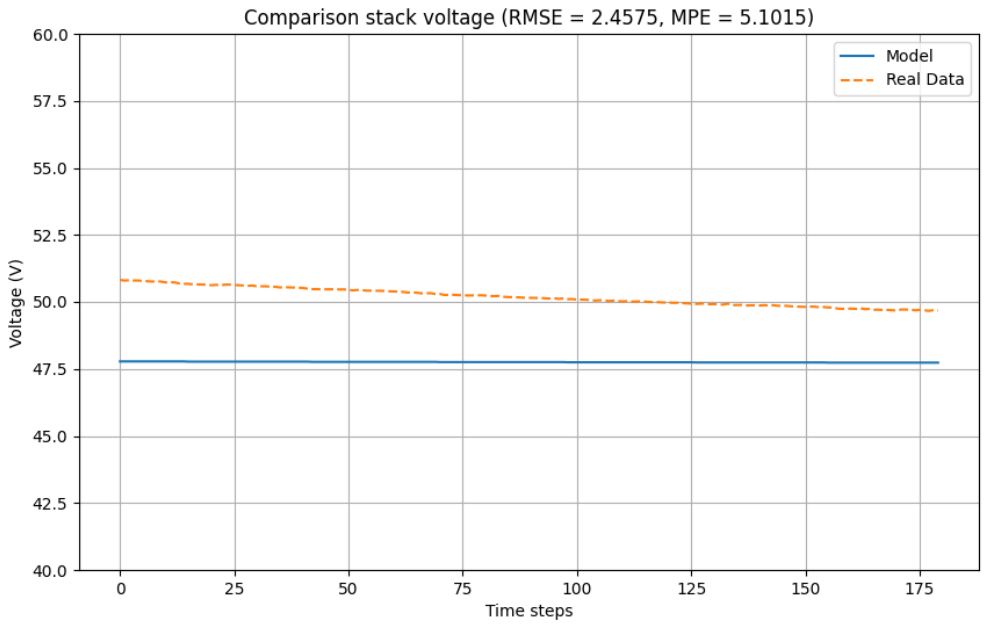

Figure 58 - Voltage evolution comparison.

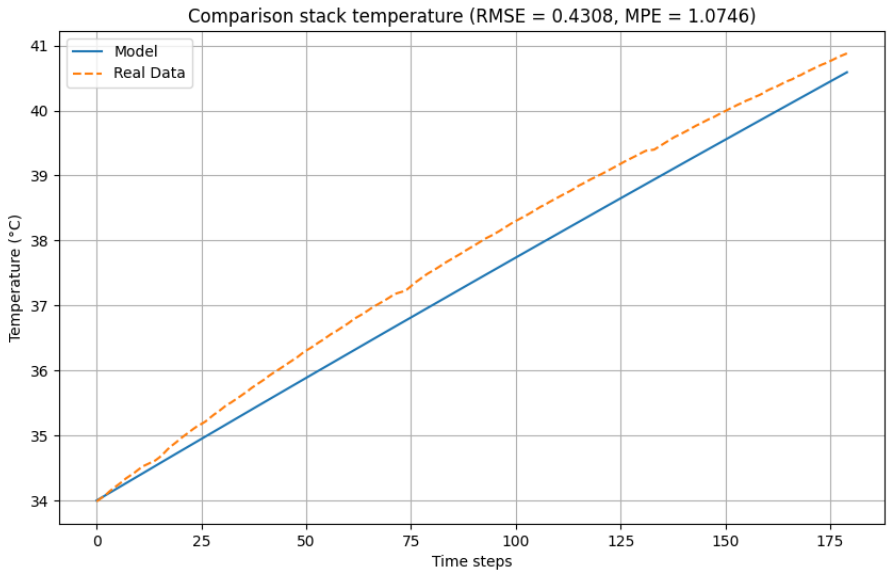

Figure 59 - Temperature evolution comparison.

Unfortunately both RMSE and MPE resulted high. Moreover, the model sensitivity to temperature is almost null. The reason of this behaviour is inherently hidden in the previous discussed Section 3.4.1. While sampling the polarisation curve, the temperature changes and the sampled points are influenced by that. The Python model requires a polarisation curve with a temperature kept constant instant by instant. The temperature provided to the boundary problem class was an average of the sampled temperatures points. This simplification is what makes the simulation not appropriately temperature dependent.

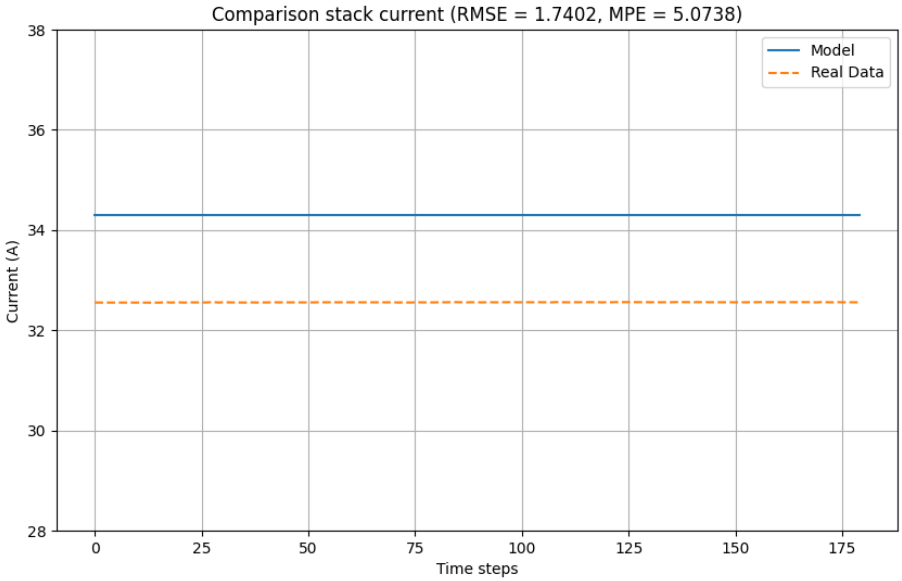

Figure 60 - Current trend comparison.

Now, analyzing the current comparison the data shift is more evident with respect to voltage one, especially checking the MPE. According to the Faraday's Law and the efficiency equation

discussed in Section 2.4.1 , this leads to an higher hydrogen production and an higher stack efficiency (respectively Figure 61 and Figure 62). Although the input polarisation curve of the model is performed from the experimental tests of the same electrolyser, it is evident that the V-I pair does not correspond. Especially by looking at the current trend.

Thanks to the Python model, the electrolyzer was regarded as faulted. After some measurements it turns out that one of the two stacks did not work properly. So its substitution was planned.

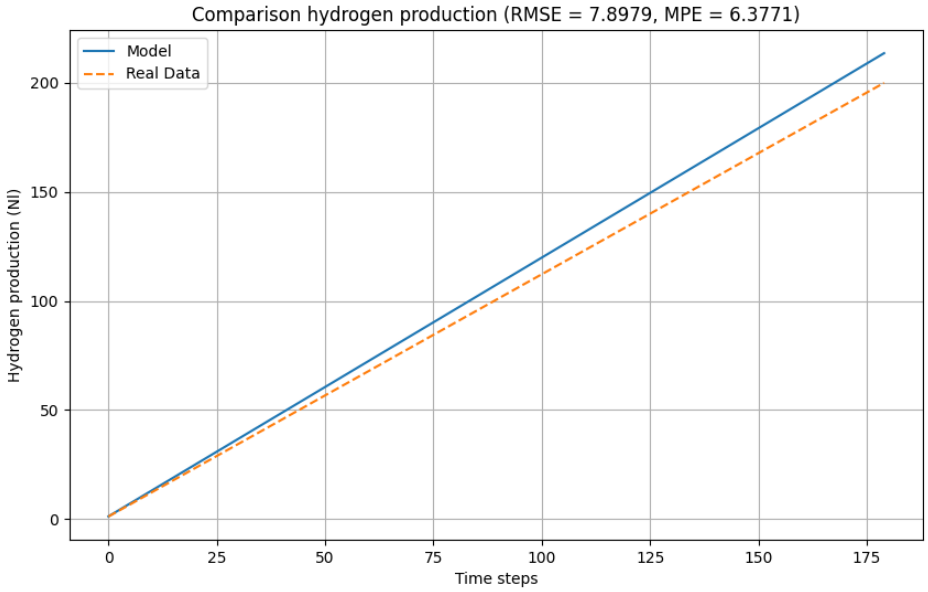

Figure 61 - Hydrogen cumulative production comparison.

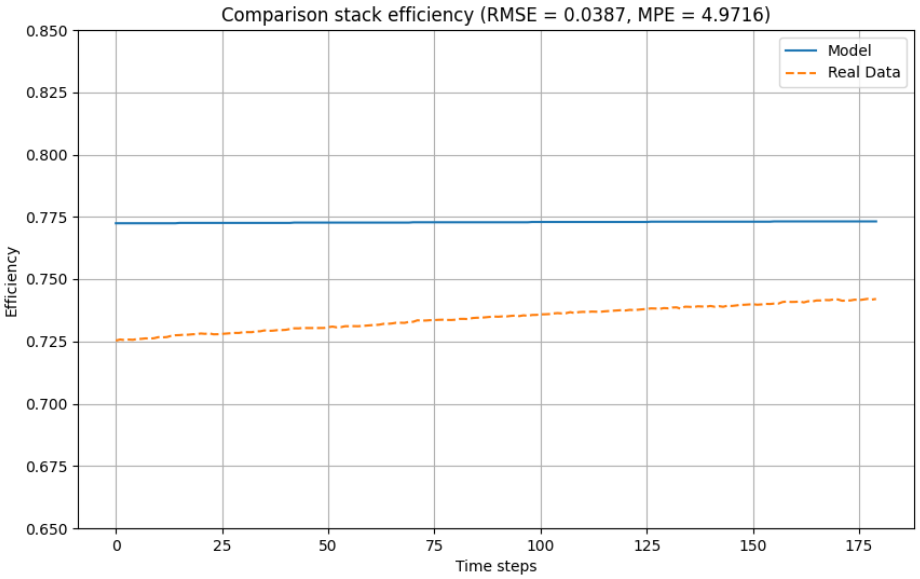

Figure 62 - Stack efficiency comparison.

As a final remark, it is important to notice the hydrogen production level. As previously stated, the model prediction is higher; nevertheless the cumulative production at the end of the simulation is consistent. By looking at Figure 61, the real data production is set at 400 Nl/h, so

in half an hour the value corresponds to 200 Nl. The predicted production instead is around 214 Nl. This represents a great result: the hydrogen production is based on the Faraday's Law which expresses a linear behaviour with respect to the current. Therefore, a simple proportion can be performed to verify whether the model predicts well the experimental hydrogen production or not. By adjusting the production with the currents, it turns out that the cumulative value corresponds to 201 Nl.

Therefore, the model approximates well the real EC behaviour.

5.2. Validation on February 2025

Now, new tests are needed to provide the correct polarisation curve of the electrolyser. This is important because it would be then used as benchmark to perform the expected long run simulations. Unfortunately, as explained in Section 3.4, only one of the two stacks was available to be tested and so current is halved.

The procedure to evaluate the polarisation curve provides for a complete hysteresis cycle, broken down into a descending part and consequently an ascending one. Only one of the two has been analyzed because it turns out to be already precise. It is the descending part of the cycle.

5.2.1.1. Boundary Problem validation

Since only one stack was available the input descending polarisation curve has been modified to simulate the integration of a second identical stack by doubling the current. The cell polarisation curve comparison is shown in the following picture.

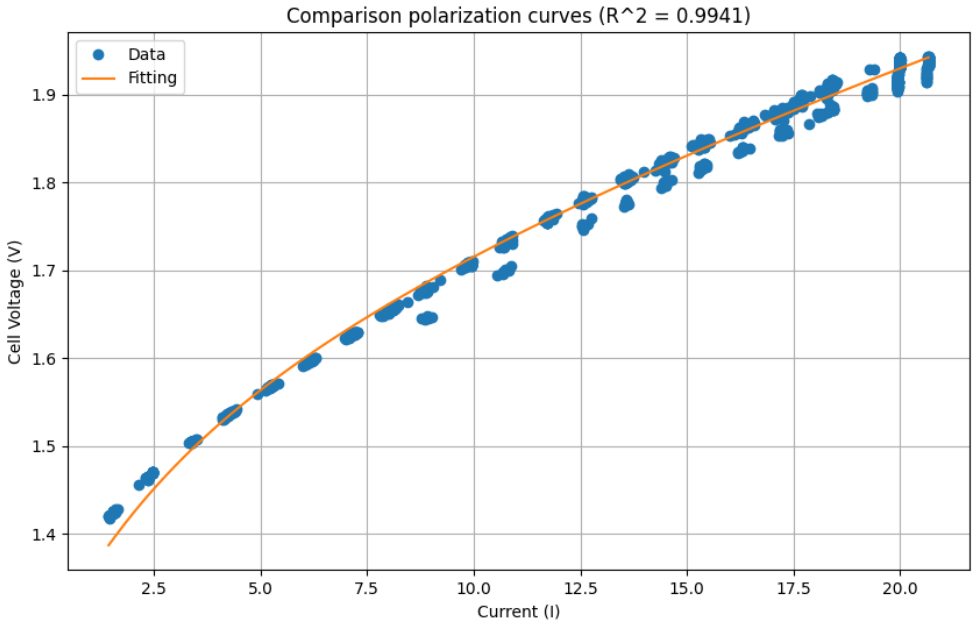

Figure 63 - Fitted descending part 5th February polarization curve.

As explained in Section 3.4.2, the activation overvoltage part has not been completely sampled. The simulation achieves a $R^2\ of\ 0.9941$ which is again a good approximation and a sign that the code can estimate polarization curves in all conditions.

5.2.1.2. Thermal Flow Balance validation

To compute this analysis, again reference was made to the results of previous experimental tests of the case study electrolyzer, the one described in the previous validation section. Initially, the comparison has not been carried out setting the input parameters of the simulation perfectly equal to the one of the experimental test. Indeed, the polarisation curve has been sampled for a single stack. Therefore, the maximum power input cannot be more than half the nominal power of the elctrolyser. On the other hand, the 2021 experimental tests were performed with a intact electrolyzer (both the stacks).
To simulate the presence of both the stacks, as explained above, and to be consistent with the experimental data, the current of the polarisation curve has been doubled and the input power restored to 1650W (same of the previous test). Doing so, two identical stacks are fictitiously integrated in the code and ready to test.

All the parameters evolution in time of the predicted model are analysed and compared to the experimental values.

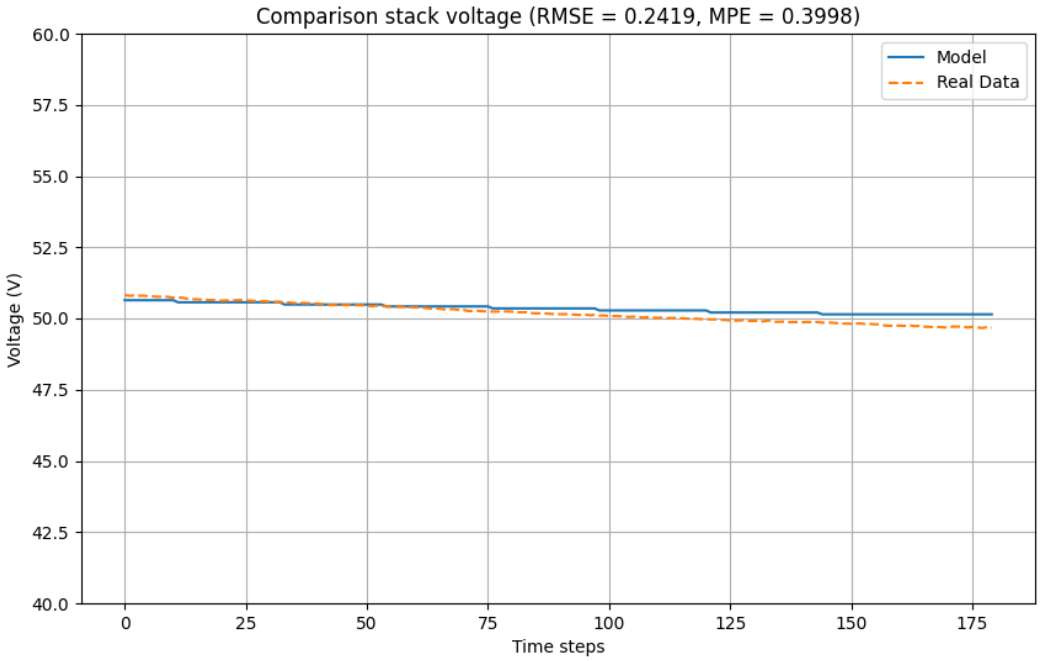

Figure 64 - Stack voltage comparison.

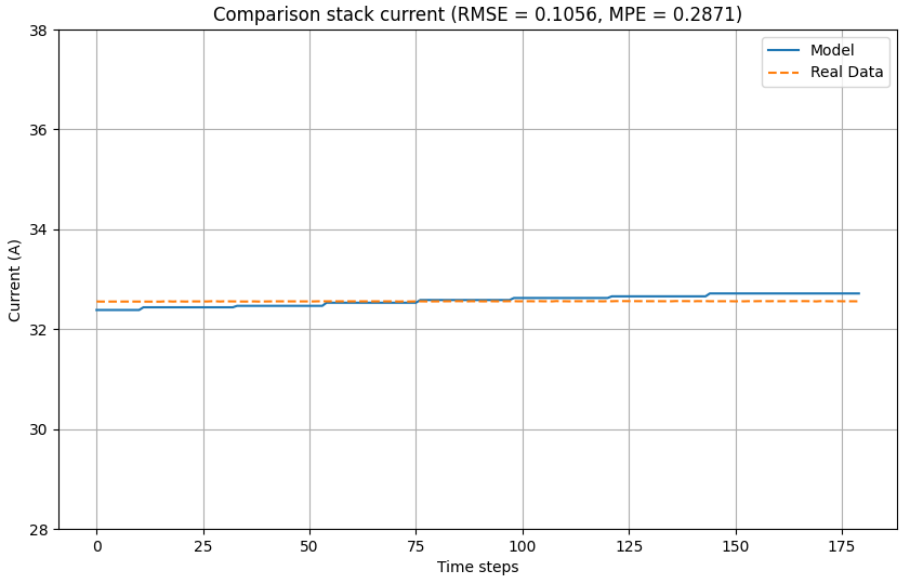

Figure 65 - Stack current comparison.

The voltage and current values are almost completely coincident. Their variation in time are now more accurate especially for the former. Indeed, the model temperature sensitivity compared to the previous validation is much more accurate. The voltage follows better the real evolution. The RMSE and MPE now are definitely lower than before.

These results point out that the previous hypothesis over the reason of the ruined stack was correct.

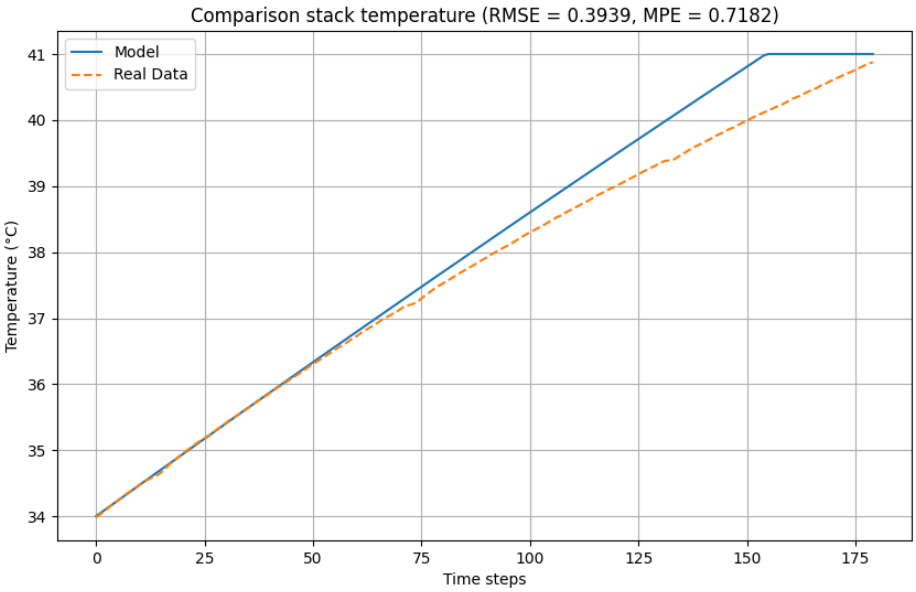

Figure 66 - Original stack temperature comparison.

The temperature evolution is similar as well, the RMSE and MPE are low. At 41°C the cooler is turned on, that is why the model prediction temperature starts to be steady. Now, differently from the previous validation, the Python code seems to predict an excessive heating up of the

electrolyser. This is due the fact that the thermal modelling has been based mainly on literature values (namely the heat exchange coefficient h) to make the model as universal as possible and not designed uniquely for the case study electrolyser.

Now, the heat exchange coefficient equation, described in Section 4.2.3, is an empirical one. It has been defined for a precise case study system electrolyser. All in all the temperature trend is well fitted. However, since already empirical, the coefficient has been optimized until the experimental and the predicted curves were almost coincident. It turns out that the equation should be multiplied by a 5 factor to reach the goal. Here as follow, the result.

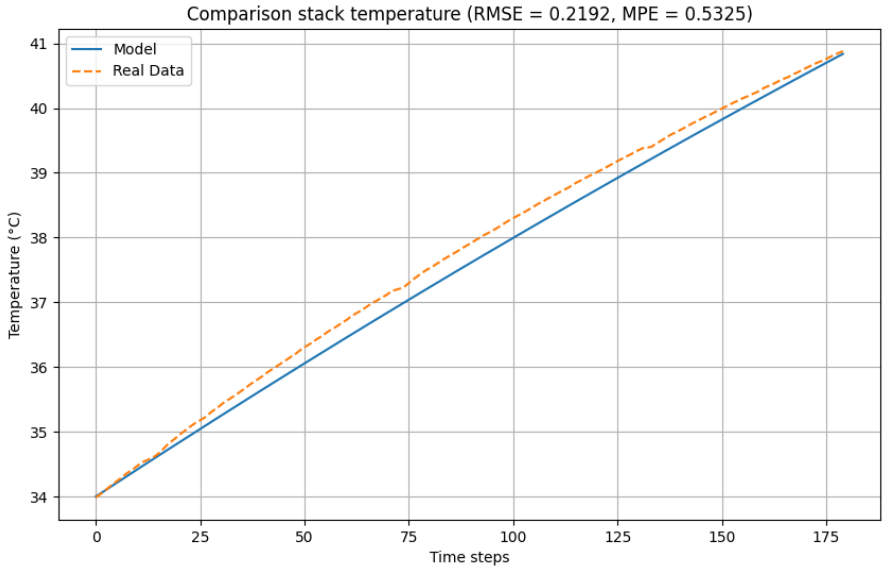

Figure 67 - h modified stack temperature comparison.

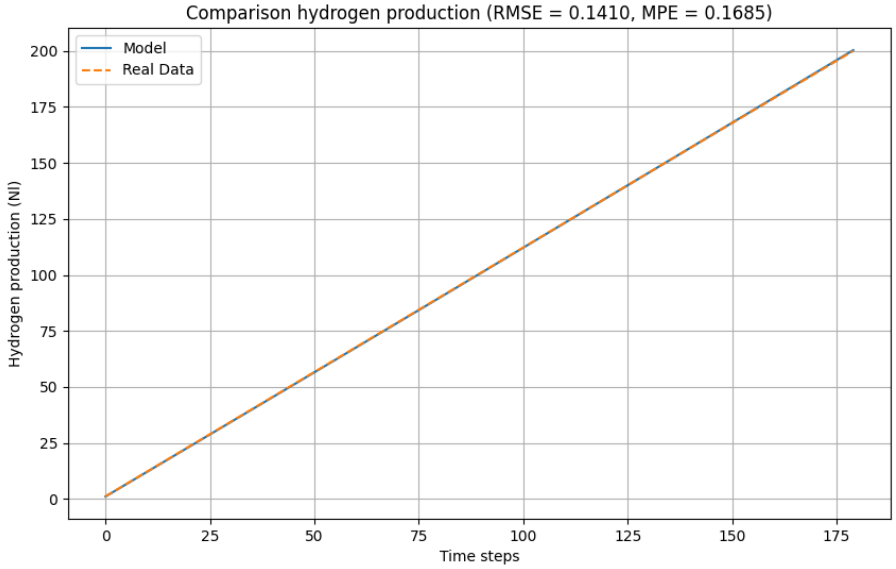

Figure 68 - Hydrogen production comparison.

The hydrogen production prediction are astonishing. The real data and the model one are almost completely coincident as well. This is proven also by the RMSE and MPE. This good result was already expected, as described in the previous validation attempt.

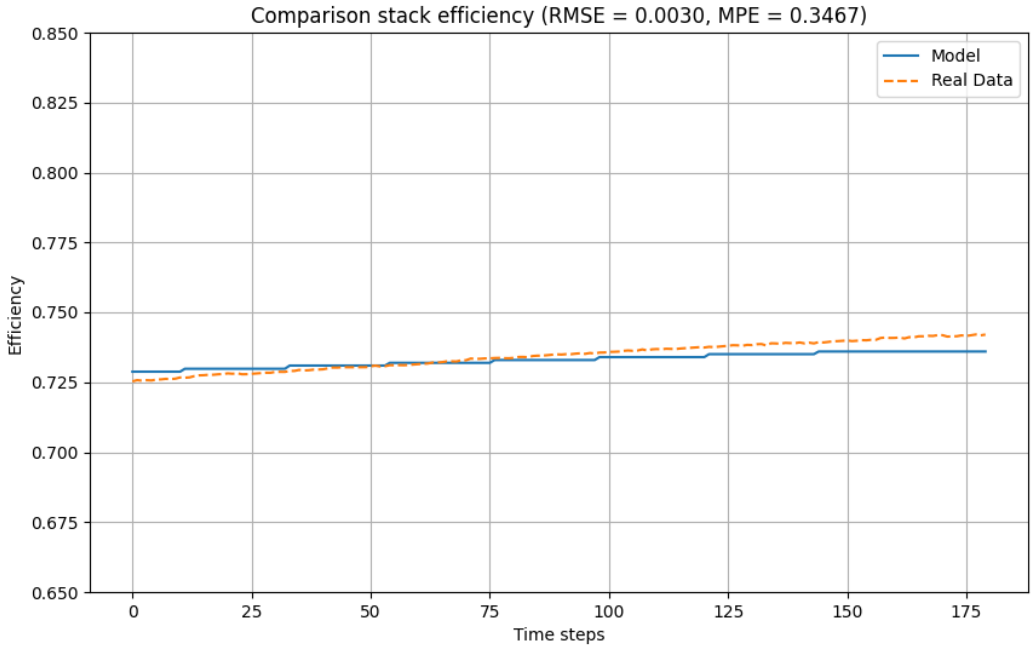

Figure 69 - Stack efficiency comparison.

The efficiency comparison reflects the previous already good result. Indeed, it depends on the voltage and current trends, which are both valid.

So, in the end, the model has been correctly validated with the descending part of the hysteresis cycle of the 5th February 2025 polarisation curve. Therefore there is no need of considering the other polarisation curves, the actual one is regarded as the correct benchmark to evaluate the next analysis.

5.3. Validations comparison

This section focuses on comparing the polarisation curve validations results and fitted parameters of the polarisation curve. The comparison is shown in Table 15.

Table 15 - Comparison between the fitted parameters results and the range of values from literature for both the validation.

Parameters	9/24 Validation	5/2/25 Validation	Range of values from literature
$i_{0,a}$	0.0085 A/cm^2	0.0107 A/cm^2	$10^{-5} < i < 1\ A/cm^2$ [54], [55]
$i_{0,c}$	0.0084A/cm^2	0.0099 A/cm^2	$10^{-5} < i < 1\ A/cm^2$ [54], [55]
λ	21	21	*14-21* [37]
$\varepsilon\left(\frac{\varepsilon-\varepsilon_p}{1-\varepsilon}\right)^{\alpha}$	0.3	0.3	0-1 [41]
t_a	0.00085 m	0.00085 m	$10^{-6} < t < 10^{-2}$ m [56], [57]
t_b	0.00085 m	0.00085 m	$10^{-6} < t < 10^{-2}$ m [56], [57]
n_d	3	3	$\sim 3\ mol_{H2O}\ (mol_{OH^-})^{-1}$ [37]
$k_{mem} = \frac{D_w}{delta_{mem}}$	640 $m\ s^{-1}$	640 $m\ s^{-1}$	$10^2 < k_{mem} < 10^5\ m\ s^{-1}$
$k_{darcy} = \frac{K_{darcy}}{delta_{mem}}$	$5 * 10^{-11}$ cm	$5 * 10^{-11}$ cm	$10^{-18} < k_{darcy} < 10^{-10}\ cm$
$d_{mem} = \frac{delta_{mem}}{A_{mem}}$	0.042 m^{-1}	0.14 m^{-1}	$10^{-2} < d_{mem} < 10^3\ m^{-1}$
$k_{koh} = \left(\frac{d_{\text{am}}}{S_a} + \frac{d_{\text{cm}}}{S_c}\right)$	0.1 m^{-1}	0.1 m^{-1}	$10^{-2} < k_{koh} < 10^2\ m^{-1}$

The code successfully managed to fit all parameters within the predefined ranges, converging with feasible data and achieving a highly accurate approximation of the polarization curves in both cases.

However, the parameters obtained in the two validation attempts differ. It is known that the February validation is the correct one, as confirmed by a comparison with real experimental data. Therefore, an explanation must be provided for why the November 2024 validation yielded incorrect results. The first reason is surely associated to the temperature variation. Below is a possible second reasoning for this discrepancy.

Before defining the parameter ranges, the membrane humidification degree (λ) was identified as the most variable parameter. Its value initially reached 28, which is excessively high for a properly functioning electrolyzer cell. Even within the defined range, λ remains maximized at 21, suggesting a potential link to the aging effects of the electrolyzer stack under study.

The simulations in the model are based on a polarization curve recorded in November 2024, while the experimental data used for validation dates back to 2021. This time gap may have led

to a change in the electrolyzer's electrochemical behaviour. However, the discrepancy cannot be attributed to voltage increase due to degradation, as described in the JRC degradation rate discussed in Section 3.5. This is because, contrary to expectations, the voltage was actually lower in the November 2024 attempt.

A plausible explanation is that the membrane sustained damage, impairing its ability to properly differentiate water molecules from electrolyte components. Under normal conditions, the hydrogen output at the cathode side retains a slight humidity level due to water vapor. However, at the end of the simulation, during the fault period, a significant presence of moisture with "oily" characteristics, similar to the water-KOH electrolyte mixture, was detected, indicating abnormal membrane behaviour.

As a consequence, the electrolyzer impedance decreased, leading to a drop in voltage and an increase in current. The root cause of this malfunction is likely related to the ram effect. When an error occurs, the water flow is abruptly stopped. Given that the system operates under pressurized hydrogen production, the resulting pressure differential downstream of the stack mechanically stresses the membrane, eventually leading to structural failure. This increases the stack's conductivity but severely compromises its normal operation.

Notably, this behaviour is successfully predicted by the model, demonstrating its ability to forecast system malfunctions under realistic operating conditions.

To confirm this hypothesis, an additional test was conducted. The data shift was found to originate specifically from the ohmic region of the polarization curve. The key parameters influencing this region are λ (membrane humidification degree), d_{mem} and k_{KOH} .

Since the correct values of these parameters were determined through the February validation, the approach taken was to fix the known correct values and allow the shifting parameter to vary, thereby validating the proposed explanation. Once again, the "boundary problem" class validation was performed, keeping all parameters affecting the ohmic region constant except for λ, which was allowed to adjust.

The fit adjustment is shown in Figure 70.

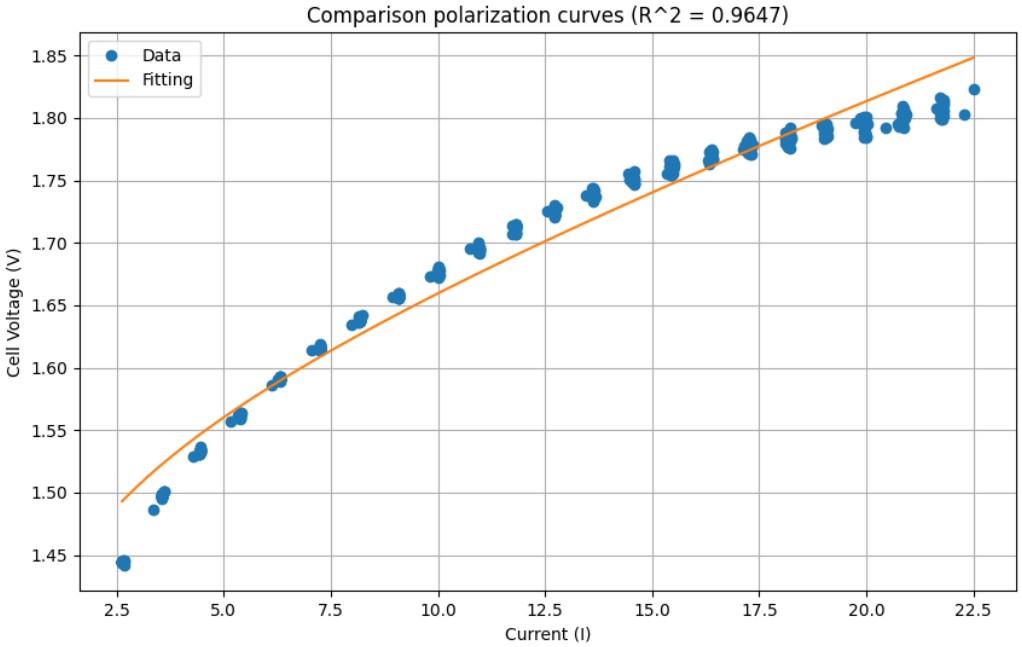

Figure 70 - Fitting process of the November polarisation curve with the new imposed parameters.

The results confirmed the hypothesis: the humidification degree converged to a value of 29, the other two parameters instead are very similar to the values of the February test: d_{mem} of $0.14\ m^{-1}$ and $k_{koh}\ of\ 0.09\ m^{-1}$.

The complete list of the other parameters in the following Table.

Table 16 - Complete list of fitted parameters.

Results	Range of values from literature
$i_{0,a}\ =\ 0.0082\ A/cm^2$	$10^{-5} < i < 1\ A/cm^2$ [54], [55]
$i_{0,c}\ = 0.0081\ A/cm^2$	$10^{-5} < i < 1\ A/cm^2$ [54], [55]
$\lambda\ =\ 29$	$14\text{-}21\ [\ mol_{H2O}\ (mol_{SO3})^{-1}]$ [37]
$\varepsilon\left(\frac{\varepsilon-\varepsilon_p}{1-\varepsilon}\right)^{\alpha} = 0.3$	0-1 [41]
$t_a\ =\ 0.00071$ m	$10^{-6} < t < 10^{-2}$ m [56], [57]
$t_b\ = 0.00085$ m	$10^{-6} < t < 10^{-2}$ m [56], [57]
$n_d\ =\ 3$	Around 3 $mol_{H2O}\ (mol_{OH^-})^{-1}$ [37]
$k_{mem} = \frac{D_w}{delta_{mem}}\ =\ 640\ m\ s^{-1}$	$10^2 < k_{mem} < 10^5\ m\ s^{-1}$
$k_{darcy} = \frac{K_{darcy}}{delta_{mem}} = 5{*}10^{-11}$ cm	$10^{-18} < k_{darcy} < 10^{-10}\ cm$
$d_{mem} = \frac{delta_{mem}}{A_{mem}} = 0.14\ m^{-1}$	$10^{-2} < d_{mem} < 10^3\ m^{-1}$

$k_{koh} = \left(\frac{d_{\text{am}}}{S_a} + \frac{d_{\text{cm}}}{S_c}\right) = 0.094\, m^{-1}$	$10^{-2} < k_{koh} < 10^{2}\, m^{-1}$

The other non-fixed values fluctuate, which is expected, as temperature variations over time influence the other parameters. However, the focus of this analysis is solely on the ohmic part of the polarization curve trend, as this is key to assessing and confirming the hypothesis of the cause of the fault in the electrolyzer.

To conclude, it is worth to note that the model tries to converge into a real polarisation curve. This is highlighted by the fitted curve which is linear and present a slight initial knee to mark the two regions, namely the activation and ohmic overvoltage predominance.

5.4. Real operation efficiency degradation results

Once the correct polarization curve was defined, a long-term performance analysis was conducted. The simulations span a one-year period, aiming to evaluate how degradation affects the normal operation of an AEM electrolyzer. The system is powered by a real fixed-panel PV plant, with a nominal capacity of approximately 1 MW. However, fluctuations in irradiance reduce the actual output power, making it well-suited for a quasi-intermittent simulation. This is relevant because, as discussed in Section 4.4, the degradation model primarily accounts for steady-state degradation.

The PV field data has a sampling interval of 15 minutes, while the simulation model operates with a timestep of 5 minutes to capture all fluctuations accurately. The reference period for the PV field data spans from January 1, 2023, to December 31, 2023, and these values are used as input for the model.

Regarding the simulation settings, multiple degrees of freedom are considered, as detailed in Section 4.3.1, with an additional parameter: the number of electrolyzers simulated. In these tests, only specific parameters are adjusted.

First, both reversible and irreversible degradation effects are examined, with simulations conducted both with and without degradation. This configuration allows for a comparative analysis to assess the overall impact on system performance.

Second, the number of electrolyzers is varied, as this parameter influences both the distribution of available input power and the degradation rate. Since the PV field's power output is shared equally among the electrolyzers, lower power availability can prevent the devices from operating.
As follow the PV peaks distribution throughout the year.

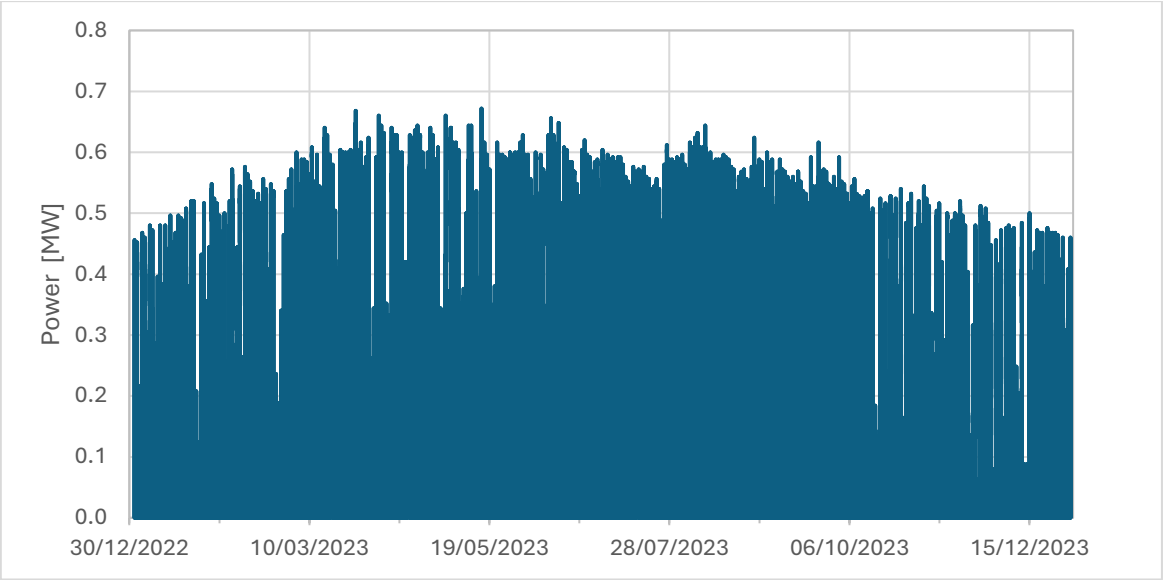

Figure 71 – Input PV field power distribution throughout the year.

It is important to note the average peak power distribution, which amounts to 0.529 MW, approximately half of the nominal power. This factor will influence the subsequent analysis.

The first test is designed to assess the effects of degradation under ideal nominal conditions, with the number of electrolyzers set so that the total nominal power matches that of the PV field, approximately 376 ECs. Subsequent tests examine the impact of degradation when fewer electrolyzers are used, specifically at half and one-third of the nominal power.

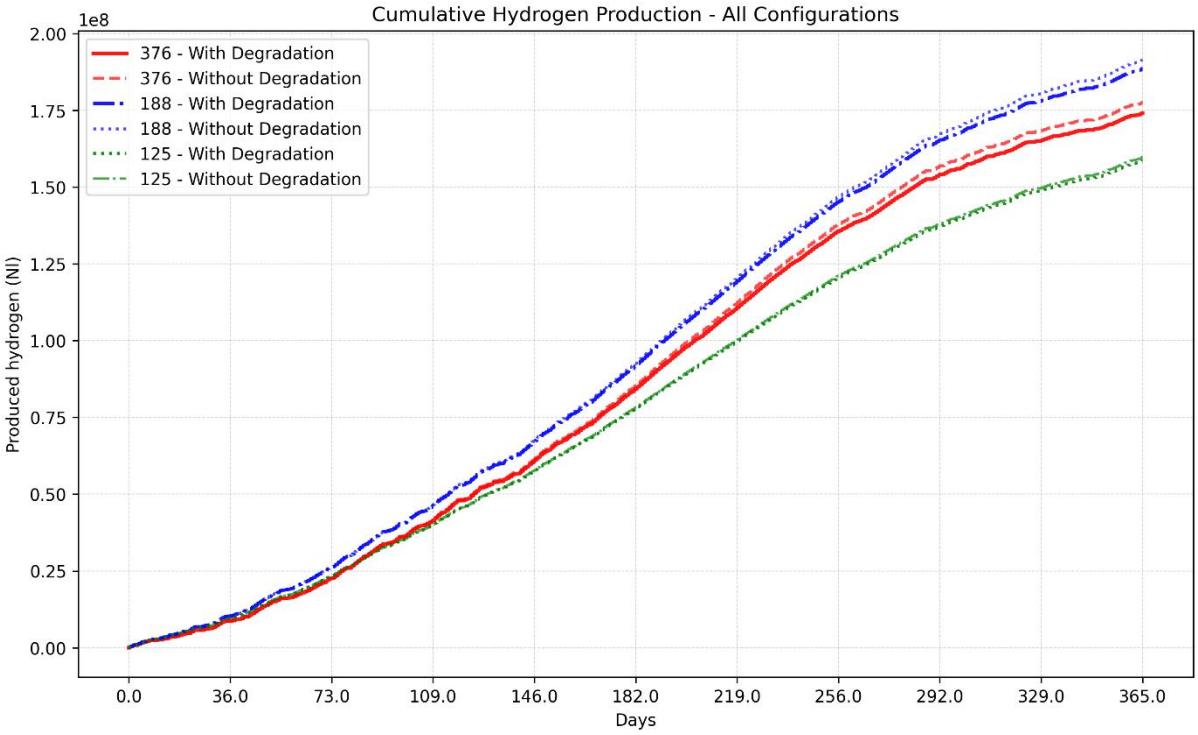

Figure 72 - Cumulative hydrogen production with 376 ECs, 188 ECs and 125 ECs.

The annual hydrogen production under nominal conditions, considering both reversible and irreversible degradation, is approximately 173,715 Nm^3, as shown in Figure 72. The curve flattens at the extremities due to reduced irradiance during the winter season. A similar trend is observed in the cumulative curve for the nominal condition without degradation, where the total hydrogen output reaches approximately 177,010 Nm^3.

The electrolyzer reaches the end of its life when the required input power or voltage increases beyond a sustainable level to maintain the same hydrogen output. Specifically, this occurs when power or voltage rises by approximately 20% over the total lifetime of the EC. Since hydrogen production is directly proportional to current, according to Faraday's law, and the ohmic region of the polarization curve exhibits a linear relationship between voltage and current, the end of life can be estimated by comparing hydrogen production with and without degradation.

The observed decline in hydrogen production corresponds to an annual degradation rate of approximately 1.9%. As degradation accumulates over time, it would take around 4.66 years to reach a 20% increase in power or voltage, marking the system's end of life. This equates to roughly 11,000 hours of operation, which, as indicated in Table 3, falls within the expected range. This approach offers a comprehensive evaluation of overall degradation effects, accounting for both reversible and irreversible components.

As supporting evidence, Figure 73 illustrates the stack voltage trends with and without degradation.

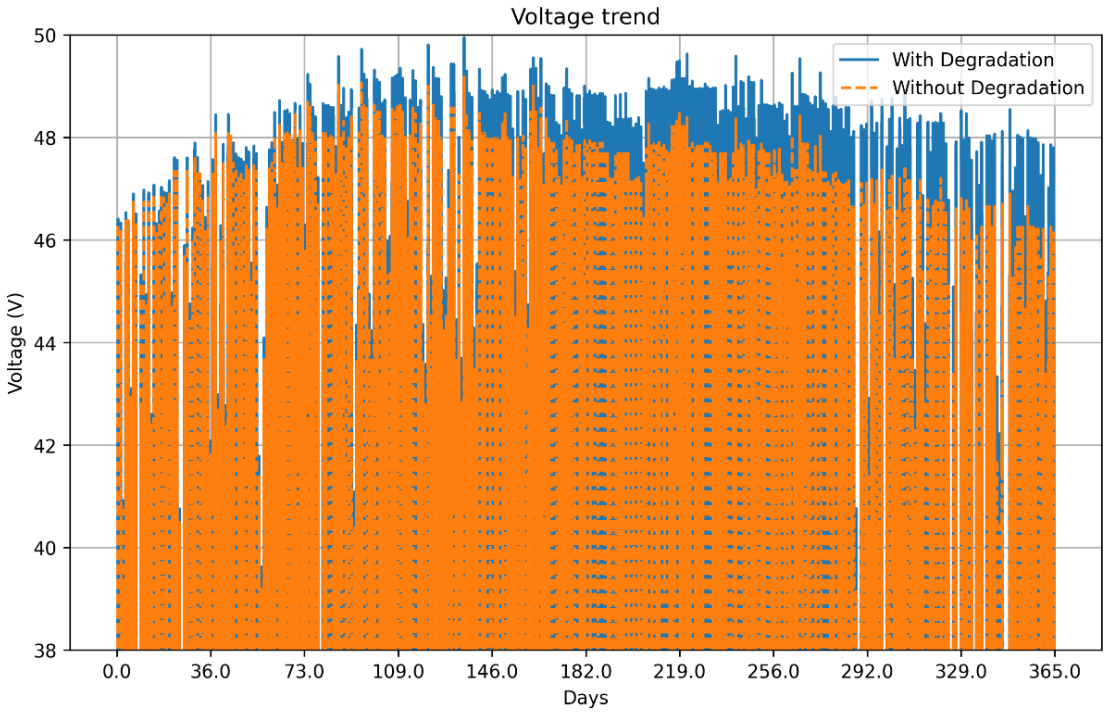

Figure 73 - Stack voltage evolution in time with 376 ECs.

Voltage increases over time, which becomes particularly evident when comparing the last days of the year, where the cumulative effect of irreversible degradation is fully reflected. The voltage values are visibly higher.

To better illustrate the impact of irreversible degradation alone, the first day of the year has been simulated again after one year of operation for a single electrolyzer. The results of this simulation are shown in Figure 74.

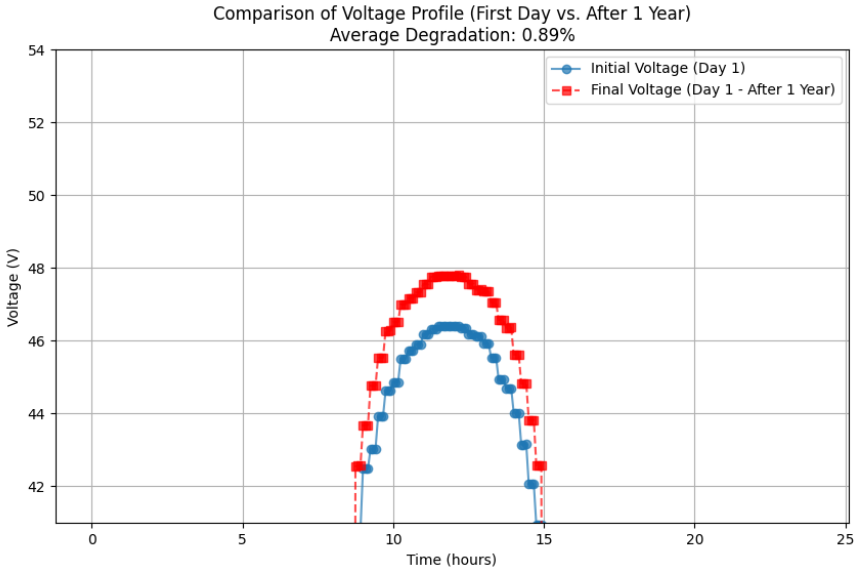

Figure 74 - Comparison of the 376 ECs voltage pattern for Day 1 after 1 year operation.

The average percentage voltage increase has been calculated accordingly, resulting in a rise of 0.89%. The irreversible degradation is cumulative unlike the reversible one.

The following figure illustrates the impact of irreversibilities on a single EC polarization curve after one year. This curve remains valid across all simulations, regardless of variations in the number of ECs.

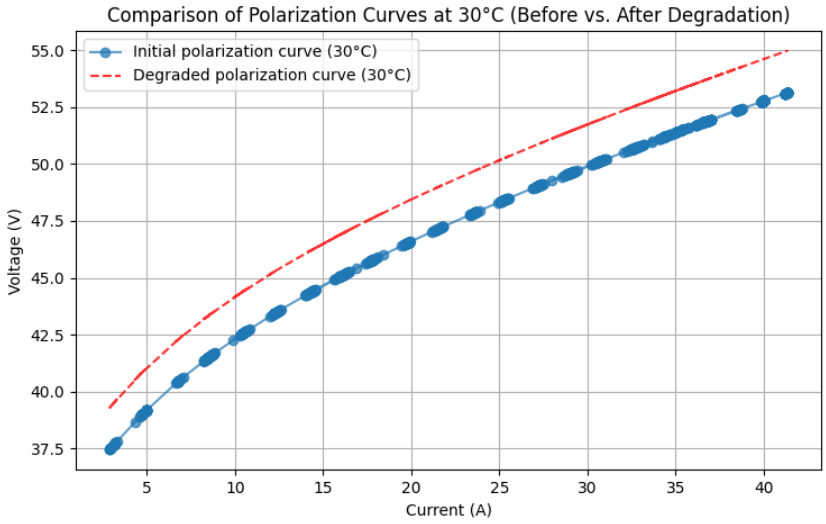

Figure 75 - Electrolyzer polarisation curve after 1 year operation.

In this condition, the irreversible voltage degradation is identified under another form, specifically represented by the average integral mean value difference between the two polarization curves. This results in a voltage increase of 1.8346 V.

Regarding tests conducted under partial power conditions, when the number of electrolyzers is halved to 188 ECs, noticeable differences emerge. Although the cumulative hydrogen production curve follows a similar trend to the previous case (see Figure 72), the total output changes. Specifically, hydrogen production reaches approximately 190,862 Nm^3 without degradation and decreases to 188,126 Nm^3 with degradation. The corresponding overall voltage degradation is reduced to 1.45%, suggesting an estimated end-of-life of around eight years. This equates to roughly 20000 hours of operation, which, as indicated in Table 3, falls within the expected range. This behaviour is anticipated, as reducing the number of ECs mitigates both reversible and irreversible degradation factors.

In the following figure, the first day after one year of operation is simulated once again.

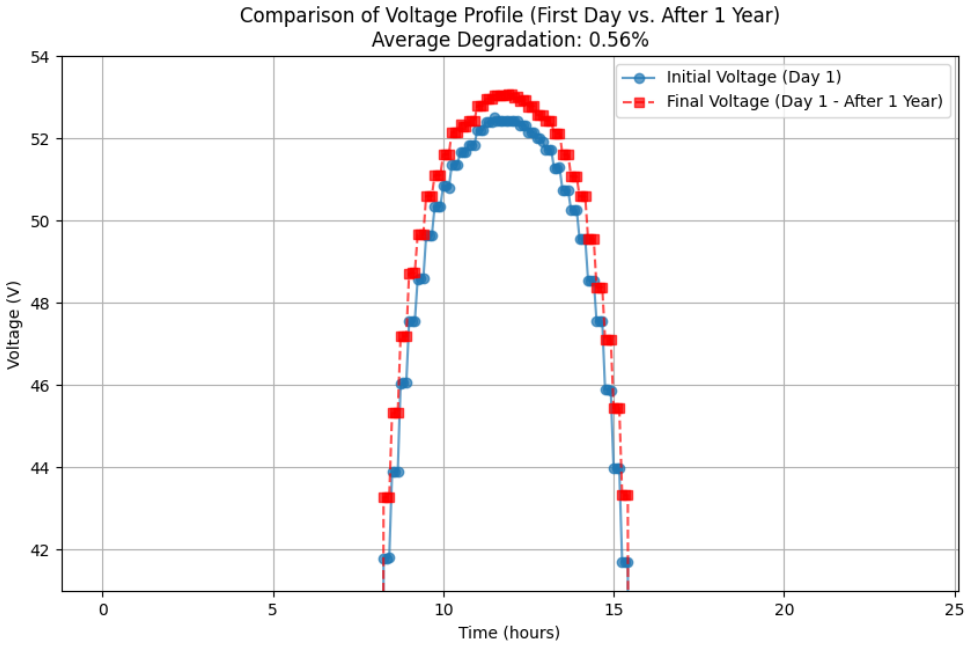

Figure 76 - Comparison of the 188ECs voltage pattern for Day 1 after 1 year operation.

The increase in irreversible degradation remains the same; however, since the electrolyzer operates under nominal conditions, its impact is minimized. Specifically, the configuration with 188 ECs achieves a nominal power of approximately 0.470 MW, while the distribution of average power peaks, as shown in Figure 71, reaches 0.529 MW. As a result, the electrolyzers function at nominal power for nearly the entire year, closely aligning with the average power output of the PV field. This effect is further illustrated in Figure 78.

In this context, current plays a crucial role in hydrogen production and should be maximized to enhance process efficiency. Since degradation leads to an increase in voltage, the required input power also rises. However, because the available average power surpasses the nominal power, the electrolyzer string can still sustain the same hydrogen output, as the current remains unchanged (see Figure 79). This effect is particularly evident in summer, when solar irradiance is high.

The impact becomes even more pronounced when simulating one-third of the nominal conditions, corresponding to 125 ECs. In this configuration, the available power is 312.5 MW, which is sufficient to operate the electrolyzers at nominal conditions throughout the entire year, across all seasons. Consequently, degradation has an almost negligible effect on hydrogen production compared to the previous tests. Under these conditions, the total hydrogen output with degradation is 158,121 Nm^3, while without degradation, it increases slightly to 159,259 Nm^3, a difference of just 0.73%. This minor variation suggests an estimated end-of-life of approximately 25 years. . This corresponds to approximately 60,000 hours of operation, which, as indicated in Table 3, does not fall within the expected range for the current year. However, that table dates back to 2022 and its projections for 2050 anticipate an operational lifespan of 100,000 hours. This suggests a continuous improvement in durability over time, aligning with expected advancements in electrolyzer technology.

The effect of irreversible degradation is further reduced, accounting for only 0.39%, as shown in Figure 77. However, the impact of lower nominal power is also evident in the same figure, indicated by the flattened peak in the middle of the day. This condition would set a limit for the hydrogen production, leading to a bad exploited solar resource.

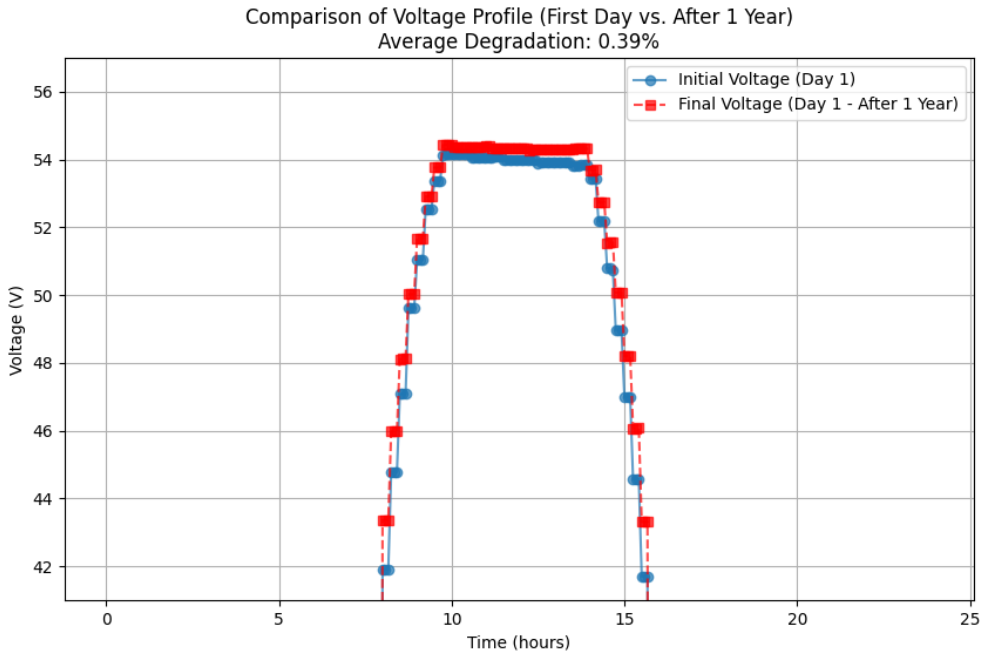

Figure 77 - Comparison of the 125 ECs voltage pattern for Day 1 after 1 year operation.

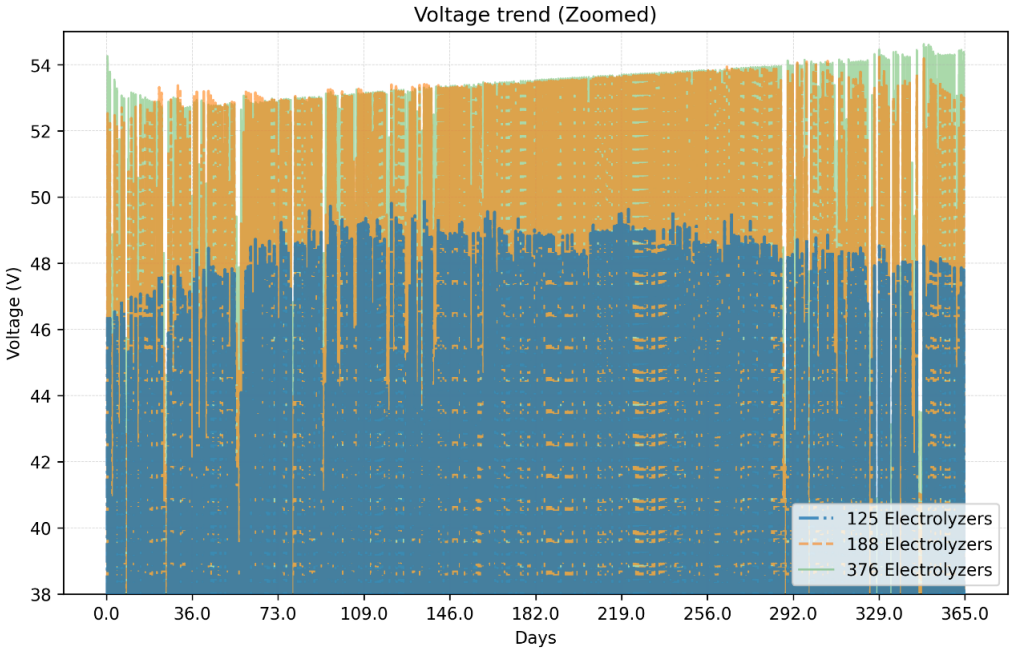

Figure 78 - Voltage comparison with degradation throughout the year between 125, 188 and 376 ECs.

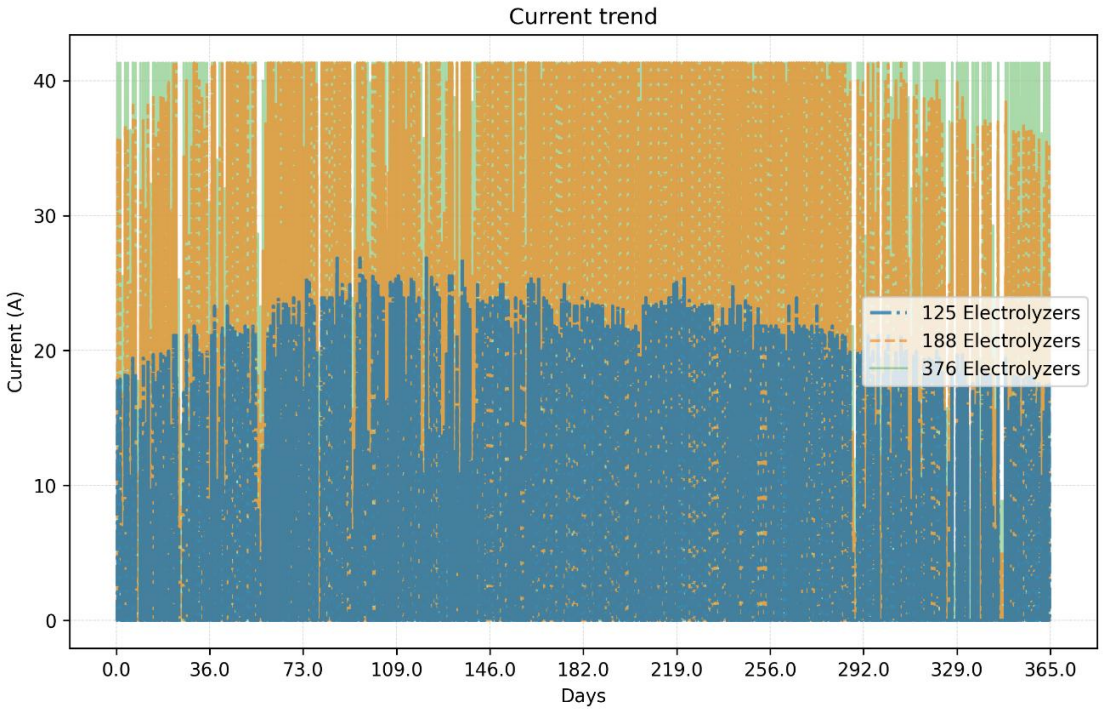

Figure 79 - Current comparison with degradation throughout the year between 125, 188 and 376 ECs.

6. Conclusions

This study developed a Python-based model capable of simulating the performance of an AEM electrolyzer under various operating conditions, with a strong focus on degradation effects. By comparing simulation results with experimental data, the model demonstrated its ability to predict key performance trends and served as a diagnostic tool for detecting operational anomalies.

A key outcome of this research is the model's ability to identify faults in electrolyzer performance. During the simulations, discrepancies between expected and actual behaviour, revealed a malfunction in one of the two stacks, which was later confirmed through experimental measurements. The model successfully detected and diagnosed the fault by analyzing the fitted parameters of the polarization curve. Specifically, the humidification degree was found to be out of range, reaching 29, whereas the upper limit should not exceed 21.
At the same time, the validation process confirmed the model's accuracy. With a coefficient of determination (R^2) of 0.9941 for the fitted polarization curve and low error metrics: a root mean square error (RMSE) of 0.1410 and a mean percentage error (MPE) of 0.1685 for cumulative hydrogen production, the model demonstrated high precision in replicating the real electrolyzer's behaviour.

From a long-term perspective, the degradation analysis offers valuable insights into the impact of both reversible and irreversible degradation on hydrogen production. While irreversible degradation progressively accumulates over time, reversible degradation remains temporary and does not compound. When the number of electrolyzers is configured so that the total nominal power matches the nominal power of the PV field, the overall degradation leads to an annual 1.9% reduction in hydrogen production. This degradation trend results in an estimated end-of-life of 4.66 years when a 20% increase in voltage or power is reached. With approximately 11,000 hours of operation, this value aligns with the expected performance at the current technology readiness level.

Regarding the irreversible voltage increase, which is relevant for all scenarios considering the number of electrolyzer cells (ECs), the average voltage rise after one year is 1.8346 V. This effect becomes more pronounced when a larger number of electrolyzers are in operation, as the power working point for each unit is lower. Consequently, the overall voltage remains lower, making degradation effects more significant during normal operation.

A key finding of this analysis is that operating the electrolyzer at nominal power helps mitigate degradation effects. When the system is properly sized to match the power output of

the PV field, degradation remains limited. However, reducing the number of electrolyzers significantly impacts performance. In a half-capacity configuration (188 ECs), the estimated lifespan extends to approximately 8 years, corresponding to an average of 20,000 hours of operation, which falls within the current technological limits. In contrast, a one-third capacity setup (125 ECs) reaches an estimated lifespan of around 25 years, equating to approximately 60,000 hours of operation, exceeding current technology limits. However, given that the reference table dates back to 2022 and its projections for 2050 anticipate an operational lifespan of 100,000 hours, durability trend increases over time, year by year. This underscores the role of optimizing current density at the operating point to counteract degradation effects, reinforcing the importance of proper system sizing based on available energy.

In conclusion, this study confirms that a well-calibrated simulation model can effectively predict electrolyzer behaviour and degradation trends, providing a valuable tool for assessing future hydrogen production scenarios.

Alongside its strengths, certain limitations must be acknowledged. The current model accounts for degradation in a steady-state context but lacks a parameter to evaluate the impact of energy intermittency. Consequently, it does not fully capture the effects of partial and fluctuating power inputs on the electrolyzer's performance. Incorporating these factors could enhance the model's ability to simulate real-world operating conditions more accurately.

Moreover, the polarization curve shifts upward with degradation. While the slope of the curve undergoes slight changes, it remains largely constant. However, degradation should theoretically increase with current, a factor that is not currently considered in the model. Introducing a parameter to account for this dependency could improve its predictive accuracy.

Another limitation pertains to the thermal management of the simulated system. The temperature evolution model is based on a thermal flow balance equilibrium applied to a simplified stack. While it effectively captures the heating phase, it tends to underestimate the cooling process, particularly during the descending phase of the temperature curve. As a result, the cooldown period is slower than observed in experimental conditions. This discrepancy could be addressed by refining the thermal management constants or enhancing the precision of the thermal behaviour modelling. Additionally, incorporating components that influence heat dissipation, such as auxiliary cooling or heating systems, could further improve the model's accuracy

References

[1] Q. Hassan *et al.*, 'Renewable energy-to-green hydrogen: A review of main resources routes, processes and evaluation', *Int. J. Hydrog. Energy*, vol. 48, no. 46, pp. 17383–17408, May 2023, doi: 10.1016/j.ijhydene.2023.01.175.

[2] 'Renewables 2023 – Analysis', IEA. Accessed: Dec. 04, 2024. [Online]. Available: https://www.iea.org/reports/renewables-2023

[3] 'Idrogeno e CCS'. Accessed: Dec. 04, 2024. [Online]. Available: https://www.snam.it/it/i-nostri-business/idrogeno.html

[4] K. Zeng and D. Zhang, 'Recent progress in alkaline water electrolysis for hydrogen production and applications', *Prog. Energy Combust. Sci.*, vol. 36, no. 3, pp. 307–326, Jun. 2010, doi: 10.1016/j.pecs.2009.11.002.

[5] M. Mori, T. Mržljak, B. Drobnič, and M. Sekavčnik, 'Integral Characteristics of Hydrogen Production in Alkaline Electrolysers', *Strojniski Vestn.*, vol. 59, pp. 585–594, Aug. 2013, doi: 10.5545/sv-jme.2012.858.

[6] P. Nikolaidis and A. Poullikkas, 'A comparative overview of hydrogen production processes', *Renew. Sustain. Energy Rev.*, vol. 67, pp. 597–611, Jan. 2017, doi: 10.1016/j.rser.2016.09.044.

[7] F. Chen, B. Chen, Z. Ma, and M. Mehana, 'Economic assessment of clean hydrogen production from fossil fuels in the intermountain-west region, USA', *Renew. Sustain. Energy Transit.*, vol. 5, p. 100077, Aug. 2024, doi: 10.1016/j.rset.2024.100077.

[8] E. S. Akyüz, E. Telli, and M. Farsak, 'Hydrogen generation electrolyzers: Paving the way for sustainable energy', *Int. J. Hydrog. Energy*, vol. 81, pp. 1338–1362, Sep. 2024, doi: 10.1016/j.ijhydene.2024.07.175.

[9] S. Baral and J. Šebo, 'Techno-economic assessment of green hydrogen production integrated with hybrid and organic Rankine cycle (ORC) systems', *Heliyon*, vol. 10, no. 4, p. e25742, Feb. 2024, doi: 10.1016/j.heliyon.2024.e25742.

[10] M. T. Muñoz Díaz, H. Chávez Oróstica, and J. Guajardo, 'Economic Analysis: Green Hydrogen Production Systems', *Processes*, vol. 11, no. 5, Art. no. 5, May 2023, doi: 10.3390/pr11051390.

[11] 'Elettrolizzatori AEMWE – Hyter'. Accessed: Jan. 14, 2025. [Online]. Available: https://hyter.it/elettrolizzatori-aemwe/

[12] M. E. Şahin, 'An Overview of Different Water Electrolyzer Types for Hydrogen Production', *Energies*, vol. 17, no. 19, Art. no. 19, Jan. 2024, doi: 10.3390/en17194944.

[13] K. Ayers, N. Danilovic, R. Ouimet, M. Carmo, B. Pivovar, and M. Bornstein, 'Perspectives on Low-Temperature Electrolysis and Potential for Renewable Hydrogen at Scale', *Annu. Rev. Chem. Biomol. Eng.*, vol. 10, pp. 219–239, Jun. 2019, doi: 10.1146/annurev-chembioeng-060718-030241.

[14] E. Taibi, R. Miranda, W. Vanhoudt, T. Winkel, J.-C. Lanoix, and F. Barth, *Hydrogen from renewable power: Technology outlook for the energy transition*. 2018.

[15] C. Santoro *et al.*, 'What is Next in Anion-Exchange Membrane Water Electrolyzers? Bottlenecks, Benefits, and Future', *ChemSusChem*, vol. 15, no. 8, p. e202200027, 2022, doi: 10.1002/cssc.202200027.

[16] I. Vincent and D. Bessarabov, 'Low cost hydrogen production by anion exchange membrane electrolysis: A review', *Renew. Sustain. Energy Rev.*, vol. 81, pp. 1690–1704, Jan. 2018, doi: 10.1016/j.rser.2017.05.258.

[17] H. A. Miller *et al.*, ‘Green hydrogen from anion exchange membrane water electrolysis: a review of recent developments in critical materials and operating conditions’, *Sustain. Energy Fuels*, vol. 4, no. 5, pp. 2114–2133, May 2020, doi: 10.1039/C9SE01240K.
[18] M. J. Bos, S. R. A. Kersten, and D. W. F. Brilman, ‘Wind power to methanol: Renewable methanol production using electricity, electrolysis of water and CO2 air capture’, *Appl. Energy*, vol. 264, p. 114672, Apr. 2020, doi: 10.1016/j.apenergy.2020.114672.
[19] ‘Demystifying Electrolyzer Production Costs - Center on Global Energy Policy at Columbia University SIPA | CGEP %’, Center on Global Energy Policy at Columbia University SIPA | CGEP. Accessed: Feb. 20, 2025. [Online]. Available: https://www.energypolicy.columbia.edu/demystifying-electrolyzer-production-costs/
[20] ‘Hydrogen Shot: Water Electrolysis Technology Assessment’, Energy.gov. Accessed: Feb. 20, 2025. [Online]. Available: https://www.energy.gov/eere/fuelcells/hydrogen-shot-water-electrolysis-technology-assessment
[21] M. David, C. Ocampo-Martínez, and R. Sánchez-Peña, ‘Advances in alkaline water electrolyzers: A review’, *J. Energy Storage*, vol. 23, pp. 392–403, Jun. 2019, doi: 10.1016/j.est.2019.03.001.
[22] N. Esfandiari *et al.*, ‘Metal-based cathodes for hydrogen production by alkaline water electrolysis: Review of materials, degradation mechanism, and durability tests’, *Prog. Mater. Sci.*, vol. 144, p. 101254, Aug. 2024, doi: 10.1016/j.pmatsci.2024.101254.
[23] Y. Shi *et al.*, ‘Hydrogen evolution electrodes: Materials and mechanisms in alkaline electrolysis’, *Desalination*, vol. 586, p. 117887, Oct. 2024, doi: 10.1016/j.desal.2024.117887.
[24] P. Trinke, P. Haug, J. Brauns, B. Bensmann, R. Hanke-Rauschenbach, and T. Turek, ‘Hydrogen Crossover in PEM and Alkaline Water Electrolysis: Mechanisms, Direct Comparison and Mitigation Strategies’, *J. Electrochem. Soc.*, vol. 165, no. 7, p. F502, May 2018, doi: 10.1149/2.0541807jes.
[25] N. Guruprasad, J. van der Schaaf, and M. T. de Groot, ‘Unraveling the impact of reverse currents on electrode stability in anion exchange membrane water electrolysis’, *J. Power Sources*, vol. 613, p. 234877, Sep. 2024, doi: 10.1016/j.jpowsour.2024.234877.
[26] L. Järvinen *et al.*, ‘Experimental study of alkaline water electrolyzer performance and frequency behavior under high frequency dynamic operation’, *Int. J. Hydrog. Energy*, vol. 67, pp. 50–61, May 2024, doi: 10.1016/j.ijhydene.2024.04.093.
[27] E. Wallnöfer-Ogris *et al.*, ‘A review on understanding and identifying degradation mechanisms in PEM water electrolysis cells: Insights for stack application, development, and research’, *Int. J. Hydrog. Energy*, vol. 65, pp. 381–397, May 2024, doi: 10.1016/j.ijhydene.2024.04.017.
[28] ‘Multi-Scale Multi-Technique Characterization Approach for Analysis of PEM Electrolyzer Catalyst Layer Degradation - IOPscience’. Accessed: Jan. 20, 2025. [Online]. Available: https://iopscience.iop.org/article/10.1149/1945-7111/ac7258/meta
[29] F. N. Khatib *et al.*, ‘Material degradation of components in polymer electrolyte membrane (PEM) electrolytic cell and mitigation mechanisms: A review’, *Renew. Sustain. Energy Rev.*, vol. 111, pp. 1–14, Sep. 2019, doi: 10.1016/j.rser.2019.05.007.
[30] D. Li *et al.*, ‘Durability of anion exchange membrane water electrolyzers’, *Energy Environ. Sci.*, vol. 14, no. 6, pp. 3393–3419, Jun. 2021, doi: 10.1039/D0EE04086J.
[31] A. K. Niaz, A. Akhtar, J.-Y. Park, and H.-T. Lim, ‘Effects of the operation mode on the degradation behavior of anion exchange membrane water electrolyzers’, *J. Power Sources*, vol. 481, p. 229093, Jan. 2021, doi: 10.1016/j.jpowsour.2020.229093.
[32] D. Grondin, J. Deseure, A. Brisse, M. Zahid, and P. Ozil, ‘Simulation of a high temperature electrolyzer’, *J. Appl. Electrochem.*, vol. 40, no. 5, pp. 933–941, May 2010, doi: 10.1007/s10800-009-0030-0.

[33] E. Rozzi, F. D. Minuto, and A. Lanzini, ‘Dynamic modeling and thermal management of a Power-to-Power system with hydrogen storage in microporous adsorbent materials’, *J. Energy Storage*, vol. 41, p. 102953, Sep. 2021, doi: 10.1016/j.est.2021.102953.
[34] F. Marangio, M. Santarelli, and M. Calì, ‘Theoretical model and experimental analysis of a high pressure PEM water electrolyser for hydrogen production’, *Int. J. Hydrog. Energy*, vol. 34, no. 3, pp. 1143–1158, Feb. 2009, doi: 10.1016/j.ijhydene.2008.11.083.
[35] S. Sood *et al.*, ‘Bond Graph based Multiphysic Modelling of Anion Exchange Membrane Water Electrolysis Cell’, in *2020 28th Mediterranean Conference on Control and Automation (MED)*, Sep. 2020, pp. 752–757. doi: 10.1109/MED48518.2020.9183344.
[36] A. S. Emam, M. O. Hamdan, B. A. Abu-Nabah, and E. Elnajjar, ‘A review on recent trends, challenges, and innovations in alkaline water electrolysis’, *Int. J. Hydrog. Energy*, vol. 64, pp. 599–625, Apr. 2024, doi: 10.1016/j.ijhydene.2024.03.238.
[37] A. Gomez Vidales, N. C. Millan, and C. Bock, ‘Modeling of anion exchange membrane water electrolyzers: The influence of operating parameters’, *Chem. Eng. Res. Des.*, vol. 194, pp. 636–648, Jun. 2023, doi: 10.1016/j.cherd.2023.05.004.
[38] L. J. Titheridge and A. T. Marshall, ‘Techno-economic modelling of AEM electrolysis systems to identify ideal current density and aspects requiring further research’, *Int. J. Hydrog. Energy*, vol. 49, pp. 518–532, Jan. 2024, doi: 10.1016/j.ijhydene.2023.08.181.
[39] A. Santistevan-Pineda, M. Jara-Vasquez, B. Ordóñez-Saca, J. Santana-Villamar, and M. Espinoza-Andaluz, ‘Membrane Electrode Assembly Selection for a Lab Scale Anion Exchange Electrolyzer: Mathematical Modeling and Comparison’, in *2023 IEEE Colombian Caribbean Conference (C3)*, Nov. 2023, pp. 1–6. doi: 10.1109/C358072.2023.10436215.
[40] E. Amores, J. Rodríguez, J. Oviedo, and A. Lucas-Consuegra, ‘Development of an operation strategy for hydrogen production using solar PV energy based on fluid dynamic aspects’, *Open Eng.*, vol. 7, Jun. 2017, doi: 10.1515/eng-2017-0020.
[41] C. Lamy and P. Millet, ‘A critical review on the definitions used to calculate the energy efficiency coefficients of water electrolysis cells working under near ambient temperature conditions’, *J. Power Sources*, vol. 447, p. 227350, Jan. 2020, doi: 10.1016/j.jpowsour.2019.227350.
[42] F. Moradi Nafchi, E. Afshari, and E. Baniasadi, ‘Anion exchange membrane water electrolysis: Numerical modeling and electrochemical performance analysis’, *Int. J. Hydrog. Energy*, vol. 52, pp. 306–321, Jan. 2024, doi: 10.1016/j.ijhydene.2023.05.173.
[43] S. Toghyani, E. Baniasadi, and E. Afshari, ‘Numerical simulation and exergoeconomic analysis of a high temperature polymer exchange membrane electrolyzer’, *Int. J. Hydrog. Energy*, vol. 44, no. 60, pp. 31731–31744, Dec. 2019, doi: 10.1016/j.ijhydene.2019.10.087.
[44] R. Qi *et al.*, ‘Thermal modeling and controller design of an alkaline electrolysis system under dynamic operating conditions’, *Appl. Energy*, vol. 332, p. 120551, Feb. 2023, doi: 10.1016/j.apenergy.2022.120551.
[45] ‘AEMWE electrolysers’, Hyter. Accessed: Feb. 04, 2025. [Online]. Available: https://hyter.it/en/aemwe-electrolysers/
[46] ‘What is a Back Pressure Valve (or Regulator)? | Kimray’. Accessed: Jan. 08, 2025. [Online]. Available: https://kimray.com/training/what-back-pressure-valve-or-regulator
[47] T. Smolinka, E. T. Ojong, and J. Garche, ‘Chapter 8 - Hydrogen Production from Renewable Energies—Electrolyzer Technologies’, in *Electrochemical Energy Storage for Renewable Sources and Grid Balancing*, P. T. Moseley and J. Garche, Eds., Amsterdam: Elsevier, 2015, pp. 103–128. doi: 10.1016/B978-0-444-62616-5.00008-5.
[48] T. Malkow, A. Pilenga, G. Tsotridis, and M. G. De, ‘EU harmonised polarisation curve test method for low-temperature water electrolysis’, JRC Publications Repository.

Accessed: Jan. 15, 2025. [Online]. Available: https://publications.jrc.ec.europa.eu/repository/handle/JRC104045
[49] N. Plankensteiner *et al.*, 'Photovoltaic–Electrolyzer System Operated at >50 mA cm−2 by Combining Large-Area Shingled Silicon Photovoltaic Module with High Surface Area Nickel Electrodes for Low-Cost Green H2 Generation', *Sol. RRL*, vol. 7, no. 7, p. 2201095, 2023, doi: 10.1002/solr.202201095.
[50] Q. Xu *et al.*, 'Anion Exchange Membrane Water Electrolyzer: Electrode Design, Lab-Scaled Testing System and Performance Evaluation', *EnergyChem*, vol. 4, no. 5, p. 100087, Sep. 2022, doi: 10.1016/j.enchem.2022.100087.
[51] G. Tsotridis and A. Pilenga, 'EU harmonised protocols for testing of low temperature water electrolysers', JRC Publications Repository. Accessed: Dec. 30, 2024. [Online]. Available: https://publications.jrc.ec.europa.eu/repository/handle/JRC122565
[52] 'What Is OOP (Object Oriented Programming)?', Spiceworks Inc. Accessed: Jan. 08, 2025. [Online]. Available: https://www.spiceworks.com/tech/devops/articles/object-oriented-programming/
[53] N. O. of D. and Informatics, 'NIST Chemistry WebBook'. Accessed: Jan. 11, 2025. [Online]. Available: https://webbook.nist.gov/chemistry/
[54] S. Fu *et al.*, 'Ultrafine and highly disordered Ni2Fe1 nanofoams enabled highly efficient oxygen evolution reaction in alkaline electrolyte', *Nano Energy*, vol. 44, pp. 319–326, Feb. 2018, doi: 10.1016/j.nanoen.2017.12.010.
[55] N. Mahmood, Y. Yao, J.-W. Zhang, L. Pan, X. Zhang, and J.-J. Zou, 'Electrocatalysts for Hydrogen Evolution in Alkaline Electrolytes: Mechanisms, Challenges, and Prospective Solutions', *Adv. Sci.*, vol. 5, no. 2, p. 1700464, 2018, doi: 10.1002/advs.201700464.
[56] Y. Li, H. Li, W. Liu, and Q. Zhu, 'Optimization of membrane thickness for proton exchange membrane electrolyzer considering hydrogen production efficiency and hydrogen permeation phenomenon', *Appl. Energy*, vol. 355, p. 122233, Feb. 2024, doi: 10.1016/j.apenergy.2023.122233.
[57] X. Wang, J. Zou, Z. Zhang, C. Zhao, M. Wang, and M. Wu, 'Optimization of anode porous transport layer's coating for enhanced proton exchange membrane electrolyzer cells', *Fuel*, vol. 381, p. 133559, Feb. 2025, doi: 10.1016/j.fuel.2024.133559.

Appendices

This appendix provides the full mathematical formulations used throughout the thesis, offering a detailed reference for the equations that were abbreviated or simplified in the main text. By presenting the complete mathematical expressions, this section ensures transparency and reproducibility of the results.

As follow the complete formulation of Eq. 3:

$$E_{\text{rev}} = E^{\circ}_{\text{rev},T} + \frac{RT}{2F}\ln\left(\frac{P_{\text{H}_2}\sqrt{P_{\text{O}_2}}}{a_{\text{H}_2\text{O}}}\right)$$

Where P_{H_2} is the hydrogen partial pressure, P_{O_2} is the oxygen partial pressure and $a_{\text{H}_2\text{O}}$ is the water activity. In turn, according to the kind of technology the partial pressures are influenced by the electrolyte properties, namely:

$$E_{\text{rev}} = E^{\circ}_{\text{rev},T} + \frac{RT}{2F}\ln\left(\frac{\left(P - P_{\text{v,KOH}}\right)\sqrt{P - P_{\text{v,KOH}}}}{a_{\text{H}_2\text{O,KOH}}}\right)$$

Where P is the rated pressure (Bar), $P_{\text{v,KOH}}$ is the water vapour pressure in KOH electrolyte and $a_{\text{H}_2\text{O,KOH}}$ is the water activity in the KOH electrolyte.

The complete formulation of Eq. 7 is:

$$N^{\dot{\text{mem}}}_{\text{H}_2\text{O}} = \frac{\frac{\text{AD}_w}{\delta_{\text{mem}}}\left[\frac{\rho_{\text{H}_2\text{O}}(T_c) - \rho_{\text{H}_2\text{O}}(T_a)}{M_{\text{H}_2\text{O}}} - \frac{\delta_c\, N^{\dot{\text{cons}}}_{\text{H}_2\text{O}}}{D_{\text{eff,c}}\, A} + \frac{\delta_a\, N^{\dot{\text{prod}}}_{\text{H}_2\text{O}}}{D_{\text{eff,a}}\, A}\right] - N^{\dot{\text{eod}}}_{\text{H}_2\text{O}} - N^{\dot{\text{pe}}}_{\text{H}_2\text{O}}}{1 - \frac{\text{D}_w}{\delta_{\text{mem}}}\left(\frac{\delta_c}{D_{\text{eff,c}}} - \frac{\delta_a}{D_{\text{eff,a}}}\right)}$$

Some of the constants have already been described. Water density $\rho_{\text{H}_2\text{O}}$ has been considered constant and temperature independent so the first term of the equation is neglected. A is the active membrane area [m2], D_w represents the membrane water diffusion coefficient [m2 s−1], δ_{mem} denotes the electrode thickness [m], Ta and Tc are the temperatures at the anode and cathode [K], δ_a and δ_c refer to the thicknesses of the anode and cathode [m], D_{eff} is the effective binary diffusion coefficient for transport at the cathode [m2 s−1], $N^{\dot{\text{cons}}}_{\text{H}_2\text{O}}$ is the molar rate of water consumed at the cathode [mol s−1], $N^{\text{prod}}_{\text{H}_2\text{O}}$ is the molar rate of water produced at the anode [mol s−1]. Finally, $N^{\text{eod}}_{\text{H}_2\text{O}}$ is the molar flow of water across the membrane due to electroosmotic

drag [mol s−1] and $N_{\mathrm{H_2O}}^{\mathrm{pe}}$ represents the molar flow of water across the membrane due to pressure effects [mol s−1]. They are represented by the following equations:

$$N_{\mathrm{H_2O}}^{\dot{\mathrm{e}}\mathrm{od}} = \frac{n_d i}{F}$$

$$N_{\mathrm{H_2O}}^{\dot{\mathrm{p}}\mathrm{e}} = \frac{K_{\mathrm{darcy}}\, A\, \nabla p}{\mu_{\mathrm{H_2O}}} \frac{\rho_{\mathrm{H_2O}}}{M_{\mathrm{m,H_2O}}} \frac{1}{\delta_{\mathrm{mem}}}$$

n_d is the electro-osmotic drag coefficient $[mol_{H2O}\,(mol_{OH^-})^{-1}]$, K_{darcy} represents the membrane permeability to water [m2], $\mu_{\mathrm{H_2O}}$ is the viscosity of water [1.1×10−3 Pa·s] and ∇p is the pressure gradient.

Eq. 8 is constituted by $C_{O_2 mem}$ and $C_{H_2 mem}$ representing the concentrations of oxygen and hydrogen, respectively, at the membrane/electrolyte interface $[mol\, m^{-3}]$. The complete equations as follow:

$$C_{O_2,mem} = \frac{p_a \left(\frac{n_{O_2}^{\cdot}}{n_{O_2}^{\cdot} + n_{H_2O,a}^{\cdot}}\right)}{RT_a} + \frac{\delta_a n_{O_2}^{\cdot}}{D_{\mathrm{eff},a}}$$

$$C_{H_2,mem} = \frac{p_c \left(\frac{n_{H_2}^{\cdot}}{n_{H_2}^{\cdot} + n_{H_2O,c}^{\cdot}}\right)}{RT_c} + \frac{\delta_c n_{H_2}^{\cdot}}{D_{\mathrm{eff},c}}$$

Some parameters have already been described: p_a and p_c denote the anode and cathode pressures [Pa], Ta and Tc represent the anode and cathode temperatures [K], $n_{O_2}^{\cdot}$, $n_{H_2}^{\cdot}$, $n_{H_2O}^{\cdot}$ refer to the molar flow rates per unit area in the electrodes [mol·s−1·m−2] (described by the Faraday Law), D_{eff} is the effective binary diffusion coefficient of mass transport [m2·s−1]. In particular, the latter has been described by Eq. **9**, it includes D_{A-B} which is the mixture diffusion coefficient. It can be calculated for a given mixture of substances of A and B. Here as follows the formulation:

$$D_{\mathrm{A\text{-}B}} = \frac{1}{p} a \left(\frac{T}{\sqrt{T_{\mathrm{crA}} T_{\mathrm{crB}}}}\right)^{b} (p_{\mathrm{crA}} p_{\mathrm{crB}})^{1/3} (T_{\mathrm{crA}} T_{\mathrm{crB}})^{5/12} \left(\frac{1}{M_{\mathrm{mA}}} + \frac{1}{M_{\mathrm{mB}}}\right)^{0.5}$$

Where: T represents the temperature in Kelvin [K], while p is the electrode pressure expressed in atmospheres [atm]. $T_{\mathrm{crA}}\ and\ T_{\mathrm{crB}}$ are the critical temperatures of components A and B, respectively, also measured in Kelvin. Similarly, $p_{\mathrm{crA}}\ and\ p_{\mathrm{crB}}$ refer to the critical pressures of components A and B, given in atmospheres. The molar masses of components A and B are denoted by $M_{\mathrm{mA}}\ and\ M_{\mathrm{mB}}$, expressed in grams per mole [g mol−1]. The coefficients a and b are dimensionless empirical values.

Acknowledgments

I would like to take a moment to acknowledge the dedication, perseverance, and passion that have guided me throughout this journey. This work is the result of countless hours of research, problem-solving, and continuous learning, often pushing me beyond my limits. I recognize the challenges I have faced, the obstacles I have overcome, and the growth I have achieved along the way. Completing this thesis is not just an academic milestone but a testament to my commitment and resilience. I am proud of the effort I have put into this work, and I carry forward the invaluable lessons learned during this experience.

I feel both the duty and the deep joy of expressing my gratitude to all those who have contributed to and actively supported my work, enabling me to achieve the best possible results.

I extend my sincere appreciation to the representatives of Edison S.p.A. for giving me the opportunity to take part in cutting-edge research aimed at addressing today's energy challenges. My heartfelt thanks go to my supervisor and co-supervisors, whose dedication and guidance have been invaluable throughout this journey.

A special and profound thank you goes to my family, who, despite the distance, has been my unwavering pillar of support throughout these five years of academic studies and beyond. Their encouragement has given me the strength to persevere, allowing me to navigate each stage of my work with commitment and determination, always striving for both personal growth and a meaningful contribution to a better world.

I also wish to express my gratitude to my professors, whose invaluable insights have helped me deepen my understanding of the challenges encountered throughout my university years. Their mentorship has further strengthened my resolve to pursue this field, with the firm belief that research holds the power to provide meaningful answers and open new horizons.

Finally, I cannot forget my old and new friends, who have stood by my side, pushing me to reach my goals and offering their support through the toughest times, making every effort and sacrifice truly worthwhile.

From the depths of my heart, thank you, thank you, thank you.